DOE Award Number: DE FE0009284

# Statistical Analysis of $CO_2$ Exposed Wells to Predict Long Term Leakage through the Development of an Integrated Neural-Genetic Algorithm

Final Scientific/Technical Report

Reporting Period Start Date: April 1, 2013
Reporting Period End Date: April 30, 2017
Principal Author: Boyun Guo, PhD

**Submitting Organizations:**

University of Louisiana at Lafayette
104 University Circle
Lafayette, Louisiana 70504

Battelle
505 King Avebue
Columbus, Ohio 43201

Missouri University of Science and Technology
1870 Miner Circle
Rolla, Missouri 65409

Date of Report: July 2017

## DISCLAIMER

## ABSTRACT

The objective of this project is to develop a computerized statistical model with the Integrated Neural-Genetic Algorithm (INGA) for predicting the probability of long-term leak of wells in $CO_2$ sequestration operations. This object has been accomplished by conducting research in three phases: 1) data mining of $CO_2$-explosed wells, 2) INGA computer model development, and 3) evaluation of the predictive performance of the computer model with data from field tests.

Data mining was conducted for 510 wells in two $CO_2$ sequestration projects in the Texas Gulf Coast region. They are the Hasting West field and Oyster Bayou field in the Southern Texas. Missing wellbore integrity data were estimated using an analytical and Finite Element Method (FEM) model. The INGA was first tested for performances of convergence and computing efficiency with the obtained data set of high dimension. It was concluded that the INGA can handle the gathered data set with good accuracy and reasonable computing time after a reduction of dimension with a grouping mechanism. A computerized statistical model with the INGA was then developed based on data pre-processing and grouping. Comprehensive training and testing of the model were carried out to ensure that the model is accurate and efficient enough for predicting the probability of long-term leak of wells in $CO_2$ sequestration operations. The Cranfield in the southern Mississippi was select as the test site. Observation wells CFU31F2 and CFU31F3 were used for pressure-testing, formation-logging, and cement-sampling. Tools run in the wells include Isolation Scanner, Slim Cement Mapping Tool (SCMT), Cased Hole Formation Dynamics Tester (CHDT), and Mechanical Sidewall Coring Tool (MSCT). Analyses of the obtained data indicate no leak of $CO_2$ cross the cap zone while it is evident that the well cement sheath was invaded by the

$CO_2$ from the storage zone. This observation is consistent with the result predicted by the INGA model which indicates the well has a $CO_2$ leak-safe probability of 72%. This comparison implies that the developed INGA model is valid for future use in predicting well leak probability.

## TABLE OF CONTENTS

## LIST OF TABLES AND FIGURES

## ACKNOWLEDGEMENTS

This work was financially supported by the United States Department of Energy's National Energy Technology Laboratory (NETL), which is gratefully acknowledged. I greatly appreciate the diligent efforts from the following individuals who contributed to this project. Dr. Runar Negaard of Missouri S&T performed numerical modelling of wellbore integrity for identifying fluid leak scenarios. Dr. Andrew Duguid of Schlumberger Carbon Services and Battelle carried out well site assessment and tests. Xiaohui Zhang tested the Integrated Neural-Genetic Algorithm (INGA) for handling data sets of high dimensions. Ben Li developed, trained, and ran a statistical INGA model with field data.

## EXECUTIVE SUMMARY

The project conducts research under DOE's *Fossil Energy Research and Development* Area of Interest 1, Studies of Existing Wellbores Exposed to Carbon Dioxide ($CO_2$). The purpose of this project is to develop a novel computer model for predicting long-term leakage risks of wells exposed to $CO_2$. The final goal is to deliver DOE and public a useful tool for evaluating the risk of long-term leakage of wells in future $CO_2$ sequestration projects. The computer model developed in this project will contribute to the DOE programs' effort of ensuring 99% $CO_2$ storage permanence in the injection zone(s) for 1000 years and support the development of Best Practices Manual.

The objective of this project is to develop a computerized statistical model with the Integrated Neural-Genetic Algorithm (INGA) for predicting the probability of long-term leak of wells in $CO_2$ sequestration operations. This objective has been accomplished by conducting research in three phases: 1) data mining of $CO_2$-explosed wells, 2) INGA computer model development, and 3) evaluation of the predictive performance of the computer model with data from field tests.

This project has been completed by the University of Louisiana at Lafayette with collaborative efforts of three subcontractors namely Missouri University of Science and Technology, Schlumberger Carbon Services, and Battelle. The University of Louisiana at Lafayette mainly carried out data mining and INGA model development. The Missouri University of Science and Technology performed numerical simulation of wellbore integrity under various well operating conditions to feed input data to the INGA model. The Schlumberger Carbon Services conducted field tests to obtain well data. The Battelle analyzed the obtained well data for INGA model evaluation.

This project was completed in five steps: 1) gathering data of $CO_2$-explosed wells sequestration wells, 2) analyzing the data to assess well integrity for identification of well leak possibility, 3) developing a computer model, 4) generating well leak scenarios, and 5) verifying leak scenarios with field data.

Data mining was conducted for 510 wells in two $CO_2$ sequestration projects in the Texas Gulf Coast region. They are the Hasting West field and Oyster Bayou field in the Southern Texas. Missing wellbore integrity data were estimated using an analytical and Finite Element Method (FEM) model. The INGA was first tested for performances of convergence and computing efficiency with the obtained data set of high dimension. It was concluded that the INGA can handle the gathered data set with good accuracy and reasonable computing time after a reduction of dimension with a grouping mechanism. A computerized statistical model with the INGA was then developed based on data pre-processing and grouping. Comprehensive training and testing of the model were carried out to ensure that the model is accurate and efficient enough for predicting the probability of long-term leak of wells in $CO_2$ sequestration operations. The Cranfield in the southern Mississippi was select as the test site. Observation wells CFU31F2 and CFU31F3 were used for pressure-testing, formation-logging, and cement-sampling. Tools run in the wells include Isolation Scanner, Slim Cement Mapping Tool (SCMT), Cased Hole Formation Dynamics Tester (CHDT), and Mechanical Sidewall Coring Tool (MSCT). Analyses of the obtained data indicate no leak of $CO_2$ cross

the cap zone while it is evident that the well cement sheath was invaded by the $CO_2$ from the storage zone. This observation is consistent with the result predicted by the INGA model which indicates the well has a $CO_2$ leak-safe probability of 72%. This comparison implies that the developed INGA model is valid for future use in predicting well leak probability.

Boyun Guo, Ph.D.

July 29, 2017

## I. INTRODUCTION

Carbon capture and storage (CCS) has been demonstrated as an effective means of storing carbon dioxide ($CO_2$) to reduce the impact of greenhouse gas on the environment. U.S. DOE's Sequestration Program began with a small appropriation of $1M in 1997 and has grown to be the largest most comprehensive CCS R&D program in the world. The U.S. DOE's sequestration program has supported a number of projects implementing $CO_2$ injection in the United States and other countries including, Canada, Algeria, Norway, Australia, and Germany. The program has also been supporting a number of complementary R&D projects investigating the science of storage, simulation, risk assessment, and monitoring the fate of the injected $CO_2$ in the subsurface. There are currently more than 20 large CCS projects in operation or under construction around the world.

The primary challenge in CCS operations is the prevention of long-term $CO_2$ leakage from the geological structures. $CO_2$ storage permanence has been an extremely important issue since the beginning of the first CCS project and has drawn more and more attention as CCS projects gain more maturity. The high corrosive property of supercritical $CO_2$, especially its reaction with cement which is most commonly used for the well completion or well abandonment, can cause significant wellbore integrity problems during $CO_2$ injection and storage. Typical wellbore integrity issues include casing failure, cement integrity failure, tubing/annulus failure, etc.[1] Among these problems, the cement integrity failure has been given a great deal of attention.[2-4] It is found that long-term exposure to $CO_2$ will cause cement degradation and create $CO_2$ leakage pathways along wellbores. As shown in **Figure 1**, these fractures are most likely to occur between the cement-casing interface, cement-shale interface, and in the cement itself.[5,6] The presence of an annular gap and/or fractures with

apertures on the order of 0.01-0.3mm leads to a significant increase in effective permeability in the range of 0.1-1 mD.[7] Hence, the potential leakage of fluids along these fractures is a primary concern in carbon sequestration.

The objective of this project is to develop a computer model with the Integrated Neural-Genetic Algorithm (INGA) for predicting the long-term leak of wells in $CO_2$ sequestration fields. The computer model will contribute to the DOE programs' effort of ensuring 99% $CO_2$ storage permanence in the injection zone(s) for 1000 years and support the development of Best Practices Manual. The computerized INGA model has been developed and tested using field data. Accomplishment details of the project are documented in three annual reports submitted to U.S. DOE.[8,9,10] This report provides a comprehensive summary of project accomplishments by integrating the contents of the first three annual reports and the work completed in the fourth year of project.

## II. RESEARCH APPROACH

This research took an integrated approach composing of three major steps namely 1) establishment of a database for $CO_2$-exposed wells, 2) development of a computer model with the Integrated Neural-Genetic Algorithm (INGA) for predicting the long-term leak of wells in $CO_2$ sequestration fields, and 3) field verification of model result.

### 2.1 Establishment of Database for $CO_2$-exposed Wells

In order to develop and valid the computer model for predicting the long-term leak of wells in $CO_2$ sequestration fields, data gathering from $CO_2$ sequestration fields is a *must.* It is also essential to make an assessment of the data and identify well conditions in terms of risk of leakage.

This project identified two $CO_2$ sequestration projects in the Texas Gulf Coast region suitable for studies. They are the Hasting West field and the Oyster Bayou field in Southern Texas. Locations of these two fields are shown in **Figure 2**. In total, 510 wells were selected from the two fields for data collection.

#### 2.1.1 Data from the Hasting West Field

The West Hastings oil field is located approximately 25 miles southeast of Houston on State Highway No. 35. Most of the field is in the Brazoria County, Texas, with a portion of the east side being in Galveston County, Texas. It is one of the largest oil reserves in the Texas Gulf Coast. The West Hastings oilfield is on a domal uplift having a structural pattern similar to many deep-seated salt domes in the Gulf Coast. It is in the prolific Frio "fairway". Oil production was from the upper Frio sands at depths ranging from 5,125 to 6,125 feet. A

major, northwesterly trending and northeasterly dipping, normal fault divides the field into two segments. Both reservoirs are productive in the upthrown, southwestern segment; whereas only the upper Frio reservoir is productive in the downthrown, northeastern segment. The continuity of these reservoirs is interrupted by many, smaller faults. Well locations in the field are shown in **Figure 3**. Basic data for 40 wells in the field are presented in **Table 1**. More data are stored in a database for this project.

The West Hastings oil field started $CO_2$ injection process in December 2010. $CO_2$ has been injected into the Frio sandstone formation at 5,700 feet with average pay zone thickness 100 feet. The average porosity of reservoir is about 30%, and the average horizontal permeability is about 900 md. The API gravity of the oil is 31°. The current bottom hole pressure is about 1,800 psig.

### 2.1.2 Data from the Oyster Bayou Field

The Oyster Bayou oil field in the Chambers County, Texas, is located at about ten miles southwest of Stowell townsite, and about seven miles southerly from Anahuac field. Oyster Bayou structural trap is on the upthrown (west) side of a large (about 450-foot) fault which strikes northeast-southwest, and is downthrown to the southeast. The structure is thought to be underlain by a non-piercement deep seated salt ridge or dome. The stringer sands (Frio No. 1, No. 2, and No. 3) are developed on the structural flanks, but tend to become thin or shale out completely in crestal wells. The Seabreeze sand is well developed and continuous over the entire productive area. The productive sands range in depth from about 8000 feet for the Frio No. 1 sand to about 8,350 feet for the Seabreeze reservoir at its lowest productive position.

Oyster Bayou oil field started the first $CO_2$ injection in June, 2010. $CO_2$ is injected into the Frio sandstone formation at 8,500 feet with an average pay thickness of 163 feet. The average porosity is 27%, and average horizontal permeability is about 1,500md. The API gravity of oil is 39°. The current bottom hole pressure is about 1,900 psig. Well locations in the field are shown in **Figure 4**. Some data for the $CO_2$ injection wells are shown in **Table 2**. More data are stored in a database for this project.

### 2.1.3 Assessment of Well Conditions

No well in the two fields was officially reported leaking of $CO_2$. Well conditions in the two fields were evaluated on the basis of wellbore cement failure analysis using analytical and numerical models.

Cement sheath is the most important well element for maintaining integrity of fluid-injection wells. Failure of cement sheath can cause loss of zonal isolation, resulting in not only severe operational difficulties, possibly leading to the loss of the well, but also detrimental impacts to personnel, equipment, and environments.

The malfunction of cement sheath may be because of improper cementing practice involving poor hole calibration, poor casing centralization, poor selection of chemical agents for mud removal, poor matching between volume/rheologies/displacement rate of the cement train, and inappropriate cement properties. All these wrong-doing items can result in isolation defect of the cement sheath due to insufficient filling of the well annulus with cement, leaving ways for fluids to pass the cement barrier, often referred to as flow-behind-pipe. The loss of zonal isolation may also be the result of secondary damage of cement sheath by the

improper well operating practice including over-pressure injection, dynamic loading, thermal loading, and corrosion.

In light of what precedes, accurate prediction of cement failure due to over-pressure injection and under-pressure fluid-production are plainly quite a challenge to achieve. Each operation of fluid injection must be assessed properly at the planning stage. This involves consideration of all possible factors that affect the stress in the cement sheath during the operation. These factors include geological conditions (in-situ stresses and temperature, pore pressure, and mechanical and thermal properties of rock), cement sheath properties (thickness, strength, and mechanical and thermal properties), casing properties (steel grade, diameter, wall thickness, strength, and mechanical and thermal properties), injection pressure, and injection temperature.

A number of researchers have investigated the failure of cement sheath under burst conditions that exist in fluid injection operations. The mechanical behavior of cement sheath drew attention in the early 1990's after some laboratory tests. Goodwin and Cook measured permeability of cement sheath under cyclic inner-casing pressures.[11] Major increases in cement sheath permeability were observed after a 4,000 psi pressure cycle and catastrophic increases in permeability developed after a 6,000 psi pressure cycle. In high-tensile-strength cements, cracks were generally initiated either within the cement sheath or at the casing/cement interface, parallel to the inner-casing surface, until tensile strength was exceeded, after which they then radiated outward to the outer-casing surface. In low-tensile-strength cements, the cracks radiated directly from the inner- to the outer-casing surface. Jackson and Murphey tested the effect of inner-casing pressure on gas flow through a sheath of set cement.[12] They confirmed Goodwin and Cook's finding of permeability change after

high-pressures applied to the cement sheath, although they did not report the cracks inside the sheath.

Thiercelin et al. published their analytical model for simulating long-term behavior of cement sheath considering that the rock, cement, and steel behave as homogenous, isotropic, and linearly elastic media up to a threshold where failure occurs.[13] Bosma et al. presented a numerical model with finite-element-method (FEM) to simulate the behavior of cement sheath. [14] It allows the use of more-efficient constitutive laws for rock and cement than in analytical models. Several modified versions of numerical models were presented after Bosma et al.'s work including those by Bois et al.[15] and Nygaard et al.[16] These sophisticated numerical models can adequately handle the effects of pressure on the stress in the cement sheath under various operating condition.

The available theoretical models mainly characterize cement-sheath damage by means of a tensile criterion at the cement/casing or cement/formation interface to simulate de-bonding, a tensile criterion in the cement to simulate cement radial cracking, and a Mohr-Coulomb criterion in the cement to simulate the damage to the cement due to compressive stress. However, these theoretical models are not very helpful for engineers who have to be conservative in designing fluid injection operations. One of the common deficiencies of these theoretical models is that they do not consider the worst scenarios such as the possible gap between the cement sheath and formation rock.

Without well failure incidence reported from the two oil fields, an investigation of well data was conducted in this study to identify wells' condition in terms of risk of leak. The research team took two approaches to assess wellbore integrity conditions. They are 1) use of safe-

operation pressure windows constructed with analytical solutions, and 2) numerical stress simulator with Finite Element Method (FEM).

#### 2.1.3.1 Safe-operation Pressure Window

The safe-operation pressure window is defined as the range of bottom hole pressures that will not cause failure of cement sheath due to either high injection pressure for fluid injection wells or pressure drawdown for fluid production and observation wells. The upper bound of the pressure range is called the Maximum Permissible Pressure (MaxPP) and the lower bound of the pressure range is called Minimum Permissible Pressure (MinPP). Mathematical models used for determining the safe-operation pressure window have been published by the research team as follows:

1. Ben Li, Boyun Guo, Hui Li, Yucai Shi. 2015. An Analytical Solution to Simulate the Effect of Cement/Formation Stiffness on Well Integrity Evaluation in Carbon Sequestration Projects, *Journal of Natural Gas Science & Engineering*, 27, 1092-1099.
2. Yucai Shi, Ben Li, Boyun Guo, Zhichuan Guan, Hui Li. 2015. An Analytical Solution to Stress State of Casing-Cement Sheath-Formation System with the Consideration of Its Initial loaded State and Wellbore Temperature Variation, *International Journal of Emerging Technology and Advanced Engineering*, Volume 5, Issue 1 (Jan. 2015), pp59-65.
3. Boyun Guo, Ben Li, and Na Wei. 2014. The Maximum Permissible Pressure in Well Stimulation Operations, paper 11715 presented at the International Petroleum Technology Conference held in Kuala Lumpur, Malaysia, 10-12 December 2014.

For simplicity of presentation only a short version of the mathematical models is provided in this report.

#### 2.1.3.1.1 The Maximum Permissible Pressure (MaxPP)

The laboratory and theoretical studies discussed in the previous section implies that, at the MaxPP, radial cracks will initiate at the casing/sheath interface due to the tensile failure of the sheath. It is expected that the MaxPP is determined by the tensile strength of set-cement and the degree of support from the formation rock for no-gap conditions or the pore fluid for fluid-gap conditions behind the sheath.

If the cement placement efficiency in the annulus is 100%, the formation rock will fully support the cement sheath with the formation stress around the wellbore. The formation stress around an injection well is higher than the formation in-situ stress. However, from engineers' point of view, using the formation in-situ stress will give a conservative value for the MaxPP. For a given rock stress around the wellbore, the radial and tangential stresses in the cement sheath can be calculated using Lame's solutions[17] if the radial stress at the inner-surface is known. Based on the analysis with simple tensile failure, the pressure at the inner-surface required to cause cement failure can be determined. A boundary condition at the casing/sheath interface is needed to relate the radial stress at the interface to the pressure inside the casing. Because the tensile strength of set-cement is very low (300 psi ~ 700 psi) as compared to its compressive strength, it is anticipated that radial cracks will initiate in the cement sheath before a significant radial deformation develops at the interface. Assuming zero radial-displacement at the interface, the radial stress at the inner-surface of sheath at failure is related to the inner-casing pressure through the classical solution described by

Timoshenko.[17] This inner-casing pressure at failure is the MaxPP. Details of derivation are shown in Appendix A. The resultant expression for the MaxPP is as follows:

$$MaxPP = \frac{[(r_{so}^2 + r_{si}^2) - \nu(r_{so}^2 - r_{si}^2)][\sigma_T(r_w^2 - r_{so}^2) + 2\sigma_h r_w^2]}{2r_{si}^2(r_{so}^2 + r_w^2)} \quad (1)$$

where $r_{so}$ = outer radius of steel casing

$r_{si}$ = inner radius of steel casing

$r_w$ = wellbore radius to sand face

$\sigma_T$ = tensile strength of set-cement

$\sigma_h$ = the minimum horizontal in-situ stress.

If the cement placement efficiency in the annulus is less than 100%, the formation fluid, not the rock, will support the cement sheath with the formation pore pressure around the wellbore. The formation pore pressure around an injection well will change with time. However, from engineers' point of view, using the initial formation pore pressure in the cap rock will give a conservative value for the MaxPP. The burst resistance of the cement sheath depends on the thickness of the sheath which relates to the cement placement efficiency in the annulus. Following the same procedure used in deriving Eq. (1), the following result is obtained (see Appendix A for derivation):

$$MaxPP = \frac{[(r_{so}^2 + r_{si}^2) - \nu(r_{so}^2 - r_{si}^2)][\sigma_T(r_{co}^2 - r_{so}^2) + 2p_P r_{co}^2]}{2r_{si}^2(r_{so}^2 + r_{co}^2)} \quad (2)$$

where $r_{co}$ = outer radius of cement sheath

$p_p$ = formation pore pressure.

Although accurate determination of the $r_{co}$ value is difficult, if not impossible, with today's technologies, it is practical to obtain an estimate of this parameter value on the basis of cement placement efficiency.

Cement Bonding Logs (CBL) have been used to estimate the cement placement efficient in oil and gas wells since 1960's.[18,19] Modern Ultrasonic Cement Logs (UCL) replaced CBL in 1980's.[20] These logs allow for estimating the volume fraction of the annular space occupied by the set-cement. If there is a gap between the cement sheath and formation rock, the data of volume fraction of cement may be utilized to estimate the outer radius of the cement sheath through

$$E_c = 1 - \frac{\pi r_w^2 - \pi r_{co}^2}{\pi r_w^2} \tag{3}$$

which gives

$$r_{co} = r_w \sqrt{E_c} \tag{4}$$

where $E_c$ is the volume fraction of the annular space occupied by the set cement. This parameter is referred to as the cement placement efficient in this study. For water injection wells, a rule of thumb accepted by the industry for the safe value of the cement placement efficiency factor is $E_c > 0.8$ over at least 50 feet of cement sheath. For $CO_2$ injection wells, such a rule of thumb has not been established. This study suggests to use a safe value of $E_c > 0.9$ over at least 50 feet of cement sheath.

#### 2.1.3.1.2 The Minimum Permissible Pressure (MinPP)

The Minimum Permissible Pressure (MinPP) is defined as the bottom hole pressure inside casing that will cause failure of the cement sheath during oil and gas production (collapse condition) operations. This parameter is extremely important for converting production wells to fluid (water and $CO_2$) injection wells. If the wells have been exposed to the wellbore pressure that are below the MinPP, they should not be selected as candidates of fluid injectors because their cement sheaths may have been damaged/cracked due to the collapse loads generated in production operations. It is expected that the MinPP is determined by the compressive strength of set-cement, properties of well casing, and the collapse pressure load from the formation rock which is dependent on the relation between the rock and the cement sheath such as the existence of fluid-gap between them. If the cement placement efficiency in the annulus is 100%, the formation rock stress will act directly on the cement sheath. If the cement placement efficiency in the annulus is less than 100%, the cement sheath should be subjected to the formation pore pressure around the wellbore. Using formation in-situ stress will give a conservative value for the MinPP due to the fact that the formation in-situ stress is much higher than the formation pore pressure.

The tangential stress at the inner wall of the cement sheath is given by (see Appendix B for derivation):

$$\sigma_{\theta ci} = \frac{p_{ci}\left(r_{ci}^2 + r_{co}^2\right) - 2p_{co}r_{co}^2}{\left(r_{co}^2 - r_{ci}^2\right)} \tag{5}$$

where

$\sigma_{\theta ci}$ = tangential stress at the inner wall of the cement sheath

$p_{ci}$ = pressure or radial stress at the inner wall of the cement sheath

$p_{co}$ = pressure or radial stress at the outer wall of the cement sheath

$r_{ci}$ = inner radius of cement sheath

$r_{co}$ = outer radius of cement sheath

The radial stress at the inner wall of the cement sheath is given by (see Appendix B for derivation):

$$\sigma_{rci} = -p_{ci} = \frac{-2p_i r_i^2}{\left(r_o^2 + r_i^2\right) - \nu\left(r_o^2 - r_i^2\right)} \tag{6}$$

where

$\sigma_{rci}$ = radial stress at the inner wall of the cement sheath

$p_{ci}$ = pressure or radial stress at the inner wall of the cement sheath

$p_i$ = casing inner pressure

$r_i$ = inner radius of casing

$r_o$ = outer radius of casing.

It can be shown that the tangential stress given by Eq. (5) is less compressive than the radial stress given by Eq. (6). These two stress components should be taken as the minimum and the maximum principal stresses, respectively, in the failure analysis with Mohr-Coulomb criterion:

$$\left|\sigma_{rci}\right| \le \frac{2C\cos\phi}{1-\sin\phi} + \left|\sigma_{\theta ci}\right| \frac{1+\sin\phi}{1-\sin\phi} \tag{7}$$

where $C$ and $\phi$ are the cohesive strength and internal friction angle of set cement, respectively. The MinPP is defined as the value of the casing inner pressure $p_i$ satisfying Eq. (7) with an equal sign.

### 2.1.4 Assessment of Wells in the Hasting West Field

Potential leak of wells in the Hasting West field were assessed using the concepts of MaxPP and MinPP. **Figure 5** presents a comparison of the maximum wellhead pressures and the calculated wellhead MaxPP's of wells without fluid gap in the cement sheaths for the West Hastings wells. Since the maximum injection pressures are less than the calculated MaxPP's for all of the wells, it is believed that these wells safe if there is not fluid gap at the sand face.

**Figure 6** shows a comparison of wellhead pressures and the calculated wellhead MaxPP's of wells with fluid gaps in the cement sheaths for the West Hastings wells. The maximum injection pressures are found greater than the calculated MaxPP's for 10 wells. It is thus believed that these wells are not safe if there are fluid gaps at the sand face. CBL's of these wells need to be evaluated to find any fluid gaps.

**Figure 7** demonstrates a comparison of wellhead pressures and the calculated wellhead MinPP's of wells with fluid gaps in the cement sheaths for the West Hastings wells. The wellhead pressures are found to be lower than the calculated MinPP's for 4 wells. It is believed that these wells are subjected to shear failure of cement sheaths.

### 2.1.5 Assessment of Wells in the Oyster Bayou Field

Potential leak of wells in the Oyster Bayou field were assessed utilizing the concepts of MaxPP and MinPP. **Figure 8** presents a comparison of the wellhead pressures and the calculated wellhead MaxPP's of wells without fluid gap in the cement sheaths for the Oyster

Bayou wells. Because the maximum injection pressures are less than the calculated MaxPP's for all of the wells, these wells are believed to be safe if there is no fluid gap at the sand face. However, **Figure 9** illustrates that the maximum injection pressures are less than the calculated MaxPP's for all wells when fluid gaps exist at the sand face. It is therefore believed that all these wells are safe even though some fluid gaps exist at the sand face.

**Figure 10** presents a comparison of wellhead pressures and the calculated wellhead MinPP's of wells with fluid gaps in the cement sheaths for the Oyster Bayou wells. The wellhead pressures are found to be lower than the calculated MinPP's for most wells. It is thus believed that these wells are subjected to shear failure of cement sheaths and possess risk of leaking in dynamic injection conditions.

### 2.1.6 Numerical Stress Simulator

Integrity conditions of the wells from the two fields were also assessed with a numerical stress simulator to consider parameters that are not included in the analytical stress window. These parameters include temperature and change in well operating conditions.

The modeling approach used to describe the effects of cement sheath degradation is a staged model. This model includes both finite element and analytical methods. The finite element methods are used to describe the in-situ stress conditions in the cement sheath. A staged modeling approach is needed to build the initial conditions. An analytical solution is superimposed on the initial conditions to simulate loading on the new Young's Modulus. The approach followed in this study is based on replicating the life of the well by including all loading steps occurring before mechanical and thermal loads caused by the injection are applied to the cased borehole. **Figure 11** shows a schematic of the borehole cross section and

the loads (mechanical and thermal) that are applied on them. The dark grey represents the casing, the light grey represents the cement sheath, and the green represents the sealing formation. Details of the steps followed in numerical simulations are also illustrated on the right side of the **Figure 11**. The mesh for finite element study was constructed in HyperMesh™ and the actual finite element simulations were conducted in Abaqus™ software[21,22]. The three-dimensional mesh has one and five meter length in z and (x,y) directions respectively and is composed of first order elements. The numerical model also assumes homogeneity in all materials including casing, cement, and formation. The main goal from numerical models is to propose a robust multi-stage modeling approach for near wellbore integrity situations and to capture effect of dynamic loads on the near wellbore area. The staged finite-element model uses the property of superposition to build the model initial conditions before the next step of loading is implemented. The advantage of building the model in several steps is to observe and record stress and deformation changes after each loading.[23] The stages of the finite element model are detailed and explained in previous quarterly reports. There are four scenarios used to analyze the cement sheath degradation. These scenarios are: the in-situ stresses with Young's Modulus E1, the injection mechanical and thermal loading applied with a Young's Modulus equal to E1, the stresses after the injection pressure is removed and thermal loading remains at the degraded Young's Modulus equal to E2, and the stresses when both mechanical and thermal loading have been removed at the degraded Young's Modulus of E2. The steps are shown in **Figure 12**. More information about the Finite Element Method (FEM) model is documented by Weideman and Nygaard.[24]

**Figure 13** presents computed profiles of radial stresses under different injection conditions. **Figure 14** illustrates computed profiles of radial stresses under different production conditions. **Figure 15** shows computed profiles of radial stresses under different depletion conditions. **Figure 16** provides computed profiles of hoop stresses for an actual well with CO2 injection. The stresses were compared with the strengths of casing, cement sheath, and formation rock to identify failure conditions and possibility of well leakage.

### 2.2 Development of Computer Model with INGA

A statistical model with the Integrated Neural-Genetic Algorithm (INGA) was developed to establish a computational tool for predicting well leakage. The procedure of developing the statistical model involves testing the performance of INGA with the large-dimension data set gathered in the first year of the project, construction of well failure index as a function of groups of variables, training the statistical INGA model, and testing the statistical model.

#### 2.2.1 Testing the INGA

The field data gathered in the project includes 510 wells in the West Hastings oil field and the Oyster Bayou oil field in southern Texas. There are 67 parameters that describe well design and operation conditions. To ensure a smooth development of a statistical model with the INGA, the INGA was first tested for convergence performance against the dimension of data set. The objective of the testing was to determine if variable grouping is required to improve data processing efficiency, i.e., to reduce computing time.

The INGA was coded in a C++ program, trained and tested to investigate its accuracy and capacity of handling different sizes of data sets. **Table 3** presents a 3-dimentional test-data set generated by:

$$y = x_1^{\,2} + x_2^{\,2} \tag{8}$$

The normalized dependent variable is defined as:

$$y_{normalized} = \frac{y - y_{\min} + 1}{y_{\max} - y_{\min} + 1} \tag{9}$$

The accuracy of the algorithm was evaluated by examining the correspondence of the model output (predicted y-value) to the model input (values of $x_1$ and $x_2$) in a system. **Figure 17** presents a cross-plot of the true and predicted values of variable $y$. It shows a good correlation between the predicted value and true value with $R^2 = 0.9994$. The quantitative analysis of accuracy was performed by calculating the average relative error defined as:

$$Error = \frac{100}{n}\sqrt{\sum_{1}^{n}\left(\frac{\text{Predicted } y_i \text{ - True } y_i}{\text{True } y_i}\right)^2}\,\% \tag{10}$$

For this data set, the average relative error was calculated to be 4%, i.e., the accuracy is 96%.

The capacity of the algorithm was analyzed by counting the CPU time required to solve problems with different populations of input data sets. **Table 4** summarizes the CPU time and error for the number of data points cut at different levels. The data is plotted in **Figure 18**, which demonstrates that the CPU time increases linearly with the population of data set. But the accuracy remains higher than 90% as long as the number of data points is greater than 20. The data set established in this project contains 510 wells with 67 parameter values for each well. This calculates the total number of data points to be 36,720 in 68 dimensions.

Based on the linear extrapolation of the trend in **Figure 18**, the computing time will be nearly 80 minutes, which is not practical. Therefore, a reduction in data dimension is required. This was done by constructing a well Leakage-Safe Probability Index (LPI) as a function of 4 failure indicators determined by 4 groups of independent variables.

### 2.2.2 Construction of Well Leakage-safe Probability Index (LPI) Function

The LPI of well is defined based on the average value of WSI, WAI, CTI, and CSII. It is between 0 and 1. The higher the LPI is, the less likely a $CO_2$ –exposed well will leak. If the average value of the four indicators for a well is less than 0.2, the well is identified as a potential-failure well and assigned with LPI = 0. If the average value is more than 0.7, the well is identified as potential-safe well and assigned with LPI = 0.95. Both potential-failure wells and potential-safe wells were used to train and test the statistical INGA model. The WSI, WAI, CTI, and CSII are explained in the following sections.

#### 2.2.2.1 Well Schematic Indicator (WSI)

The U.S. Environmental Protection Agency (EPA) is mandated under the Underground Injection Control (UIC) Program of the Safe Drinking Water Act (SDWA) to protect Underground Source of Drinking Water (USDW) and the health of people from underground injection. USDW means an aquifer or its part that currently supplies any public water system or contains a sufficient quantity of ground water to supply a public water system; and currently supplies drinking water for human consumption or contains fewer than 10,000 mg/L total dissolved solids. Based on the Texas Administrative Code (TAC) Rule 5.203, Geologic Storage and Associated Injection of Anthropogenic Carbon Dioxide, the operator of a geologic storage facility must ensure that all anthropogenic $CO_2$ injection wells are

constructed and completed to prevent the movement of injection $CO_2$ into any areas where it could endanger USDW.

Carbon dioxide can leak along the interfaces between casing and cement sheath, cement sheath and formation, and fractures inside the cement sheath. The leakage can lead to the impacts to USDW or atmosphere. If the surface casing depth is below the USDW, the potential leakage pathways of $CO_2$ are shown in **Figure 19**. Descriptions of the routines are as follows: Routine (a) means that the $CO_2$ escapes to the atmosphere through the annuli between the production casing and formation, and between the production casing and surface casing. This leakage should be due to the de-bonding or poor bonding of the cement sheath as well as cement failure. The $CO_2$ could also flow to the USDW through routine (b) due to the defect of cement sheath set in the annulus between surface casing and formation, and between the production casing and formation. The $CO_2$ could also leak through routine (b) to the surface rather than the USDW due to the cement sheath fail in the casing and formation annulus along the whole wellbore. This pathway is named as routine (c). Most of the newly constructed $CO_2$ injection wells must fulfill the requirement of TAC and EPA. However, some existing wells drilled before 1940 were also converted to the $CO_2$ injection wells for economic purposes in the two fields studied. The surface casing depth of these wells may be above the USDW due to the regulation at that time did not consider USDW or the USDW was not clear when these wells were drilled. These wells should be carefully examined for potentials problems shown in **Figure 20**. If the cement sheath of production casing fails to cover the whole column, $CO_2$ leak through routine (a) and pathway (b) will happen at the same time, which means $CO_2$ could leak to USDW and atmosphere simultaneously. The risk of $CO_2$ leakage is more likely to happen on this sort of wells because only the failure of the

production casing cement sheath will lead to the leakage of $CO_2$. There is no barrier to postpone the $CO_2$ escaping to the surface or USDW. In order to develop a method to identify well leakage potential, surface casing depth should be considered as a key parameter. This is because most of the $CO_2$ injection wells do not have intermediate casing in the studied fields. The base of usable quality water (BQUW) and the cement tops of surface casing and production casing should also be considered. The $CO_2$ injection well could be classified into three groups by two criteria. Criterion one is the relationship between the surface casing depth and the BUQW; and the second criterion is the relation between the cement sheath top of the production casing (CSPC) and the BUQW. **Table 5** presents a summary of the well classification criteria and the Well Schematic Indicator (WSI) assignment. Reliable wells are assigned with WSI = 1 while highly risky wells are assigned with WSI = 0.

#### 2.2.2.2 Well Age Indicator (WAI)

The age of $CO_2$ injection wells should be considered as a factor for well wellbore integrity due to time-dependent corrosion. The age of a well can be classified as the well construction age defined from the year the well was drilled and $CO_2$ exposed age defined from the beginning of $CO_2$ injection. The reference year in this study is set to January 1, 2015.

Since the ages of $CO_2$ injection wells vary widely in the studied field, data normalization was used to standardize the range of data in the domain of [0, 1]. The formula for data scaling is defined as:

$$WAI = \frac{x_{max} - x}{x_{max} - x_{min}} \tag{11}$$

where WAI is well age indicator (normalized well age) and $x$ is the original age of $CO_2$ injection well. For example, the wells in the Hasting West field have ages span between 2.25 years and 79.05 years. To rescale the well age, we first subtract the ages of $CO_2$ injection wells from the maximum age (79.05) and then divide the result by 76.80 (the difference between the maximum and minimum well ages). If the WAI value is closed to 1, the well is a relatively new well. A well with WAI = 0 means the well is the oldest well in the field.

#### 2.2.2.3 Cement Type Indicator (CTI)

Most cements used in the oil industry are Portland cement, burned blends of limestone and clay. The crystals seen in set cement include $C_3S$ - tricalcium silicate, $C_2S$ – dicalcium silicate, $C_4AF$ - tetracalcium aluminoferrite, $C_3A$ - tricalcium aluminate, MgO - periclase or magnesium oxide, and CaO - free lime. American Petroleum Institute (API) classifies the cements into classes of A through I based on the composition and properties of Portland cements. **Table 6** gives the API designated classes for oil well cements. “HTHP” denotes high temperature and high pressure in this table.

Improper cement type can cause cement sheath failure due to high pressure and dynamical temperature change. For example, if the casing of a $CO_2$ injection well with depth larger than 6,000ft is cemented using Class C cement, the cement sheath may not stand with the downhole conditions and thus lose its integrity. The cement sheath with suitable cement class is identified in suitable cement design with Cement Type Indicator (CTI) set to 1. If the cement type is unsuitable for the casing depth, the CTI is set to 0, which means problematic cement design. The CTI for a well with both the surface casing and long string casing (production casing) is assigned to an average value of the two casing sections.

#### 2.2.2.4 Cement Sheath Integrity Indicator (CSII)

Carbon dioxide–exposed wells were classified into three groups based on the stress levels calculated by the analytical model presented in the previous section. The first group contains safe wells in which the bottom hole pressure is in the range between the Maximum Permissible Pressure (MaxPP) and the Minimum Permissible Pressure (MinPP), considering well cement sheath with and without fluid gap. The Cement Sheath Integrity Indicator (CSII) for a safe well is set to 1. The second group contains potentially safe wells in which the bottom hole pressure is either in the range between the MaxPP's without fluid gap and with fluid gap, or in the range between the MinPP's without fluid gap and with fluid gap. The cement sheath integrity indicator of this kind of well is set 0.5. This is because it is difficult to determine whether the well has a fluid gap between the cement sheath and formation. The third group contains potential leakage wells, meaning that the wellbore pressure is lower than the MinPP with fluid gap, or greater than the MaxPP without fluid gap. These sort of wells are in the dangerous range of cement sheath failure whether due to burst for injection wells and collapse for shut-in/plugged-in wells. The cement sheath integrity indicator for this type of wells is assigned to 0.

### 2.2.3 Description of Interface of the Statistical INGA Model

The statistical INGA model was built in MS Excel. The graphical user interface (GUI) of the model is briefly described in this section. The computer program consists of 6 sheets namely User Guide, Basic Data, Mechanical Analysis Data, Frame, Training, and New Well Evaluation. The User Guide (**Figure 2**1) sheet provides basic steps to run the program. The Basic Data sheet (**Figure 2**2) is for the user to input basic well data from well design and

operations. Mechanical Analysis Data sheet (**Figure 23**) is for the user to input well parameter values useful for well integrity analysis. Frame sheet (**Figure 24**) is for the user to specify parameter values for Neural Network and Genetic Algorithm and well failure criteria. Training sheet (**Figure 25**) performs training of the model with the data provided in the Basic Data sheet and Mechanical Analysis Data sheet. New Well Evaluation sheet (**Figure 26**) carries out prediction of the leakage probability of new wells added to the Basic Data sheet.

### 2.2.4 Obtaining Field Data for Model Verification

A test site was selected in the Cranfield Field, Adams County, Mississippi, shown in **Figure 27**. Wells CFU31F2 and CFU31F3 were logged for reservoir characterization, tested for pressure build up, and sampled for cement integrity identification. As shown in **Figure 28**, CFU31F2 and CFU31F3 are monitoring wells constructed in 2009 and P&A'd in 2015. They have very similar constructions with 7-in 26lb N80 casing set to ~10,200ft, 7 5/8-in Bluebox 2500 set from ~10,200 to ~10,700ft, 7-in 26lb N80 casing set to ~10,700ft to TD (~10,790ft). Electrodes and other jewelry were constructed in the wells. The wells were drilled with 12 ¼-inch bit (large cemented annulus). Well CFU31F2 penetrates production reservoir from ~10,435ft to ~10,518ft.

The existing data for wells CFU31F2 and CFU31F3 include 1) Gas ($CO_2$) saturation changes between 2009 and 2015 recorded by a reservoir saturation tool; 2) Casing maps, cement maps, solid, liquid, and gas identification, jewelry locations from an Ultrasonic Imager Tool (**Figure 29**); and well construction records giving joint locations, material changes, electrode locations, and gauge locations.

**Figure 30** presents pressure data recorded in well CFU31F2 CHDT at test depth of 9,535 feet. **Figure 31** shows sidewall coring intervals in well CFU31F2. **Figure 32** illustrates the fiberglass casing set in well CFU31F3. Some core samples taken from the sidewall in the well are presented in **Figure 33** for further analysis to identify wellbore integrity problems. A complete data analysis and well integrity assessment are given by Duguid, et al.[25]

## III. RESULT AND DISCUSSION

Result of the statistical INGA model was tested by test data from three oilfields namely the West Hasting oil field (WH), the Oyster Bayou oil field (OB), and the Cranfield Field. Result and discussion are presented in this section.

### 3.1 Training of the Statistical INGA Model

The statistical INGA model was trained and tested using the assigned LPI values of 22 wells in the West Hasting oil field (WH) and the Oyster Bayou oil field (OB) in the Texas Gulf Coast region. The results are shown in **Table 7**. Ten wells were randomly selected for training the model. **Figure 34** illustrates the performance of training. The average relative error is 0.51%.

### 3.2 Testing of the Statistical INGA Model

The statistical model was thoroughly tested using the remaining data from the WH and OB fields, the data generated by the FEM model, and data from the Cranfield Field.

#### 3.2.1 Testing of the Statistical INGA Model with Data from WH and OB

After training, the statistical INGA model was tested using the assigned LPI values of the remaining 13 wells in the WH and OB fields. **Figure 35** demonstrates a comparison of model-predicted and true values of the LPI's of the 13 wells. The average relative error is only 0.95%, indicating the super accuracy of the statistical model.

#### 3.2.2 Testing of the Statistical INGA Model with Data from FEM Model

Well leak scenarios were created using the FEM well stress model for 3 wells as candidates for $CO_2$ injection in the West Hasting oil field and the Oyster Bayou oil field, Texas, in the Texas Gulf Coast region. Major concerns are from the possible $CO_2$ leak behind casing due to inadequate coverage of cement columns. The following scenarios were considered:

Scenario 1: Using a well with a cement volume of 1,348 sacks for the long casing string in the West Hasting field for $CO_2$ injection.

Scenario 2: Using a well with a cement volume of 300 sacks for the surface casing string in the West Hasting field for $CO_2$ injection.

Scenario 3: Using a well with a cement volume of 300 sacks for the surface casing string in the Oyster Bayou oil field for $CO_2$ injection.

Result of the FEM well stress model indicates that the cement in well Scenario 1 is in safe condition while and cement in well Scenarios 2 and 3 are in failure conditions. Running the statistical INGA model gave the predicted LPI values of 0.919, 0.373, and 0.121, for Scenarios 1, 2, and 3, respectively (**Table 8**). This result implies that it is safe to use the well with a cement volume of 1,348 sacks for the long casing string in the West Hasting. However, it is not safe to use the two wells with cement volume of 300 sacks for the surface casing string in the 2 fields. This result is consistent with that obtained from the FEM stress model.

### 3.2.3 Testing of the Statistical INGA Model with Data from the Cranfield Field

The 2009 image logs in the tested wells in the Cranfield Field show generally high (8 Mrayl) to middle (5 Mrayl) acoustic impedance cements from 2773.7m (9100 ft) to the bottom of the log at 3243.7 m (10642 ft). These values indicate solid cement in the annulus between the casing and formation. Above 2773.7 m (9100 ft) the acoustic impedance is generally lower

indicating debonded solid or liquid behind the casing. The collection of a solid cement core sample at 2407.9 m (7900 ft) does show that competent cement reached well above the sections where the logs show good cement/good bond. Cables or control lines are visible as low acoustic impedance features between the $CO_2$ reservoir at 3181.5 m (10438 ft) and 2444.5 m (8020 ft) where low acoustic impedance values in the log generally transition from being interpreted as debonded solid to fluid. The low acoustic impedance values in the area of the cable and hardware in the well indicate that the cable and hardware is not bonded to the casing and could represent a pathway along the casing. Deterioration of the acoustic impedance and CBL signals in the logs are evident over much of the section that was relogged in 2015. The reason for the deterioration of cement bond and acoustic impedance is not readily apparent. The zone showing little change, between 2813.3 and 2835.8 m (9230 and 9304 ft), probably rules out differences in the tools as the cause. The 2015 ultrasonic image maps also shows the cables and monitoring hardware running between about 2743.2 m (9000 ft) and the bottom of the log. Above 2743.2 m (9000 ft) the overall low acoustic impedance in the Raw Acoustic Impedance track makes identifying the cable impossible. The identification of the monitoring equipment on the outside of the casing is a concern for CCUS monitoring for this and other projects. Control lines and cables for downhole sensors and gauges must run from the surface to the zone being monitored. The low acoustic impedance values that make up these features in the log indicate that there is weak or no cement or cement bond. The combination of low acoustic impedance and the necessity of vertical control lines could allow a direct path for $CO_2$ out of the reservoir if there is monitoring technology located below the reservoir seal.

Each of the cored depths showed large changes in acoustic impedance and CBL amplitude but yielded solid cements. The cores collected at 2407.9 and 2987.0 m (7900 and 9800 ft) have indications that the cement has reacted since placement; exhibited by discolored fronts in the core. Further work is needed to determine the nature of the reaction. The existence of a reaction fronts indicates that isolation at these points in the well was compromised but does not indicate the overall integrity of the well was compromised. The reactions appear to emanate from the interfaces in the well; the casing-cement interface in the case of the 2407.9 m (7900 ft) sample and the formation-cement interface in the case of the 2987.0 m (9800 ft) sample. This is in general agreement with Duguid et al.[26] and Carey et al.[27] who have found that the interfaces in the well are more conductive than the porous network of the cement. Details of data analysis is documented elsewhere by Duguid.[28]

In conclusion, the CFU31F-2 and CFU31F-3 monitoring wells were constructed to test monitoring technologies in and above a commercial $CO_2$-EOR project. Time-lapse comparison of cement bond amplitude data and acoustic impedance maps show a deterioration of signal that implies a deterioration of cement bond or cement along much of the cemented annulus in the long-string section. The existence of a section between 2813.3 and 2835.8 m (9230 and 9304 ft) that showed little change likely rules out difference in tools as the cause of the deterioration. Both the 2009 and 2015 ultrasonic image logs clearly show that there is reduced or no bond under the cables running from the reservoir to the point in the log were they can no longer be identified implying that they may represent a vertical leakage risk. The statistical model predicts that the wells have predicted LPI values of 0.72, indicating a high probability of fluid leakage.

### 3.3 Discussion

The statistical model developed in this project has been tested with limited data. More verification work needs to be done using data from confirmed $CO_2$ leakage incidents. For those who do not have access to the statistical model, the mathematical models used in developing the model can be evaluated and tested. These mathematical models are disseminated in the following technical papers published during this project:

1) Ben Li, Boyun Guo, Hui Li, Yucai Shi. 2015. An Analytical Solution to Simulate the Effect of Cement/Formation Stiffness on Well Integrity Evaluation in Carbon Sequestration Projects, *Journal of Natural Gas Science & Engineering*, 27, 1092-1099.
2) Ben Li, Boyun Guo, Hui Li, Yin Feng and Jim Lee. 2015. Leak Risk Assessment for Plugged Wells in Carbon Sequestration Projects, *Journal of Sustainable Energy Engineering,* Vol. 3, No. 1, 44-65.
3) Ben Li, Boyun Guo, Hui Li, and Yuanlong Zhou. 2015. Well Degradation Assessment and Leakage Risk Prediction in a Carbon Sequestration Project Using Neural Networks, *Journal of Sustainable Energy Engineering*, Vol. 2, No. 4, pp. 331-349(19).
4) Yucai Shi, Ben Li, Boyun Guo, Zhichuan Guan, Hui Li. 2015. An Analytical Solution to Stress State of Casing-Cement Sheath-Formation System with the Consideration of Its Initial loaded State and Wellbore Temperature Variation, *International Journal of Emerging Technology and Advanced Engineering*, Volume 5, Issue 1 (Jan. 2015), pp59-65.

5) Xiaohui Zhang and Boyun Guo. "A Review of $CO_2$ Behavior During Geological Storage and Leakage Assessment," *International Journal of Recent Development in Engineering and Technology* (October, 2014), Vol. 3 (4), 14-23.
6) Boyun Guo, Ben Li, and Na Wei. 2014. The Maximum Permissible Pressure in Well Stimulation Operations, paper 17715 presented at the International Petroleum Technology Conference held in Kuala Lumpur, Malaysia, 10-12 December 2014.
7) Ben Li, Boyun Guo, Hui Li. 2015. Plugged Well Leakage Risk Assessment in a Carbon Sequestration Project, paper 403711 presented at 2015 AIChE Annual Meeting held in Salt Lake November 8-13, 2015.
8) Andrew Duguid, Boyun Guo, and Rona Nygaard, Well integrity assessment of monitoring wells at an active CO2-EOR flood, paper presented at the 13th International Conference on Greenhouse Gas Control Technologies (GHGT-13) held in Lausanne, Switzerland, 14-18 November 2016.

Once fully tested and validated the statistical model can be utilized to create risk maps, workover candidate selection, and design new wells for carbon sequestration. An outline of this work is presented in the following sections.

### 3.3.1 Creating Risk Maps

Risk maps should be created for $CO_2$ injection and observation wells. These maps should be presented in form of Operating Net Pressure (ONP) windows in which the $CO_2$ exposed wells should be operated. The ONP should be chosen between the Maximum Permissible Net Pressure (MaxPNP) and the Minimum Permissible Net Pressure (MinPNP). The MaxPNP is defined as the difference between the maximum permissible wellbore pressure and the

reservoir pore pressure for fluid injection wells. The MinPNP is defined as the difference between the reservoir pore pressure and the minimum permissible wellbore pressure for fluid production and observation wells. Figures 36 through 50 present ONP windows for wells completed with typical casings and cements used in the oil and gas industry.

### 3.3.2 Workover Candidate Selection

$CO_2$ injection wells in carbon sequestration projects are normally wells that were previously used for water and $CO_2$ injection in $CO_2$-EOR projects. Some $CO_2$ profile observation wells are converted from oil production wells. Before these wells are employed for $CO_2$ sequestration, their integrity should be carefully examined. Wells candidates for workover should be selected from those that have never been operated outside the Operating Net Pressure (ONP) windows during their injection or production histories. Other criteria for workover candidate's selection include cemented intervals relative to casing depths, aquifer locations, and the bonding quality of cement sheaths. Wells of over 40 years old should not be selected as workover candidates for $CO_2$ injection or observation wells. Cement bonding quality of the candidate wells should be evaluated using the criteria that are listed in the next section for new well construction.

### 3.3.3 New Well Construction

If new wells are drilled for a $CO_2$ sequestration project, the wells should be constructed in a way to ensure 99% $CO_2$ storage permanence in the injection zone(s) for 1000 years. Recommendations for well construction are outlined as follows. All aquifer zones should be sealed by either a surface casing or an intermediate casing.

1) The cement placement efficiency in the intervals above and below the aquifer zone should be higher than 99% for at least 50 feet. If not, cement squeezing should be carried out to improve sealing quality.

2) If the cement placement efficiency in the interval against the aquifer zone is lower than 90% for over 30 feet, cement squeezing should be performed to enhance sealing of the aquifer zone.

3) Cased-hole well completion method should be used in $CO_2$ sequestration projects with corrosion-resistant casing (steel grade N-80). The production casing should be cemented in the entire interval with cement return to a level of minimum 150 feet above the top of the $CO_2$ storage zone.

4) The cement placement efficiency in the interval above the $CO_2$ storage zone should be higher than 99% for at least 50 feet. If not, cement squeezing should be carried out to improve sealing quality.

5) If the cement placement efficiency in the interval against the aquifer zone is lower than 90% for over 30 feet, cement squeezing should be performed to enhance sealing of the $CO_2$ storage zone.

6) Wellbore pressure in all well stimulation and workover operations should be controlled at a level lower than the formation pressure plus the MaxPNP.

7) Wellbore pressure in all well production and shut-in operations should be controlled at a level higher than the formation pressure minus the MinPNP.

## IV. CONCLUSIONS

The objective of this project is to develop a computerized statistical model with the Integrated Neural-Genetic Algorithm (INGA) for predicting the probability of long-term leak of wells in $CO_2$ sequestration operations. This object has been accomplished by conducting research in data mining of $CO_2$-exposed wells, INGA computer model development, and evaluation of the predictive performance of the computer model with data from field tests. The following technical conclusions are drawn.

1. Field data was gathered from 510 wells in the West Hastings field and the Oyster Bayou field of Texas in this project, allowing for establishment a database for $CO_2$-exposed wells. Unfortunately, no well was reported officially to leak $CO_2$ in the past. An indirect approach has to be taken to assess well integrity conditions.

2. To assess the well integrity in the two fields, an analytical model was developed to predict the Maximum Permissible Pressure (MaxPP) and the Minimum Permissible Pressure (MinPP) for assessment of cement sheaths in CO2 sequestration wells. A numerical stress model with Finite Element method (FEM) was adopted to further evaluate well integrity considering temperature and change in well operating conditions.

3. Application of the analytical and numerical models to the wells in the West Hastings field and the Oyster Bayou field allowed for identification of wells with risk of leakage. In the West Hastings field, 10 wells were identified to be risky due to fluid injection with over-pressure. In addition, 4 wells were found in the condition of under-pressure, which can cause failure of cement sheath. In the Oyster Bayou field,

well pressures are found to be lower than the calculated Minimum Permissible Pressures for most wells. It is thus believed that these wells are subjected to shear failure of cement sheaths and possess high risk of leaking in dynamic injection conditions.

4. In development of a statistical model with Integrated Neural-Genetic Algorithm (INGA), the INGA was tested for accuracy and converging efficiency against data dimension and sample size. It was found that, with today's computing technology, the algorithm is slow and infeasible for processing the data set obtained from the 510 wells in the West Hasting field and the Oyster Bayou field. The controlling factor is the large number of independent variables (67 well design and operating parameters affecting leak probability).
5. A statistical model was developed using the INGA with a data-dimension reduction mechanism. This mechanism makes the well leakage probability as a function of 4 variables that are pre-evaluated using the values of 67 well parameters before data processing.
6. The developed statistical INGA model was trained with the LPI data for the wells in the West Hasting field and the Oyster Bayou field. The model output matched the ample data with a relative error of 0.51%.
7. The trained statistical INGA model was tested with different data from the wells in the West Hasting field and the Oyster Bayou field. The model-predicted LPI-values were found to have an average error of 0.95%.
8. To verify the accuracy of the statistics model, a field test was conducted on wells CFU31F2 and CFU31F3 in the Cranfield Field, Adams County, Mississippi. Both the

2009 and 2015 ultrasonic image logs clearly show that there is reduced or no bond under the cables running from the reservoir to the point in the log were they can no longer be identified implying that they may represent a vertical leakage risk. However, this type of cement deficiency was not observed in the wellbore section against the cap rock. The statistics model predicts a Leakage-safe Probability Index (LPI) of 0.72, which is consistent with the test result.

**9.** Risk maps should be constructed using the statistical model developed in this project for evaluating well operating conditions, selecting workover candidate wells for $CO_2$ injection, and designing new wells for $CO_2$ injection. These maps should be presented in form of Operating Net Pressure (ONP) windows in which the $CO_2$ exposed wells should be operated. The ONP should be chosen between the Maximum Permissible Net Pressure (MaxPNP) and the Minimum Permissible Net Pressure (MinPNP). Before any wells are employed for $CO_2$ sequestration, their integrity should be carefully examined. Wells candidates for workover should be selected from those that have never been operated outside the Operating Net Pressure (ONP) windows during their injection or production histories. Other criteria for workover candidate's selection include cemented intervals relative to casing depths, aquifer locations, and the bonding quality of cement sheaths. Wells of over 40 years old should not be selected as workover candidates for $CO_2$ injection or observation wells.

**References**


1. Hossain, M.M. and Amro, M.M. "Drilling and completion challenges and remedies of $CO_2$ injected wells with emphasis to mitigate well integrity issues", paper SPE 133830 presented at the SPE Asia Pacific Oil &Gas Conference and Exhibition held in Brisbane, Queensland, Australia, October 18-20, 2010.
2. Barlet-Gouedard,V., Rimmele, G. Goffe, B., and Porcherie, O. "Well technologies for $CO_2$ geological storage: $CO_2$-resistant cement", Oil & Gas and Technology –Rev. IFP 62 (2007) 325-334.
3. Viswanathan, H. S., Pawar, R. J. , Stauffer, P. H., Kaszuba, J. P., Carey, J. W., Olsen, S. C., Keating, G. N., Kavetski, D., and Guthrie, G. D. " Development of a hybrid process and system model for the assessment of wellbore leakage at a geologic $CO_2$ sequestration site", Environmental Science & Technology 42 (2008) 7280-7286.
4. Benge, G. "Improving wellbore seal integrity in $CO_2$ injection wells", paper SPE 119267 presented at the SPE/IADC Drilling Conference and Exhibition held in Amsterdam, The Netherlands, March 17-19, 2009.
5. Duguid, A. "The effect of carbonic acid on well cements as identified through lab and field studies", paper SPE 119504 presented at the SPE Eastern Regional/AAPG Eastern Section Joint Meeting held in Pittsburgh, Pennsylvania, October 11-15, 2008.
6. Carey, J. W. Svec, R. Grigg, R., Zhang, J. and Crow, W. "Experimental investigation of wellbore integrity and $CO_2$-brine flow along the casing-cement microannulus", International Journal of Greenhouse Gas Control 4 (2010) 272-282.
7. Um, W., Jung, H.B., Kabilan, S., Suh, D.M. and Fernandez, C.A. "Geochemical and geomechanical effects on wellbore cement fractures: Data information for wellbore

reduced order model", prepared for the U.S. Department of Energy under Contract DE-AC05-76RL01830, Pacific Northwest National Laboratory, January 2014.

8. Guo, B. "Statistical Analysis of $CO_2$ Exposed Wells to Predict Long Term Leakage through the Development of an Integrated Neural-Genetic Algorithm." Year-1 Report summited to U.S. DOE for Project DE FE0009284, 2014.

9. Guo, B. "Statistical Analysis of $CO_2$ Exposed Wells to Predict Long Term Leakage through the Development of an Integrated Neural-Genetic Algorithm." Year-2 Report summited to U.S. DOE for Project DE FE0009284, 2015.

10. Guo, B. "Statistical Analysis of $CO_2$ Exposed Wells to Predict Long Term Leakage through the Development of an Integrated Neural-Genetic Algorithm." Year-3 Report summited to U.S. DOE for Project DE FE0009284, 2016.

11. Goodwin, K.J., and Cook, R.J. 1992. Cement Sheath Stress Failure, SPE Drill Eng. 7 (4): 291-296.

12. Jackson, P.B. and Murphey, C.E. 1993. Effect of Casing Pressure on Gas Flow through a Sheath of Set Cement, paper SPE 25698 presented at the SPE Drilling Conference held February 23-25, 1993 in Amsterdam.

13. Thiercelin, M.J., Dargaud, B., Baret, J.F., and Rodriquez, W.J. 1998. Cement Design Based on Cement Mechanical Response, SPE Drilling & Completion, 13 (4). 266-273.

14. Bosma, M., Ravi, K., van Driel, W., and Schreppers, G.J. 1999. Design Approach to Sealant Selection for the Life of the Well. Paper SPE 56536 presented at the SPE Annual Technical Conference and Exhibition held October 3-6, 1999 in Houston, Texas.

15. Bois, A.-P., Garnier A., Rodot, F., Saint-Marc, J., and Aimaid, N. 2011. How To Prevent Loss of Zonal Isolation Through a Comprehensive Analysis of Microannulus Formation, SPE Drilling & Completion (March 2011), 13-31.

16. Nygaard, R., Salehi, S., and Lavoie, R. 2011. Effect of Dynamic Loading on Wellbore Leakage for the Wabamun Area $CO_2$ Sequestration Project, paper CSUG/SPE 146640 presented at the SPE Canadian Unconventional Resources Conference held November 15-17, 2011 in Calgary, Canada.

17. Timoshenko, S.P. and Goodier, J.N. 1961. Theory of Elasticity, 3rd edition, McGraw-Hill Book Co., New York City. 121-125.

18. Bade, J.F. 1963. Cement Bond Logging Techniques – How They Compare and Some Variables Affecting Interpretation, *J. Pet. Tech.* (January 1963), 17-22.

19. Pardue, G.H., Morris, R.L., Gollwitzer, L.H., and Moran, J.H. 1963. Cement Bond Log – A Study of Cement and Casing Variables, *J. Pet. Tech.* (May 1963), 545-555.

20. Sheives, T.C., Tello, L.N., Maki Jr., V.E., Standley, T.E., and Blankinship, T.J. 1986. A Comparison of New Ultrasonic Cement and Casing Evaluation Logs With Standard Cement Bond Logs, paper SPE 15436 presented at the SPE Annual Technical Conference and Exhibition held in New Orleans, LA October 5-8, 1986.

21. Altair (2010), *Altair Hypermesh User's Guide*, http://www.altairhyperworks.com.

22. SIMULIA (2011), *Abaqus/CAE User's Manual*, http://www.simulia.com/support/documentation.html.

23. Gray, K. E., Podnos, E., & Becker, E. (2009, March 1). *Finite-Element Studies of Near-Wellbore Region During Cementing Operations: Part I. Society of Petroleum Engineers*. doi:10.2118/106998-PA

24. Weideman, B. and Nygaard, R. 2014. How Cement Operations affect your Cement Sheath Short and Long Term Integrity, 2014 AADE Fluids Technical Conference and Exhibition, April 15-16, 2014, Houston, Texas. AADE-14-FTCE-20.

25. Duguid, A., Guo, B., and Nygaard, R. Well integrity assessment of monitoring wells at an active CO2-EOR flood, paper presented at the 13th International Conference on Greenhouse Gas Control Technologies (GHGT-13) held in Lausanne, Switzerland, 14-18 November 2016.

26. Duguid, A., Butsch, R., Carey, J.W., Celia, M., Chugunov, N., Gasda, S., Ramakrishnan, T.S., Stamp, V., and Wang, J., Pre-injection Baseline Data Collection to Establish Existing Wellbore Leakage Properties, 11th International Conference on Greenhouse Gas Technologies, Kyoto,Japan, September 2012, Energy Procedia, 2013:37:5661 – 5672.

27. Carey, J.W., Wigand, M., Chipera, S.J., WoldeGabriel, G., Pawar, R., Lichtner, P.C., Wehner, S.C., Raines, M.A., Guthrie, G.D.: Analysis and performance of oil well cement with 30 years Of CO2 exposure from the SACROC Unit, West Texas, USA. International J of Greenhouse Gas Control 2007:1:75–85.

28. Duguid, A., Well Integrity Assessment of CFU31-F2 and CFU-31F3 for Statistical Analysis of $CO_2$ Exposed Wells to Predict Long Term Leakage through the Development of an Integrated Neural-Genetic Algorithm. Final report submitted to University of Louisiana at Lafayette for DOE Project DE FE0009284, May 23, 2017.

Table 1: $CO_2$ Injection Well Structure and Operation Data from the West Hastings Oil Field

| Well No. | Lease No. | Hole Size (in) | Casing Size (in) | Well Depth (ft) | Casing Weight (lb/ft) | Casing ID (in) | Max. Injection Pressure Water (psig) | Max. Injection Pressure $CO_2$ psig) | Tubing Size (in) | Current BHP (psig) |
|---|---|---|---|---|---|---|---|---|---|---|
| 1708 | 19054 | 7.875 | 5.5 | 6050 | 11 | 5.012 | 2900 | 4350 | 2.875 | 1800 |
| 1194 | 19054 | 9.875 | 7 | 6661 | 26 | 6.276 | 3080 | 4620 | 3.5 | 1800 |
| 1190 | 19054 | 9.875 | 7 | 6445 | 26 | 6.276 | 2985 | 4478 | 3.5 | 1800 |
| 1191 | 19054 | 8.625 | 5.5 | 6550 | 9.2 | 2.94 | 3000 | 4500 | 2.875 | 1800 |
| 1192 | 19054 | 8.625 | 5.5 | 6255 | 9.2 | 2.94 | 2975 | 4462 | 2.875 | 1800 |
| 1308 | 19054 | 9.875 | 7 | 6314 | 26 | 6.276 | 2920 | 4380 | 3.5 | 1800 |
| 1310 | 19054 | 9.875 | 7 | 6622 | 26 | 6.276 | 3050 | 4575 | 3.5 | 1800 |
| 1608 | 19054 | 8.625 | 5.5 | 6525 | 9.5 | 2.94 | 3000 | 4500 | 2.875 | 1800 |
| 1616 | 19054 | 9.875 | 7 | 7017 | 26 | 6.276 | 3225 | 4838 | 3.5 | 1800 |
| 1710 | 19054 | 9.875 | 7 | 6594 | 26 | 6.276 | 3053 | 4579 | 3.5 | 1800 |
| 1818 | 19054 | 9.875 | 7 | 6150 | 26 | 6.276 | 2870 | 4305 | 3.5 | 1800 |
| 2402w | 19054 | 9.875 | 7 | 6217 | 23 | 6.366 | 2915 | 4373 | 3.5 | 1800 |
| 2702 | 19054 | 9.875 | 7 | 5825 | 18 | 6.538 | 2775 | 4162 | 3.5 | 1800 |
| 3106 | 19054 | 9.875 | 7 | 6000 | 26 | 6.276 | 2785 | 4170 | 3.5 | 1800 |
| 3401 | 19054 | 9.875 | 7 | 6114 | 24 | 6.366 | 2862 | 4293 | 3.5 | 1800 |
| 4304 | 19054 | 9.875 | 7 | 6618 | 26 | 6.276 | 2705 | 4057 | 3.5 | 1800 |
| 4701 | 19054 | 6.125 | 5 | 5961 | 18 | 4.276 | 2850 | 4275 | 3.5 | 1800 |
| 4702 | 19054 | 6.125 | 5 | 7000 | 15 | 4.408 | 2870 | 4305 | 2.875 | 1800 |
| 4805w | 19054 | 7.875 | 5 | 6074 | 15 | 4.408 | 2907 | 4361 | 2.875 | 1800 |
| 4820w | 19054 | 6.125 | 5 | 6525 | 18 | 4.276 | 2988 | 4481 | 2.875 | 1800 |
| 4845 | 19054 | 9.875 | 7 | 6800 | 26 | 6.276 | 3100 | 4650 | 3.5 | 1800 |
| 4847 | 19054 | 9.875 | 7 | 6550 | 26 | 6.276 | 3050 | 4575 | 3.5 | 1800 |
| 6011 | 19054 | 9.875 | 7 | 6000 | 26 | 6.276 | 2785 | 4177 | 3.5 | 1800 |
| 6116 | 19054 | 9.875 | 7 | 6265 | 26 | 6.276 | 2910 | 4365 | 3.5 | 1800 |
| 6117 | 19054 | 9.875 | 7 | 6185 | 26 | 6.276 | 2880 | 4320 | 3.5 | 1800 |
| 6120 | 19054 | 9.875 | 7 | 6500 | 26 | 6.276 | 3000 | 4500 | 3.5 | 1800 |
| 7605 | 19054 | 6.125 | 5 | 5015 | 15 | 4.408 | 2175 | 3262 | 2.875 | 1800 |
| 7803 | 19054 | 6.125 | 5 | 5764 | 15 | 4.408 | 2150 | 3225 | 2.875 | 1800 |
| 7328 | 19054 | 6.125 | 7 | 6350 | 26 | 4 | 2987 | 4481 | 2.875 | 1800 |
| 7343 | 19054 | 9.875 | 7 | 6800 | 26 | 6.276 | 3100 | 4650 | 3.5 | 1800 |
| 8409 | 19054 | 9.875 | 7 | 5884 | 24 | 6.366 | 2925 | 4388 | 3.5 | 1800 |
| 7345 | 19054 | 9.875 | 7 | 6868 | 26 | 6.276 | 3200 | 4800 | 3.5 | 1800 |
| 7342 | 19054 | 9.875 | 7 | 6582 | 26 | 6.276 | 3108 | 4662 | 3.5 | 1800 |
| 3706 | 19054 | 8.75 | 5.5 | 6093 | 17 | 4.892 | 2800 | 4200 | 2.875 | 1800 |
| 2401w | 19054 | 9.875 | 7 | 6079 | 24 | 6.366 | 2900 | 4350 | 3.5 | 1800 |
| 5204 | 19054 | 9.625 | 7 | 5468 | 24 | 6.366 | 2905 | 4357 | 3.5 | 1800 |
| 5101 | 19054 | 6.125 | 5 | 6078 | 15 | 4.408 | 2907 | 4361 | 2.875 | 1800 |

| | | | | | | | | | | |
|---|---|---|---|---|---|---|---|---|---|---|
| 3802 | 19054 | 7 | 5 | 5695 | 18 | 4.276 | 2679 | 4018 | 2.875 | 1800 |
| 7611 | 19054 | 7 | 5 | 5904 | 18 | 4.276 | 2675 | 4237 | 2.875 | 1800 |
| 2101 | 19054 | 7 | 5 | 5951 | 18 | 4.276 | 2812 | 4218 | 2.875 | 1800 |

Table 2: $CO_2$ Injection Well Structure and Operation Data from the Oyster Bayou Oil Field

| Well | Lease | Hole | Casing | Well | Casing | Casing ID | Maximum Injection Pressure | | Tubing | Current |
|---|---|---|---|---|---|---|---|---|---|---|
| Name | No. | Size | Size | Depth | Weight | | Water | $CO_2$ | Size | BHP |
| | | (in) | (in) | (ft) | (lb/ft) | (in) | (psig) | (psig) | (in) | (psig) |
| 102 | 25515 | 9.88 | 7 | 8800 | 26 | 6.276 | 4150 | 6225 | 3.5 | 1900 |
| 108 | 25515 | 9.88 | 7 | 8550 | 26 | 6.276 | 4149 | 6224 | 3.5 | 1900 |
| 203 | 25515 | 9.88 | 7 | 8525 | 26 | 6.276 | 4100 | 6150 | 3.5 | 1900 |
| 402 | 25515 | 9.88 | 7 | 8560 | 26 | 6.276 | 4166 | 6249 | 3.5 | 1900 |
| 504 | 25515 | 9.88 | 7 | 8540 | 26 | 6.276 | 4140 | 6209 | 3.5 | 1900 |
| 1033 | 25515 | 8.75 | 5.5 | 8481 | 15 | 4.95 | 4082 | 6123 | 2.875 | 1900 |
| 1043 | 25515 | 8.75 | 5.5 | 8500 | 15 | 4.95 | 4073 | 6109 | 2.875 | 1900 |
| 105 | 25515 | 9.75 | 7 | 8800 | 26 | 6.276 | 4150 | 6225 | 3.5 | 1900 |
| 103 | 25515 | 9.88 | 7 | 8800 | 26 | 6.276 | 4150 | 6225 | 3.5 | 1900 |
| 47 | 3312 | 8.75 | 5.5 | 8450 | 17 | 4.892 | 4100 | 6155 | 2.875 | 1900 |
| 67 | 3312 | 8.63 | 5.5 | 8170 | 15.5& 17 | 4.921 | 4070 | 6105 | 2.875 | 1900 |
| 14 | 3312 | 8.63 | 5.5 | 8375 | 15.5& 17.2 | 4.921 | 4090 | 6140 | 2.875 | 1900 |
| 4 | 3312 | 9.88 | 7 | 8291 | 24 | 6.366 | 4060 | 6095 | 3.5 | 1900 |
| 1 | 3313 | 8.63 | 5.5 | 8379 | 17 | 4.892 | 4095 | 6145 | 2.875 | 1900 |
| 24 | 3312 | 8.63 | 5.5 | 8376 | 17 | 4.892 | 4095 | 6142 | 2.875 | 1900 |
| 47 | 3312 | 8.75 | 5.5 | 8450 | 17 | 4.892 | 4100 | 6155 | 2.875 | 1900 |
| 1056 | 25515 | 8.75 | 7 | 8603 | 23 | 6.366 | 4063 | 6094 | 3.5 | 1900 |
| 1044 | 25515 | 8.75 | 7 | 8600 | 23 | 6.366 | 4065 | 6097 | 3.5 | 1900 |
| 104 | 25515 | 9.88 | 7 | 8675 | 26 | 6.276 | 4150 | 6225 | 3.5 | 1900 |
| 106 | 25515 | 9.88 | 7 | 8850 | 26 | 6.276 | 4150 | 6225 | 3.5 | 1900 |

Table 3: Data Set to Train and Test the INGA

| No. | $x_1$ | $x_2$ | $y=x_1^2+x_2^2$ | True $y_{normalized}$ | Predicted $y_{normalized}$ |
|---|---|---|---|---|---|
| 1 | 9.61 | 8.73 | 168.565 | 0.991553 | 0.976585 |
| 2 | 7.49 | 1.9 | 59.7101 | 0.354095 | 0.361341 |
| 3 | 1.2 | 3.4 | 13 | 0.080559 | 0.076307 |
| 4 | 1.75 | 7.51 | 59.4626 | 0.352646 | 0.354708 |
| 5 | 2.46 | 7.11 | 56.6037 | 0.335904 | 0.338334 |
| 6 | 1.45 | 3.33 | 13.1914 | 0.08168 | 0.077509 |
| 7 | 6.63 | 1.4 | 45.9169 | 0.273322 | 0.27825 |
| 8 | 6.32 | 0.75 | 40.5049 | 0.241629 | 0.245471 |
| 9 | 2.4 | 2.22 | 10.6884 | 0.067022 | 0.06412 |
| 10 | 4.32 | 7.13 | 69.4993 | 0.411421 | 0.417668 |
| 11 | 3.21 | 8.87 | 88.981 | 0.525507 | 0.524973 |
| 12 | 5.48 | 2.17 | 34.7393 | 0.207865 | 0.208081 |
| 13 | 8.32 | 7.23 | 121.4953 | 0.715911 | 0.727853 |
| 14 | 8.88 | 0.3 | 78.9444 | 0.466732 | 0.473013 |
| 15 | 3.18 | 4.28 | 28.4308 | 0.170922 | 0.166695 |
| 16 | 3.56 | 5.74 | 45.6212 | 0.27159 | 0.272273 |
| 17 | 4.22 | 6.96 | 66.25 | 0.392393 | 0.398136 |
| 18 | 3.96 | 1.14 | 16.9812 | 0.103873 | 0.101878 |
| 19 | 1.87 | 8.64 | 78.1465 | 0.462059 | 0.462051 |
| 20 | 7.42 | 6.59 | 98.4845 | 0.581159 | 0.596187 |
| 21 | 8.57 | 3.78 | 87.7333 | 0.5182 | 0.526511 |
| 22 | 4.35 | 7.19 | 70.6186 | 0.417976 | 0.424361 |
| 23 | 0.87 | 1.93 | 4.4818 | 0.030676 | 0.031275 |
| 24 | 8.74 | 5.48 | 106.418 | 0.627618 | 0.638334 |
| 25 | 6.91 | 9.16 | 131.6537 | 0.775399 | 0.776708 |
| 26 | 5.54 | 1.8 | 33.9316 | 0.203135 | 0.203792 |
| 27 | 1.58 | 5.08 | 28.3028 | 0.170173 | 0.166871 |
| 28 | 8.14 | 8.18 | 133.172 | 0.784291 | 0.791806 |
| 29 | 8.42 | 2.18 | 75.6488 | 0.447433 | 0.454907 |
| 30 | 7.1 | 7 | 99.41 | 0.586579 | 0.60135 |
| 31 | 1.05 | 1.36 | 2.9521 | 0.021718 | 0.024756 |
| 32 | 7.07 | 1.14 | 51.2845 | 0.304755 | 0.311149 |
| 33 | 8.88 | 4.62 | 100.1988 | 0.591198 | 0.599704 |
| 34 | 2.43 | 9.66 | 99.2205 | 0.585469 | 0.57766 |
| 35 | 7.4 | 4.89 | 78.6721 | 0.465137 | 0.476771 |

| | | | | | |
|---|---|---|---|---|---|
| 36 | 0.78 | 0.44 | 0.802 | 0.009127 | 0.015595 |
| 37 | 4.67 | 4.47 | 41.7898 | 0.249153 | 0.249069 |
| 38 | 8.71 | 3.96 | 91.5457 | 0.540526 | 0.548642 |
| 39 | 6.15 | 9.34 | 125.0581 | 0.736775 | 0.736084 |
| 40 | 2.15 | 2.45 | 10.625 | 0.066651 | 0.063568 |
| 41 | 1.42 | 8.21 | 69.4205 | 0.41096 | 0.41196 |
| 42 | 3.19 | 3.4 | 21.7361 | 0.131718 | 0.126547 |
| 43 | 1.33 | 7.63 | 59.9858 | 0.35571 | 0.357202 |
| 44 | 6.61 | 1.65 | 46.4146 | 0.276236 | 0.281004 |
| 45 | 2.95 | 7.19 | 60.3986 | 0.358127 | 0.36124 |
| 46 | 5.78 | 3.62 | 46.5128 | 0.276811 | 0.27929 |
| 47 | 3.76 | 7.91 | 76.7057 | 0.453622 | 0.45797 |
| 48 | 5.53 | 3.22 | 40.9493 | 0.244231 | 0.244982 |
| 49 | 7.35 | 8.61 | 128.1546 | 0.754909 | 0.761633 |
| 50 | 4.17 | 6.27 | 56.7018 | 0.336478 | 0.34055 |
| 51 | 5.63 | 2.15 | 36.3194 | 0.217118 | 0.217915 |
| 52 | 8.38 | 2.75 | 77.7869 | 0.459954 | 0.46758 |
| 53 | 7.01 | 5.42 | 78.5165 | 0.464226 | 0.476619 |
| 54 | 3.81 | 5.39 | 43.5682 | 0.259568 | 0.259686 |
| 55 | 6.07 | 0.09 | 36.853 | 0.220243 | 0.222217 |
| 56 | 6.71 | 3.09 | 54.5722 | 0.324007 | 0.329506 |
| 57 | 1.23 | 8.51 | 73.933 | 0.437385 | 0.437218 |
| 58 | 4.17 | 3.92 | 32.7553 | 0.196247 | 0.193166 |
| 59 | 8.39 | 1.38 | 72.2965 | 0.427802 | 0.435593 |
| 60 | 4.25 | 1.38 | 19.9669 | 0.121358 | 0.119201 |
| 61 | 9.75 | 2.26 | 100.1701 | 0.59103 | 0.591267 |
| 62 | 8.27 | 4.29 | 86.797 | 0.512717 | 0.522758 |
| 63 | 8.44 | 8.41 | 141.9617 | 0.835763 | 0.83914 |
| 64 | 2.77 | 4.69 | 29.669 | 0.178173 | 0.174497 |
| 65 | 3.4 | 5.64 | 43.3696 | 0.258405 | 0.25841 |
| 66 | 3.99 | 3.85 | 30.7426 | 0.18446 | 0.1808 |
| 67 | 7.53 | 1.78 | 59.8693 | 0.355027 | 0.362376 |
| 68 | 3.44 | 2.07 | 16.1185 | 0.098821 | 0.095071 |
| 69 | 1.1 | 1.99 | 5.1701 | 0.034707 | 0.034937 |
| 70 | 2.45 | 0.37 | 6.1394 | 0.040383 | 0.042009 |
| 71 | 9.68 | 1.32 | 95.4448 | 0.563359 | 0.565071 |
| 72 | 9.94 | 1.42 | 100.82 | 0.594836 | 0.59395 |
| 73 | 5.53 | 1.33 | 32.3498 | 0.193872 | 0.194835 |

| | | | | | |
|---|---|---|---|---|---|
| 74 | 3.5 | 7.13 | 63.0869 | 0.37387 | 0.377898 |
| 75 | 6.43 | 1.15 | 42.6674 | 0.254292 | 0.258574 |
| 76 | 9.46 | 1.04 | 90.5732 | 0.534831 | 0.538459 |
| 77 | 6.67 | 1.15 | 45.8114 | 0.272704 | 0.277829 |
| 78 | 9.15 | 4.23 | 101.6154 | 0.599494 | 0.605654 |
| 79 | 6.04 | 5.66 | 68.5172 | 0.40567 | 0.415465 |
| 80 | 2.32 | 3.88 | 20.4368 | 0.124109 | 0.119164 |
| 81 | 7.02 | 6.91 | 97.0285 | 0.572633 | 0.587382 |
| 82 | 4.85 | 6.31 | 63.3386 | 0.375344 | 0.382022 |
| 83 | 4.85 | 8.1 | 89.1325 | 0.526394 | 0.533124 |
| 84 | 1.86 | 0.25 | 3.5221 | 0.025056 | 0.028889 |
| 85 | 4.07 | 1.7 | 19.4549 | 0.118359 | 0.115507 |
| 86 | 0.94 | 3.46 | 12.8552 | 0.079711 | 0.075192 |
| 87 | 9.13 | 6.14 | 121.0565 | 0.713342 | 0.721592 |
| 88 | 2.08 | 7.01 | 53.4665 | 0.317532 | 0.319453 |
| 89 | 2.81 | 5.47 | 37.817 | 0.225888 | 0.224442 |
| 90 | 0.47 | 0.15 | 0.2434 | 0.005856 | 0.012745 |
| 91 | 9.93 | 8.45 | 170.0074 | 1 | 0.983164 |
| 92 | 1.04 | 9.92 | 99.488 | 0.587036 | 0.576023 |
| 93 | 3.14 | 5.14 | 36.2792 | 0.216883 | 0.214825 |
| 94 | 4.16 | 0.4 | 17.4656 | 0.10671 | 0.105191 |
| 95 | 9.92 | 3.11 | 108.0785 | 0.637342 | 0.635471 |
| 96 | 8.1 | 8.62 | 139.9144 | 0.823774 | 0.827279 |
| 97 | 5.17 | 0.41 | 26.897 | 0.16194 | 0.161848 |
| 98 | 1.63 | 4.69 | 24.653 | 0.1488 | 0.14478 |
| 99 | 4.8 | 3.75 | 37.1025 | 0.221704 | 0.220341 |
| 100 | 2.29 | 8.65 | 80.0666 | 0.473304 | 0.473458 |

Table 4: The Effect of Number of Data Samples on the CPU Time and Accuracy of INGA

| No. of Data Samples | CPU Time (min.) | Accuracy (%) | Error (%) |
|---|---|---|---|
| 10 | 0.07 | 17.25 | 82.75 |
| 20 | 0.13 | 90.27 | 9.73 |
| 30 | 0.16 | 93.38 | 6.62 |
| 40 | 0.20 | 94.37 | 5.63 |
| 50 | 0.25 | 96.16 | 3.84 |
| 60 | 0.28 | 95.05 | 4.95 |
| 70 | 0.33 | 95.31 | 4.69 |
| 80 | 0.37 | 94.85 | 5.15 |
| 90 | 0.41 | 92.30 | 7.70 |
| 100 | 0.46 | 94.98 | 5.02 |
| 200 | 0.88 | 96.44 | 3.56 |
| 300 | 1.30 | 96.87 | 3.13 |
| 400 | 1.71 | 99.04 | 0.96 |
| 500 | 2.12 | 97.27 | 2.73 |
| 600 | 2.55 | 97.58 | 2.42 |
| 700 | 2.94 | 98.52 | 1.48 |
| 800 | 3.51 | 98.98 | 1.02 |
| 900 | 3.83 | 98.00 | 2.00 |
| 1000 | 4.24 | 98.71 | 1.29 |
| 1500 | 7.52 | 99.06 | 0.94 |
| 2000 | 8.32 | 97.73 | 2.27 |
| 2500 | 10.26 | 98.97 | 1.03 |
| 3000 | 12.37 | 98.87 | 1.13 |
| 3500 | 14.96 | 98.43 | 1.57 |
| 4000 | 16.42 | 99.11 | 0.89 |

Table 5: Assignment of Well Schematic Indicator (WSI)

| Groups | Criteria 1 | Criteria 2 | WSI |
|---|---|---|---|
| 1 | SCD < BUQW | CSPC > BUQW | 0 |
| 2 | SCD < BUQW | CSPC < BUQW | 0.5 |
| 3 | SCD > BUQW | CSPC < BUQW | 1 |

Table 6: API Cement Classes

| API Class | Compounds, % | | | | Usable Depth | Feature |
|---|---|---|---|---|---|---|
| | $C_3S$ | $C_2S$ | $C_3A$ | $C_4AF$ | feet | |
| A | 53 | 24 | 8+ | 8 | 0-6,000 | |
| B | 47 | 32 | 5- | 12 | 0-6,000 | Sulfate Resistance |
| C | 58 | 16 | 8 | 8 | 0-6,000 | High Early Strength |
| D | | | | | 6,000-10,000 | HTHP Resistance |
| E | | | | | 10,000-14,000 | HTHP Resistance |
| F | | | | | 10,000-16,000 | Extremely HTHP Resistance |
| G | 50 | 30 | 5 | 12 | 0-8,000 | |
| H | 20 | 30 | 5 | 12 | 0-8,000 | |
| I | | | | | 12,000-16,000 | Extremely HTHP Resistance |

Table 7: The LPI's of 22 Wells in the WH and OB Fields

| Well Name | Well Series No. | LPI |
|---|---|---|
| WH-1 | 1 | 0.95 |
| WH-2 | 2 | 0.95 |
| WH-3 | 3 | 0.95 |
| WH-4 | 4 | 0.95 |
| WH-5 | 6 | 0 |
| WH-7 | 7 | 0.95 |
| WH-8 | 8 | 0 |
| WH-9 | 9 | 0.95 |
| WH-11 | 11 | 0.95 |
| WH-12 | 12 | 0.95 |
| WH-13 | 13 | 0.95 |
| WH-15 | 15 | 0.95 |
| WH-16 | 16 | 0.95 |
| OB-1 | 17 | 0 |
| OB-6 | 22 | 0.95 |
| OB-7 | 23 | 0.95 |
| OB-9 | 25 | 0.95 |
| OB-10 | 26 | 0 |
| OB-11 | 27 | 0 |
| OB-12 | 28 | 0 |
| OB-14 | 30 | 0.95 |
| OB-15 | 31 | 0 |

Table 8: Result of Scenario Analysis with the Statistical INGA Model

| **Scenario** | Predicted LPI |
|---|---|
| 1. Using a well with a cement volume of 1,348 sacks for the long casing string in the West Hasting field for $CO_2$ injection. | 0.919 |
| 2. Using a well with a cement volume of 300 sacks for the surface casing string in the West Hasting field for $CO_2$ injection. | 0.373 |
| 3. Using a well with a cement volume of 300 sacks for the surface casing string in the Oyster Bayou oil field for $CO_2$ injection. | 0.121 |

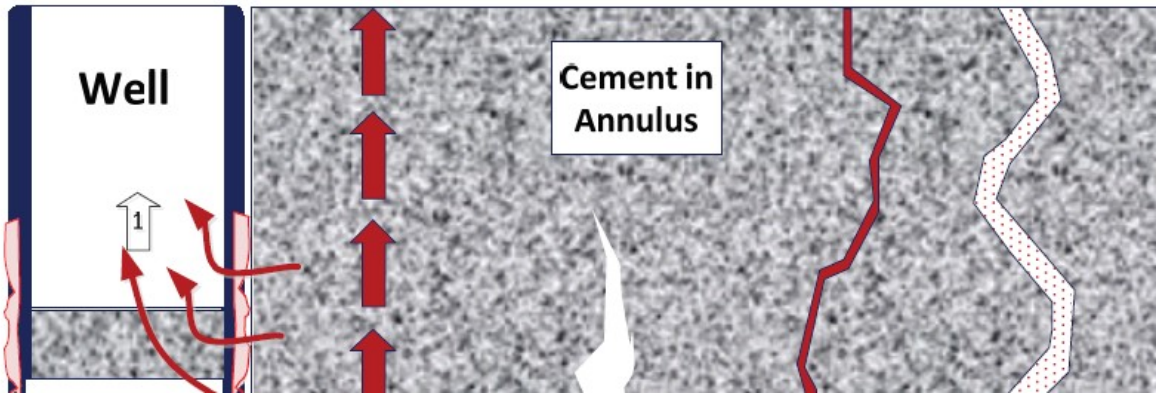


Figure 1: Schematic of potential pathways for $CO_2$ leakage around the wellbore.

(1) leaking through casing due to corrosion or erosion, (2) casing-cement interface, (3) cement matrix, (4) bulk dissolution induced pathway, (5) induced fracture, (6) cement defect/mud channel and (7) cement-cap rock interface.[3]


Figure 2: The West Hastings and Oyster Bayou oil fields, Texas.

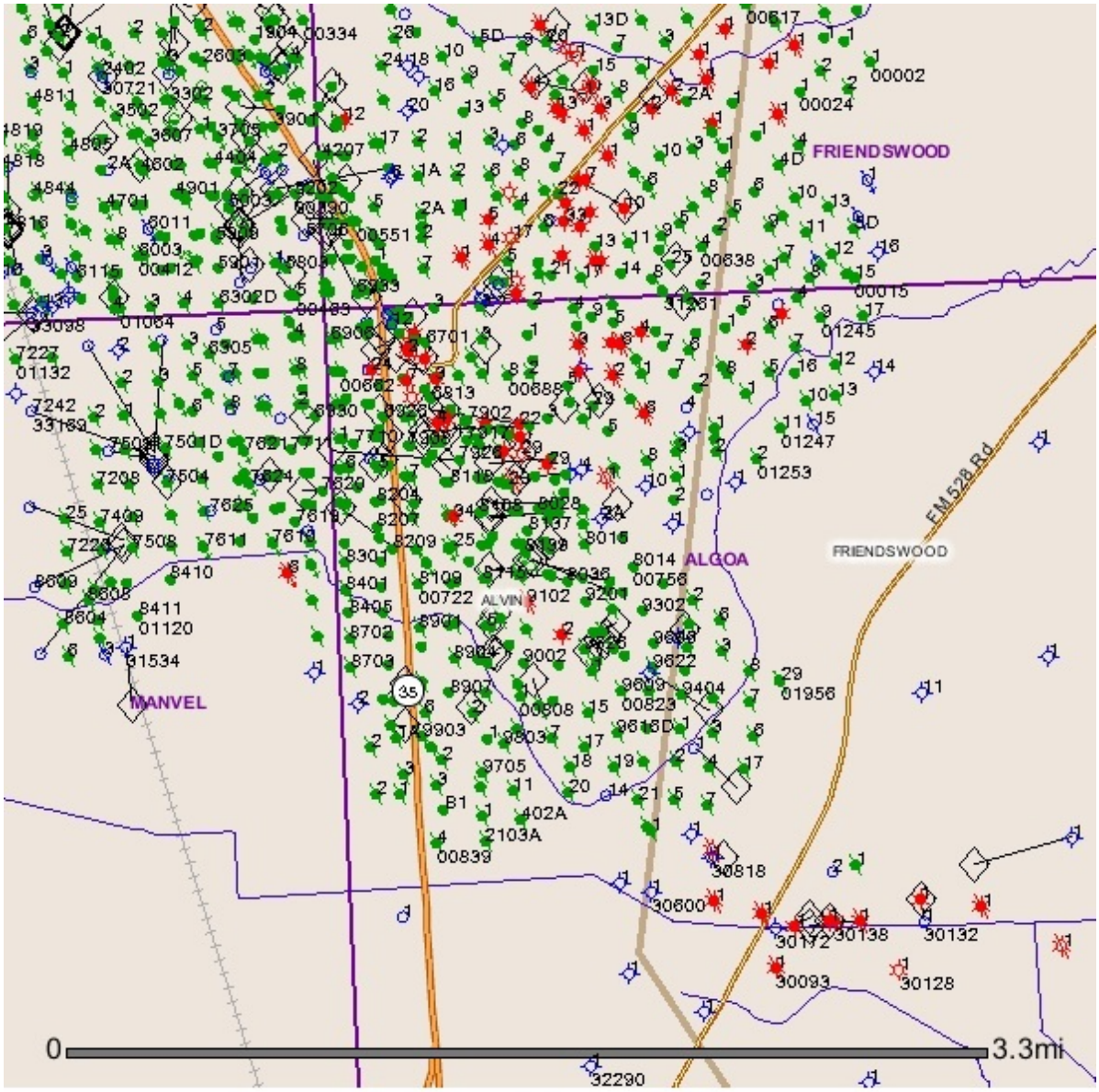


**West Hastings Oil Field**

Figure 3: Well locations in the West Hastings oil field.

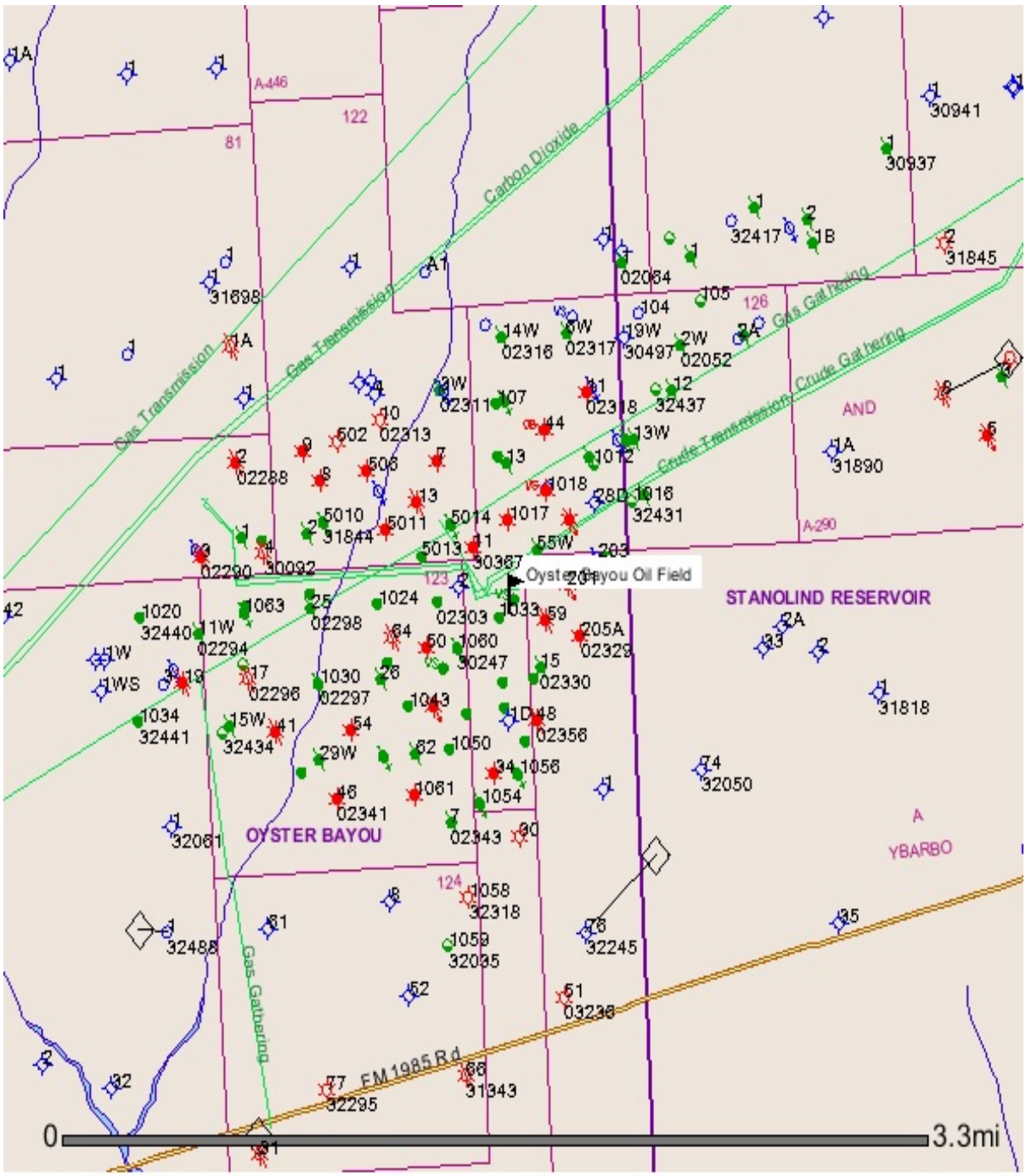


Figure 4: Well locations in the Oyster Bayou oil field.

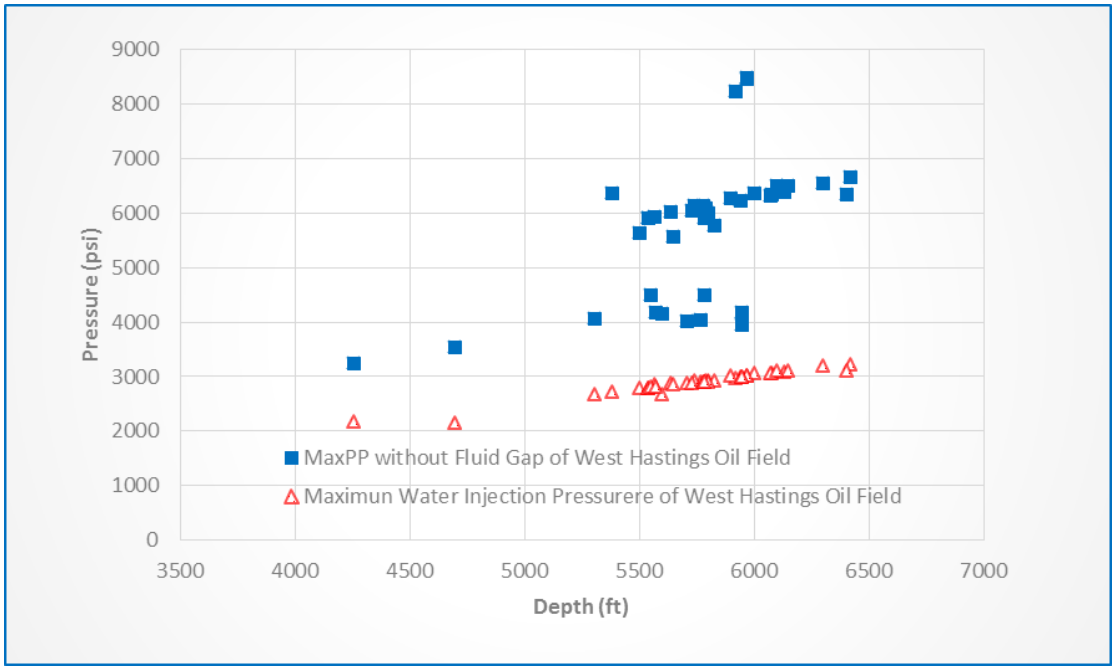


Figure 5: Comparison of the maximum wellhead pressures and the calculated wellhead MaxPP's without fluid gap in the cement sheath for the wells in the West Hastings oil field.

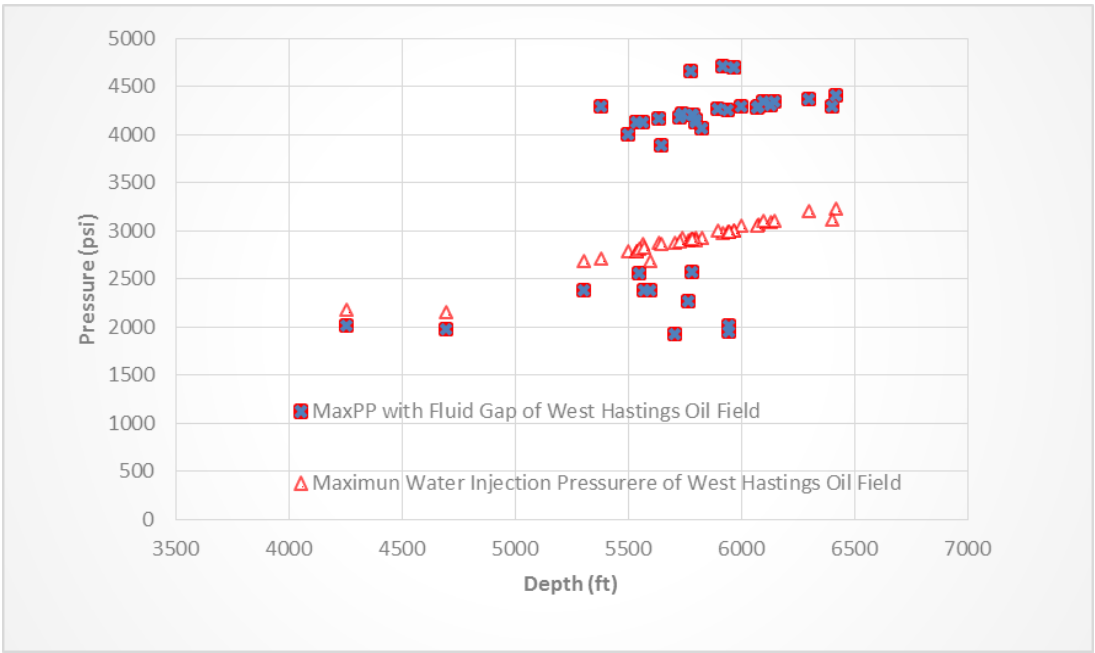


Figure 6: Comparison of the maximum wellhead pressures and the calculated wellhead MaxPP's with fluid gaps in the cement sheaths for the wells in the West Hastings oil field.

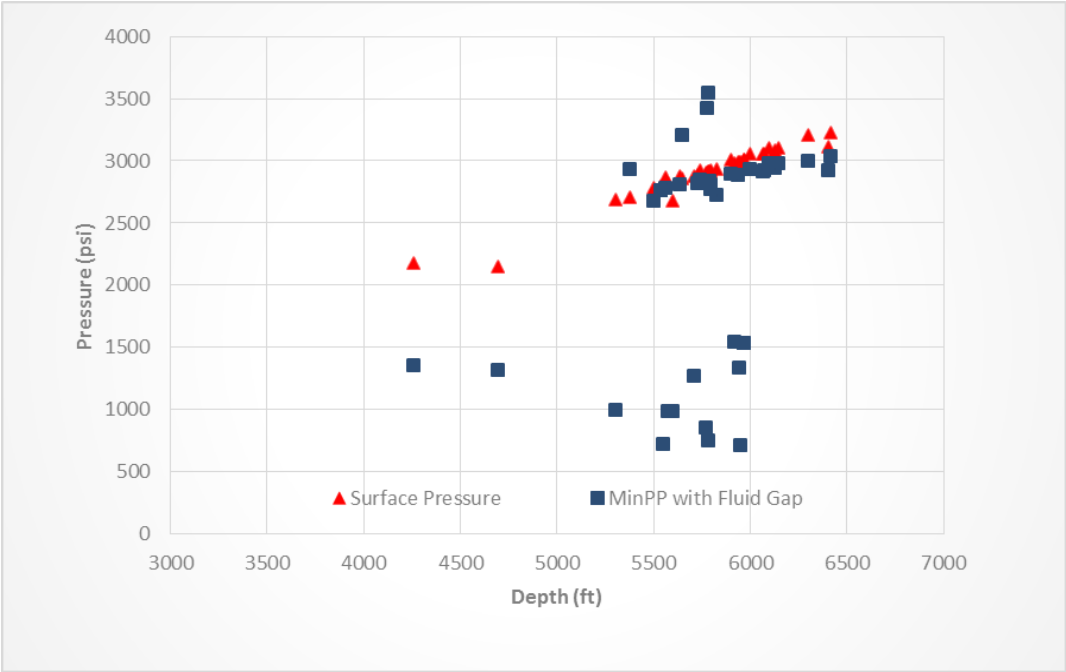


Figure 7: Comparison of wellhead pressures and the calculated wellhead MinPP's with fluid gaps in the cement sheaths for the wells in the West Hastings oil field.

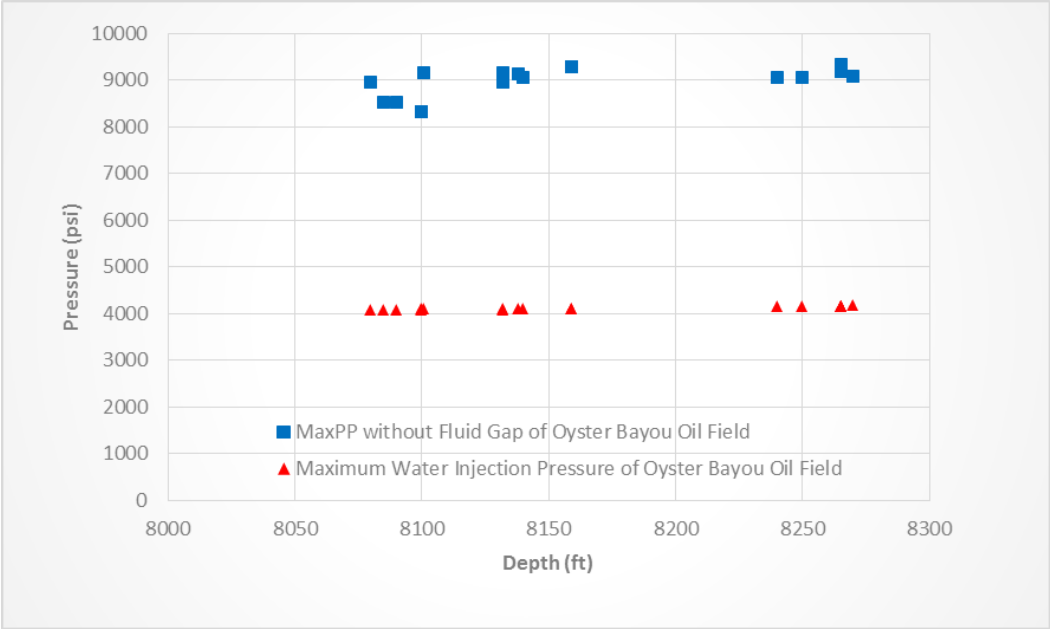


Figure 8: Comparison of wellhead pressures and the calculated wellhead MaxPP's without fluid gap in the cement sheath for the wells in the Oyster Bayou oil field.

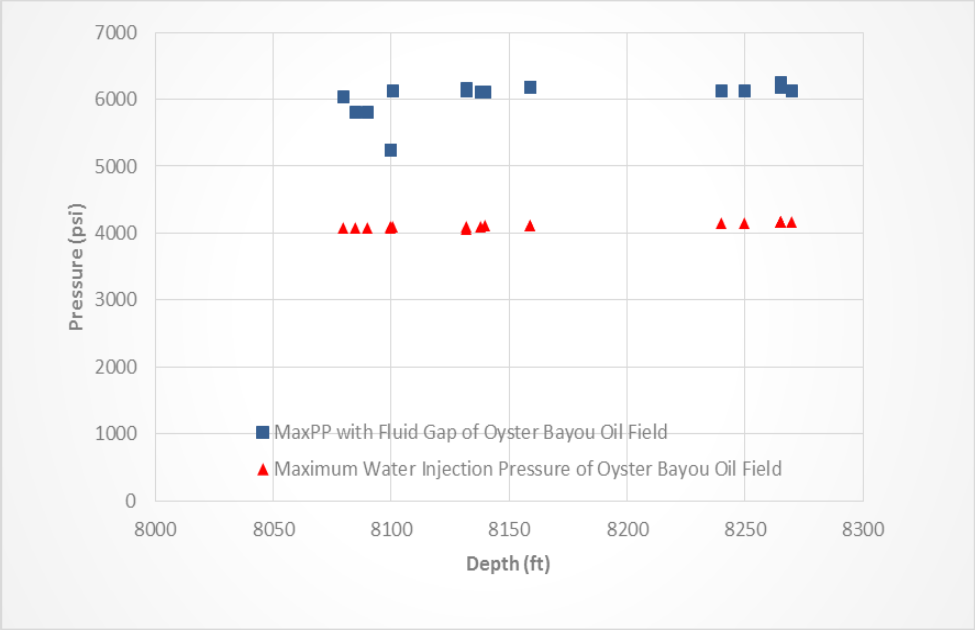


Figure 9: Comparison of wellhead pressures and the calculated wellhead MaxPP's with fluid gaps in the cement sheaths for the wells in the Oyster bayou oil field

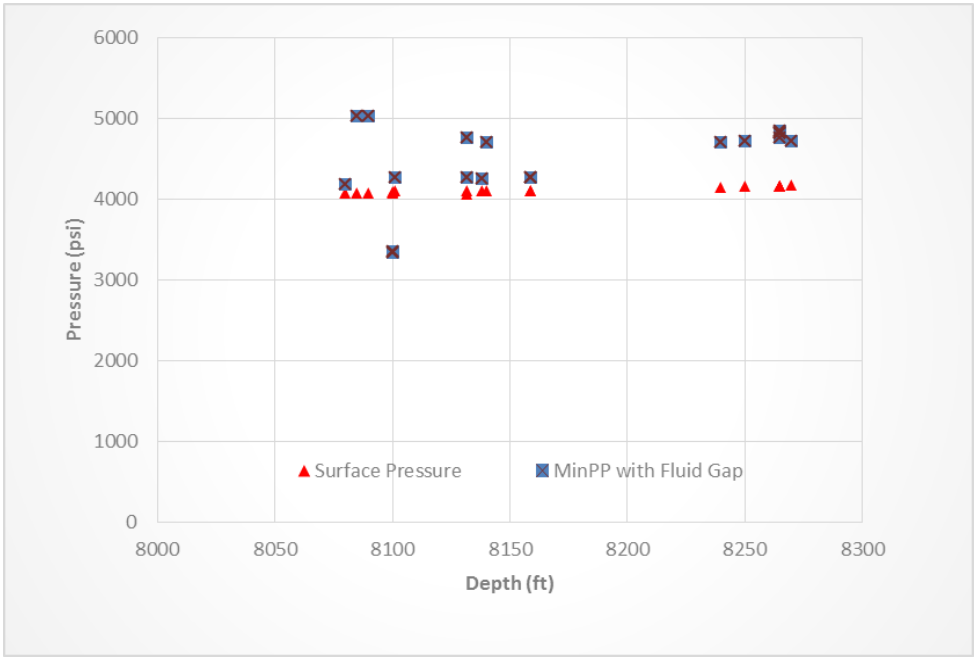


Figure 10: Comparison of wellhead pressures and the calculated wellhead MinPP's with fluid gaps in the cement sheaths for the wells in the Oyster Bayou oil field.

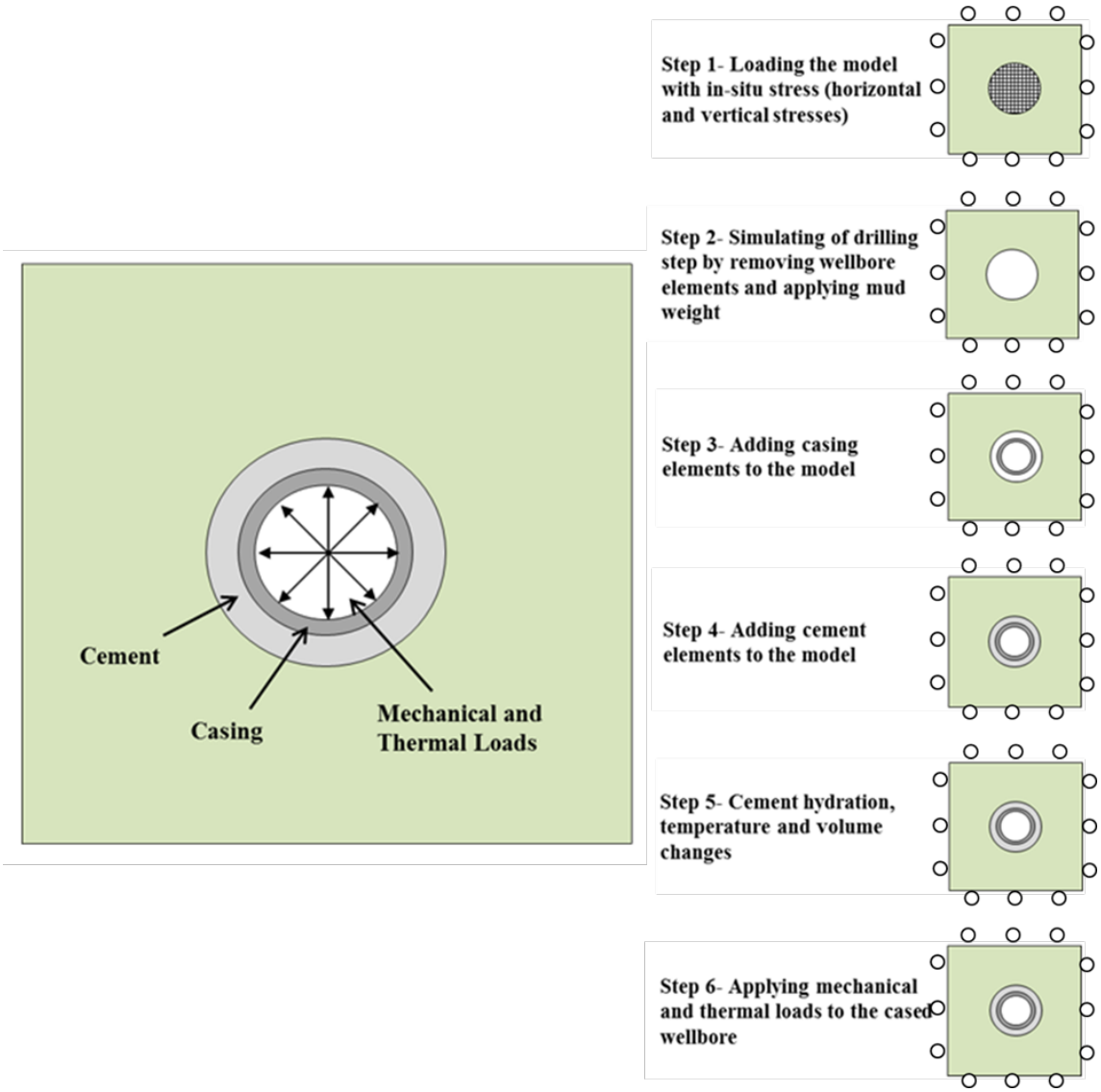


Figure 11: Overall sketch of the model (left) and the simulation step details (right). Model size was adjusted based on actual wellbores from the WASP study area.

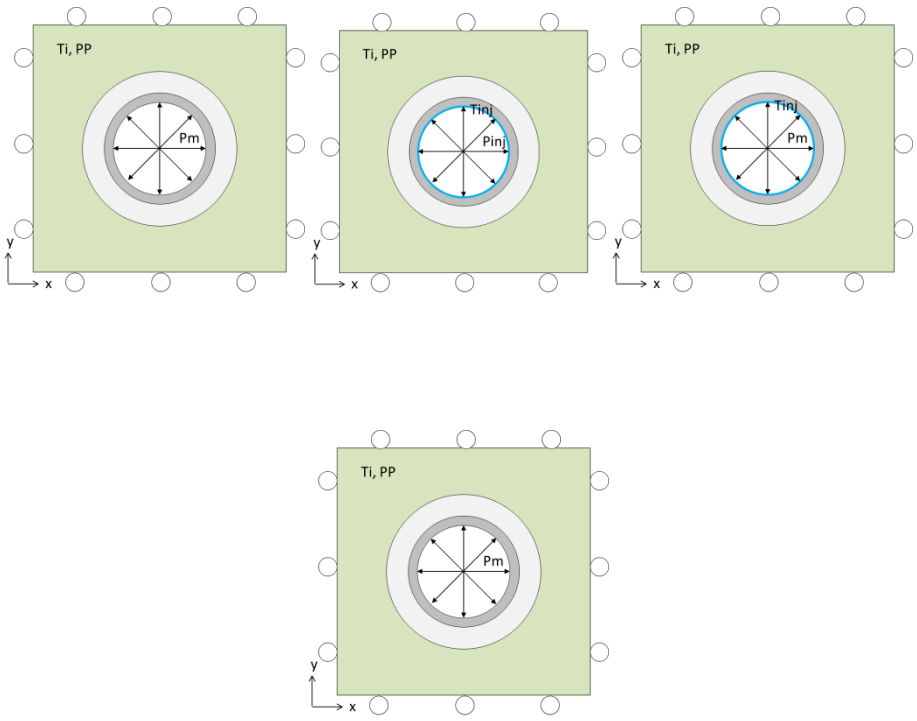


Figure 12: Wellbore cross-section sketches of the 4 scenarios of interest to determine the effects of $CO_2$ degradation on the cement sheath.

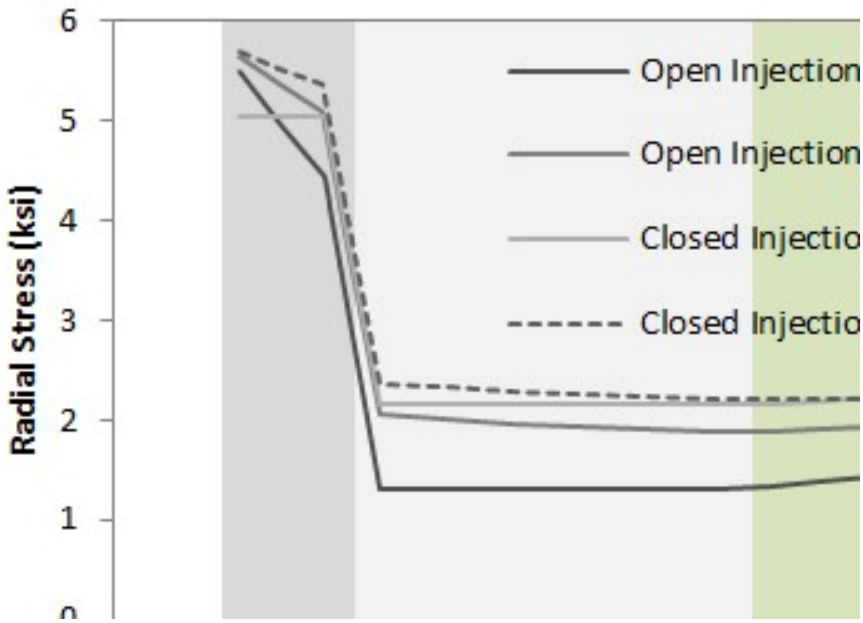


Figure 13: Computed profiles of radial stresses under different injection conditions.

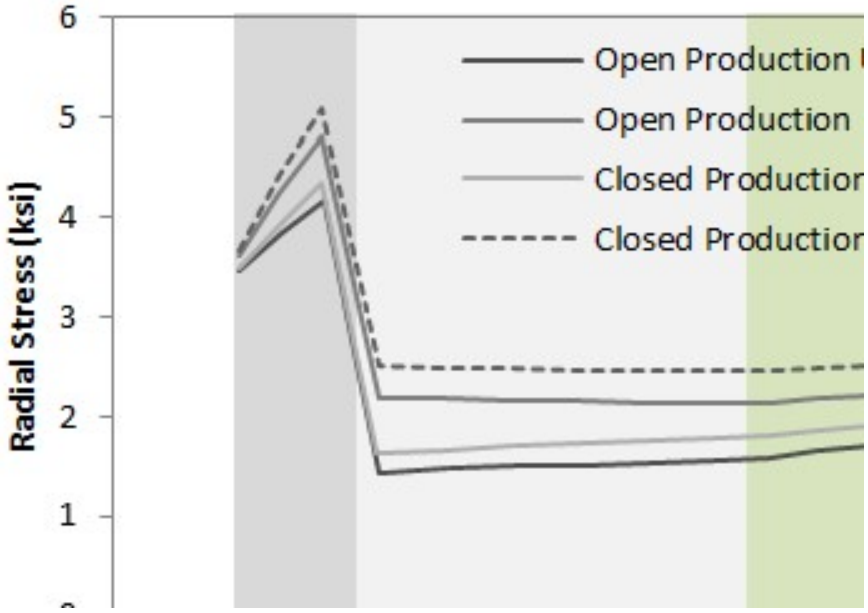


Figure 14: Computed profiles of radial stresses under different production conditions.

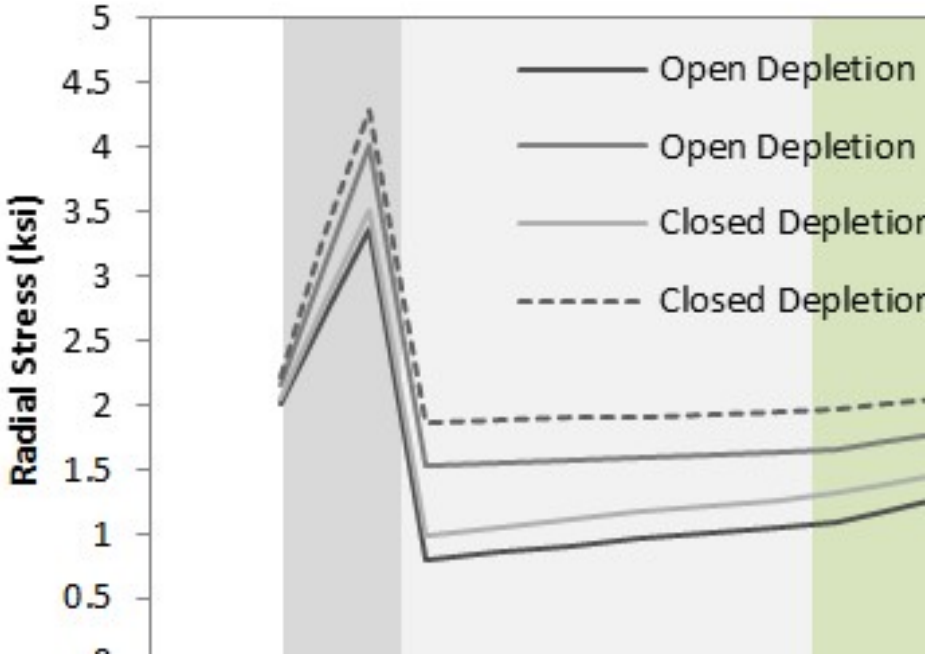


Figure 15: Computed profiles of radial stresses under different depletion conditions.

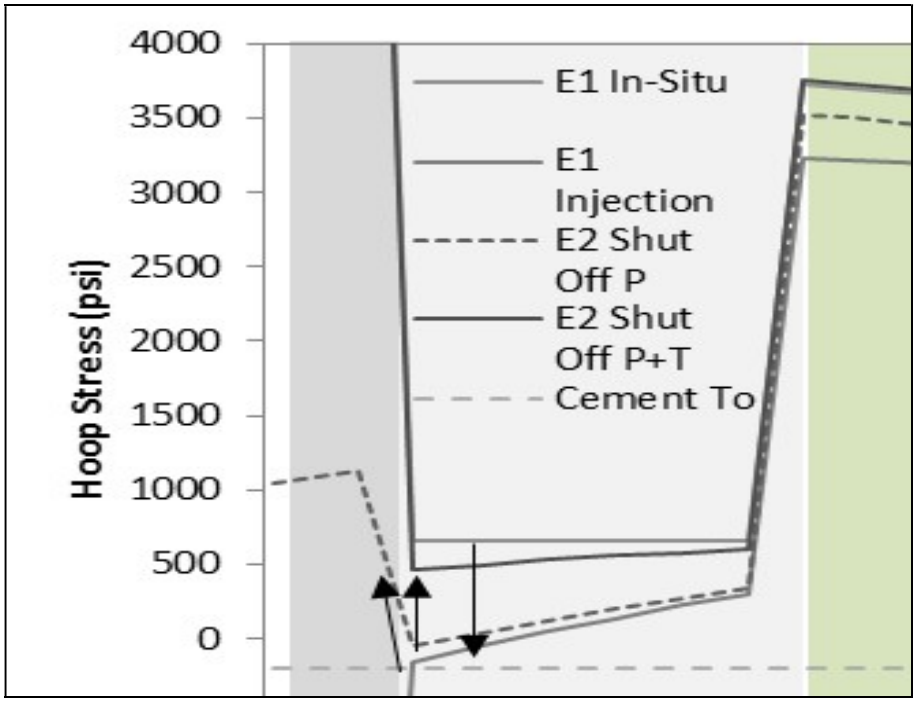


Figure 16: Computed profiles of hoop stresses for an actual well with $CO_2$ injection.

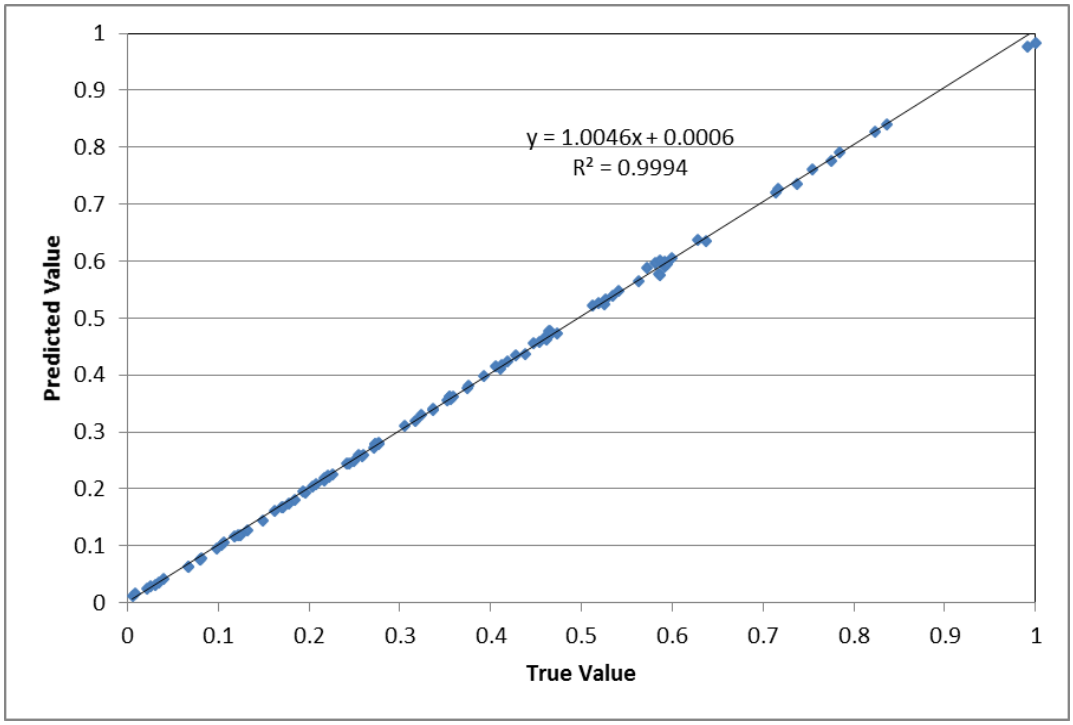


Figure 17: Cross-plot of the True and Predicted Function Values.

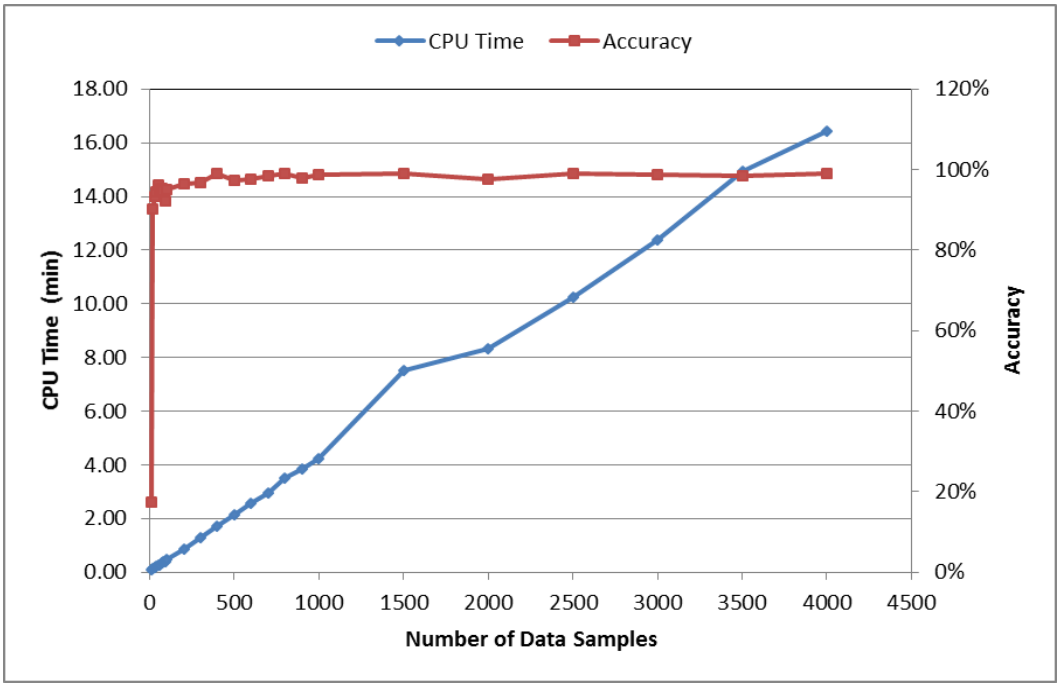


Figure 18: The Effect of Number of Data Samples on the CPU Time and Accuracy of INGA.

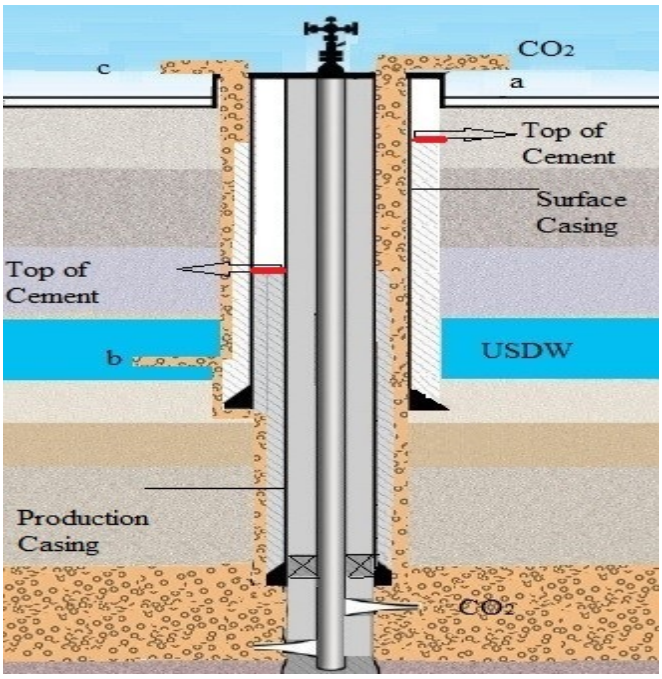


Figure 19: Possible leakage pathways through a proper schematic $CO_2$ injection well.

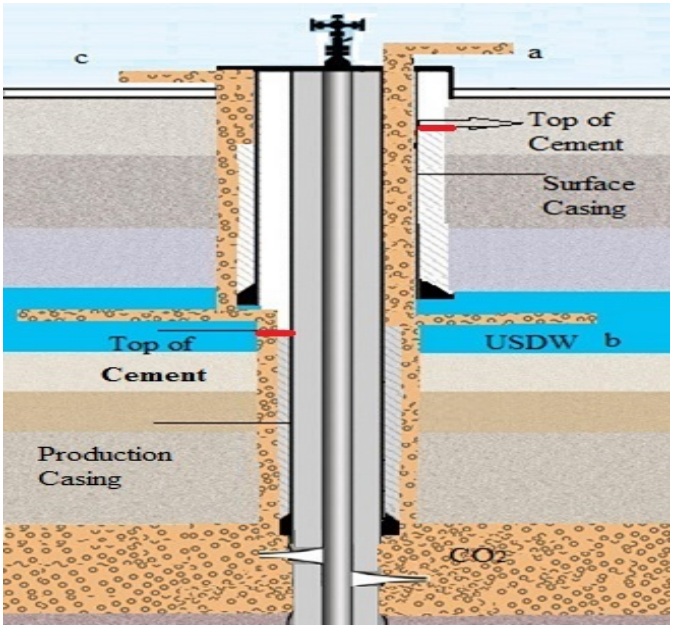


Figure 20: Possible leakage pathways through an improper schematic $CO_2$ injection Well.

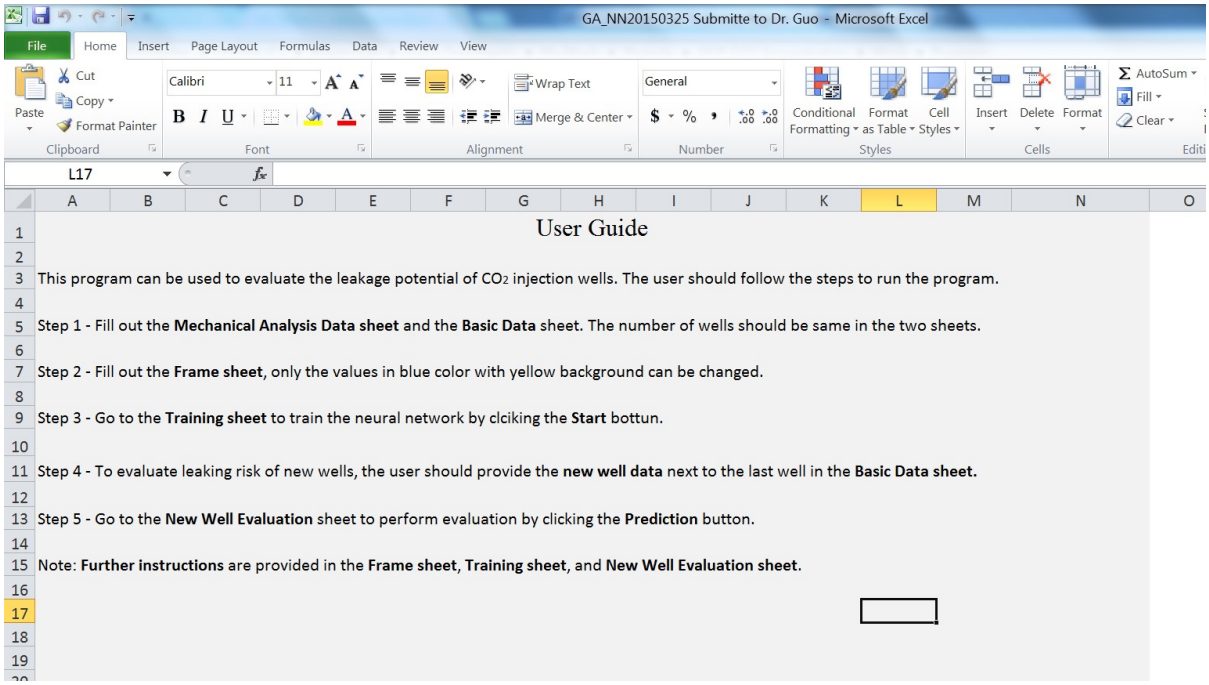

GA_NN20150325 Submitte to Dr. Guo - Microsoft Excel

File Home Insert Page Layout Formulas Data Review View

Cut Copy Format Painter Paste Clipboard

Calibri 11 Font

Wrap Text Merge & Center Alignment

General Number

Conditional Formatting Format as Table Cell Styles Styles

Insert Delete Format Cells

AutoSum Fill Clear Editi

L17

## User Guide

This program can be used to evaluate the leakage potential of $CO_2$ injection wells. The user should follow the steps to run the program.

Step 1 - Fill out the **Mechanical Analysis Data sheet** and the **Basic Data** sheet. The number of wells should be same in the two sheets.

Step 2 - Fill out the **Frame sheet**, only the values in blue color with yellow background can be changed.

Step 3 - Go to the **Training sheet** to train the neural network by clciking the **Start** bottun.

Step 4 - To evaluate leaking risk of new wells, the user should provide the **new well data** next to the last well in the **Basic Data sheet.**

Step 5 - Go to the **New Well Evaluation** sheet to perform evaluation by clicking the **Prediction** button.

Note: **Further instructions** are provided in the **Frame sheet**, **Training sheet**, and **New Well Evaluation sheet**.

Figure 21: User Guide sheet of the Statistical INGA model.

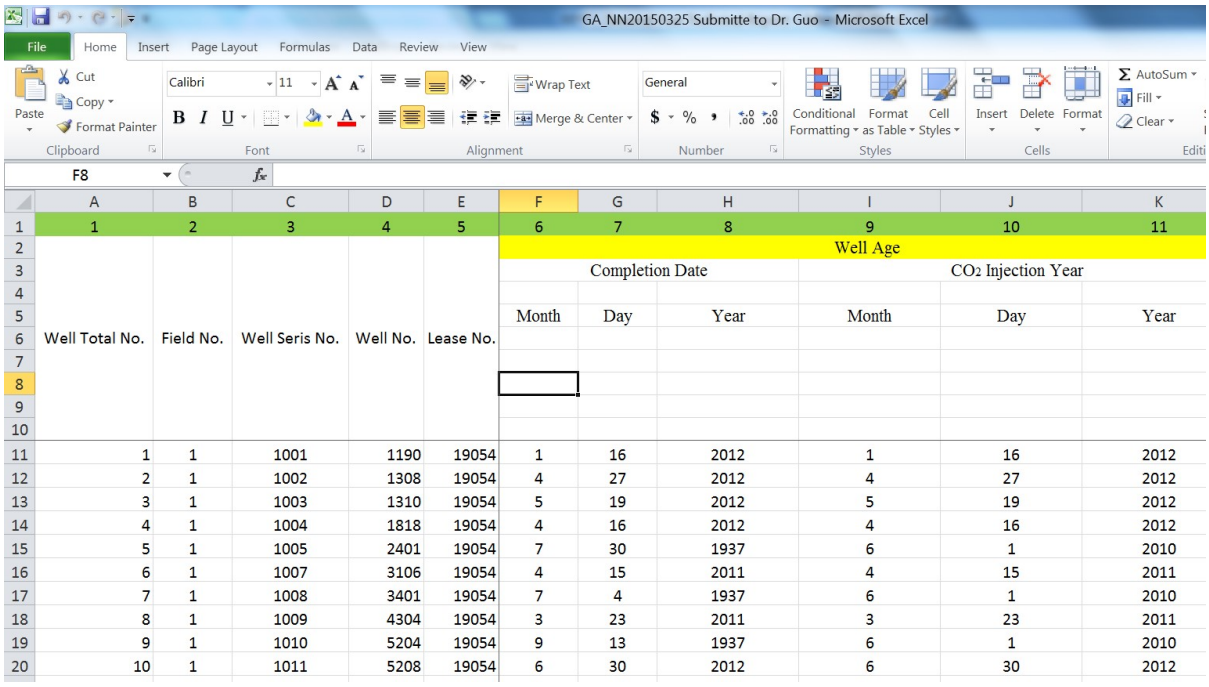

GA_NN20150325 Submitte to Dr. Guo - Microsoft Excel

File Home Insert Page Layout Formulas Data Review View

Cut Copy Format Painter Paste Clipboard

Calibri 11 Font

Wrap Text Merge & Center Alignment

General Number

Conditional Formatting Format as Table Cell Styles Styles

Insert Delete Format Cells

AutoSum Fill Clear Editi

F8

| | A | B | C | D | E | F | G | H | I | J | K |
|---|---|---|---|---|---|---|---|---|---|---|---|
| 1 | 1 | 2 | 3 | 4 | 5 | 6 | 7 | 8 | 9 | 10 | 11 |
| 2 | | | | | | Well Age | | | | | |
| 3 | | | | | | Completion Date | | | $CO_2$ Injection Year | | |
| 4 | | | | | | | | | | | |
| 5 | | | | | | Month | Day | Year | Month | Day | Year |
| 6 | Well Total No. | Field No. | Well Seris No. | Well No. | Lease No. | | | | | | |
| 7 | | | | | | | | | | | |
| 8 | | | | | | | | | | | |
| 9 | | | | | | | | | | | |
| 10 | | | | | | | | | | | |
| 11 | 1 | 1 | 1001 | 1190 | 19054 | 1 | 16 | 2012 | 1 | 16 | 2012 |
| 12 | 2 | 1 | 1002 | 1308 | 19054 | 4 | 27 | 2012 | 4 | 27 | 2012 |
| 13 | 3 | 1 | 1003 | 1310 | 19054 | 5 | 19 | 2012 | 5 | 19 | 2012 |
| 14 | 4 | 1 | 1004 | 1818 | 19054 | 4 | 16 | 2012 | 4 | 16 | 2012 |
| 15 | 5 | 1 | 1005 | 2401 | 19054 | 7 | 30 | 1937 | 6 | 1 | 2010 |
| 16 | 6 | 1 | 1007 | 3106 | 19054 | 4 | 15 | 2011 | 4 | 15 | 2011 |
| 17 | 7 | 1 | 1008 | 3401 | 19054 | 7 | 4 | 1937 | 6 | 1 | 2010 |
| 18 | 8 | 1 | 1009 | 4304 | 19054 | 3 | 23 | 2011 | 3 | 23 | 2011 |
| 19 | 9 | 1 | 1010 | 5204 | 19054 | 9 | 13 | 1937 | 6 | 1 | 2010 |
| 20 | 10 | 1 | 1011 | 5208 | 19054 | 6 | 30 | 2012 | 6 | 30 | 2012 |

Figure 22: Basic Data sheet of the Statistical INGA model.

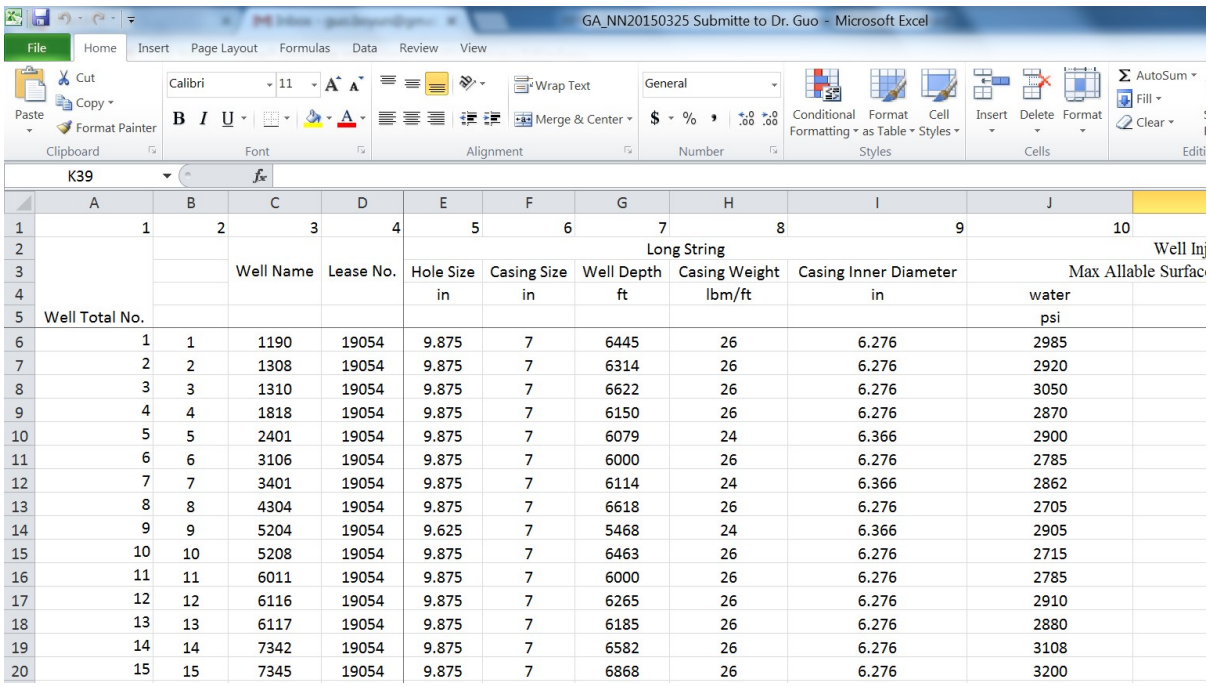

GA_NN20150325 Submitte to Dr. Guo - Microsoft Excel

| | A | B | C | D | E | F | G | H | I | J |
|---|---|---|---|---|---|---|---|---|---|---|
| 1 | 1 | 2 | 3 | 4 | 5 | 6 | 7 | 8 | 9 | 10 |
| 2 | | | | | Long String | | | | | Well Inj |
| 3 | | | Well Name | Lease No. | Hole Size | Casing Size | Well Depth | Casing Weight | Casing Inner Diameter | Max Allable Surfac |
| 4 | | | | | in | in | ft | lbm/ft | in | water |
| 5 | Well Total No. | | | | | | | | | psi |
| 6 | 1 | 1 | 1190 | 19054 | 9.875 | 7 | 6445 | 26 | 6.276 | 2985 |
| 7 | 2 | 2 | 1308 | 19054 | 9.875 | 7 | 6314 | 26 | 6.276 | 2920 |
| 8 | 3 | 3 | 1310 | 19054 | 9.875 | 7 | 6622 | 26 | 6.276 | 3050 |
| 9 | 4 | 4 | 1818 | 19054 | 9.875 | 7 | 6150 | 26 | 6.276 | 2870 |
| 10 | 5 | 5 | 2401 | 19054 | 9.875 | 7 | 6079 | 24 | 6.366 | 2900 |
| 11 | 6 | 6 | 3106 | 19054 | 9.875 | 7 | 6000 | 26 | 6.276 | 2785 |
| 12 | 7 | 7 | 3401 | 19054 | 9.875 | 7 | 6114 | 24 | 6.366 | 2862 |
| 13 | 8 | 8 | 4304 | 19054 | 9.875 | 7 | 6618 | 26 | 6.276 | 2705 |
| 14 | 9 | 9 | 5204 | 19054 | 9.625 | 7 | 5468 | 24 | 6.366 | 2905 |
| 15 | 10 | 10 | 5208 | 19054 | 9.875 | 7 | 6463 | 26 | 6.276 | 2715 |
| 16 | 11 | 11 | 6011 | 19054 | 9.875 | 7 | 6000 | 26 | 6.276 | 2785 |
| 17 | 12 | 12 | 6116 | 19054 | 9.875 | 7 | 6265 | 26 | 6.276 | 2910 |
| 18 | 13 | 13 | 6117 | 19054 | 9.875 | 7 | 6185 | 26 | 6.276 | 2880 |
| 19 | 14 | 14 | 7342 | 19054 | 9.875 | 7 | 6582 | 26 | 6.276 | 3108 |
| 20 | 15 | 15 | 7345 | 19054 | 9.875 | 7 | 6868 | 26 | 6.276 | 3200 |

Figure 23: Mechanical Analysis sheet of the Statistical INGA model.

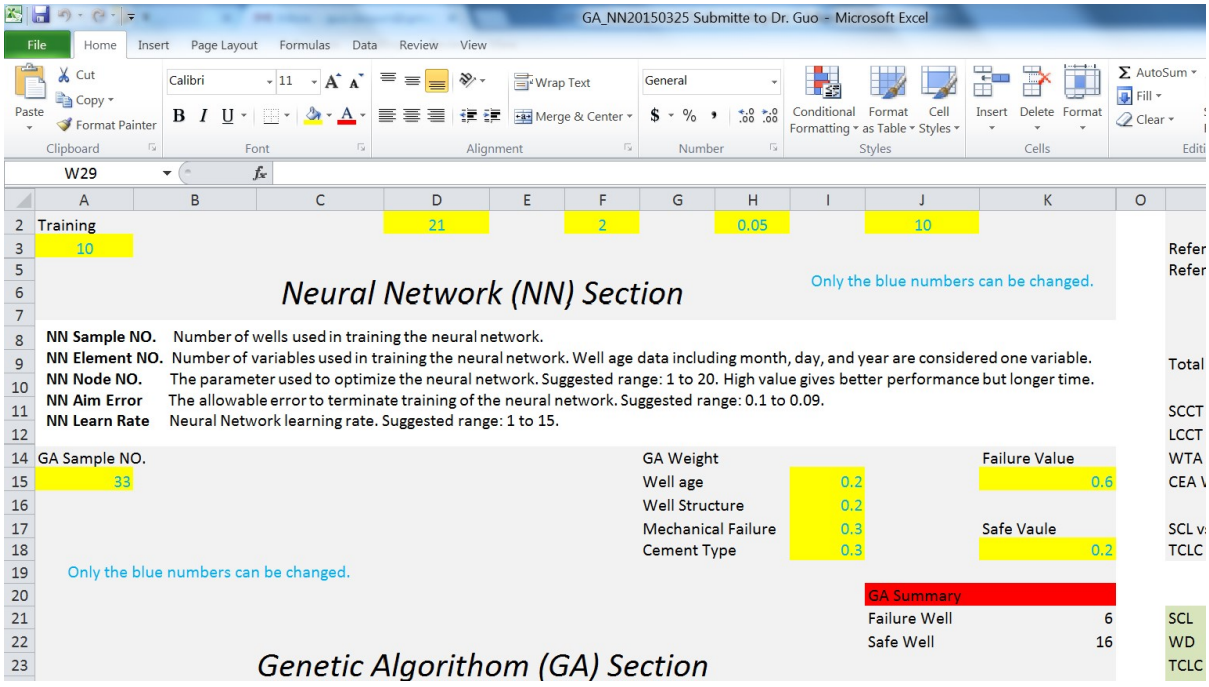

GA_NN20150325 Submitte to Dr. Guo - Microsoft Excel

| | A | B | C | D | E | F | G | H | I | J | K | O |
|---|---|---|---|---|---|---|---|---|---|---|---|---|
| 2 | Training | | | 21 | | 2 | | 0.05 | | 10 | | |
| 3 | 10 | | | | | | | | | | | |
| 5 | | | | | | | | | | | | |
| 6 | | | | *Neural Network (NN) Section* | | | | | Only the blue numbers can be changed. | | | |
| 7 | | | | | | | | | | | | |
| 8 | **NN Sample NO.** Number of wells used in training the neural network. | | | | | | | | | | | |
| 9 | **NN Element NO.** Number of variables used in training the neural network. Well age data including month, day, and year are considered one variable. | | | | | | | | | | | |
| 10 | **NN Node NO.** The parameter used to optimize the neural network. Suggested range: 1 to 20. High value gives better performance but longer time. | | | | | | | | | | | |
| 11 | **NN Aim Error** The allowable error to terminate training of the neural network. Suggested range: 0.1 to 0.09. | | | | | | | | | | | |
| 12 | **NN Learn Rate** Neural Network learning rate. Suggested range: 1 to 15. | | | | | | | | | | | |
| 14 | GA Sample NO. | | | | | | GA Weight | | | Failure Value | | |
| 15 | 33 | | | | | | Well age | 0.2 | | 0.6 | | |
| 16 | | | | | | | Well Structure | 0.2 | | | | |
| 17 | | | | | | | Mechanical Failure | 0.3 | | Safe Vaule | | |
| 18 | | | | | | | Cement Type | 0.3 | | 0.2 | | |
| 19 | Only the blue numbers can be changed. | | | | | | | | | | | |
| 20 | | | | | | | | | GA Summary | | | |
| 21 | | | | | | | | | Failure Well | 6 | | |
| 22 | | | | | | | | | Safe Well | 16 | | |
| 23 | | | | *Genetic Algorithom (GA) Section* | | | | | | | | |

Figure 24: Frame sheet of the Statistical INGA model.

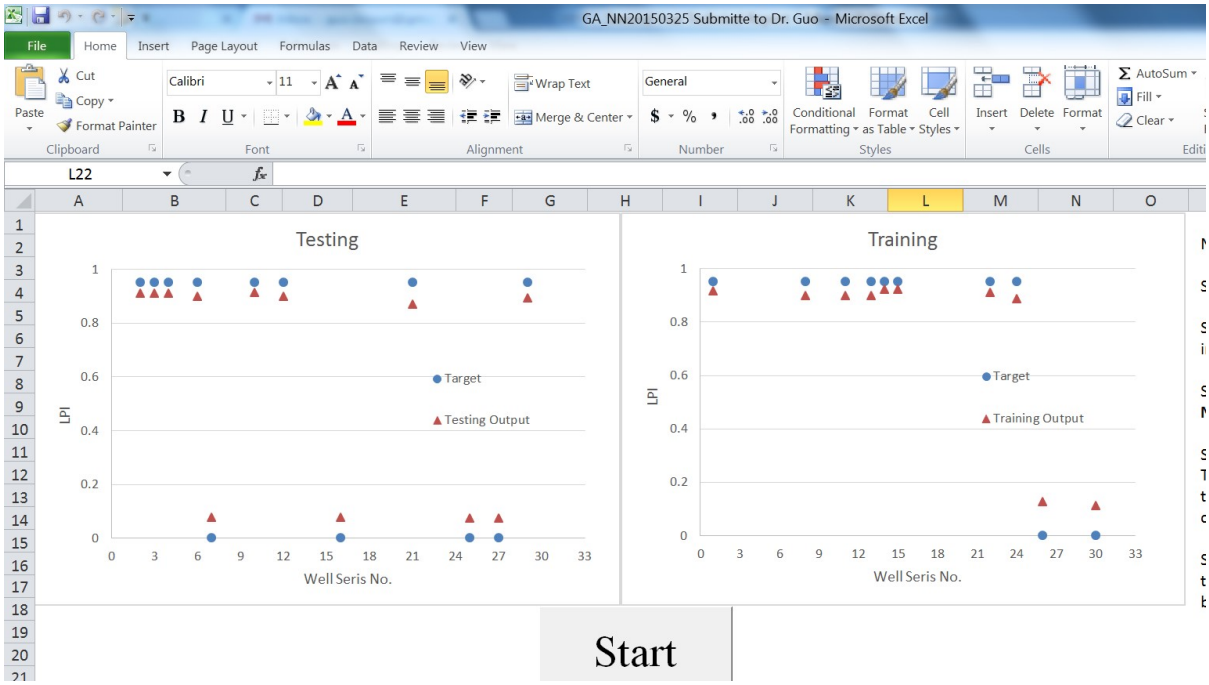


Figure 25: Training sheet of the Statistical INGA model.

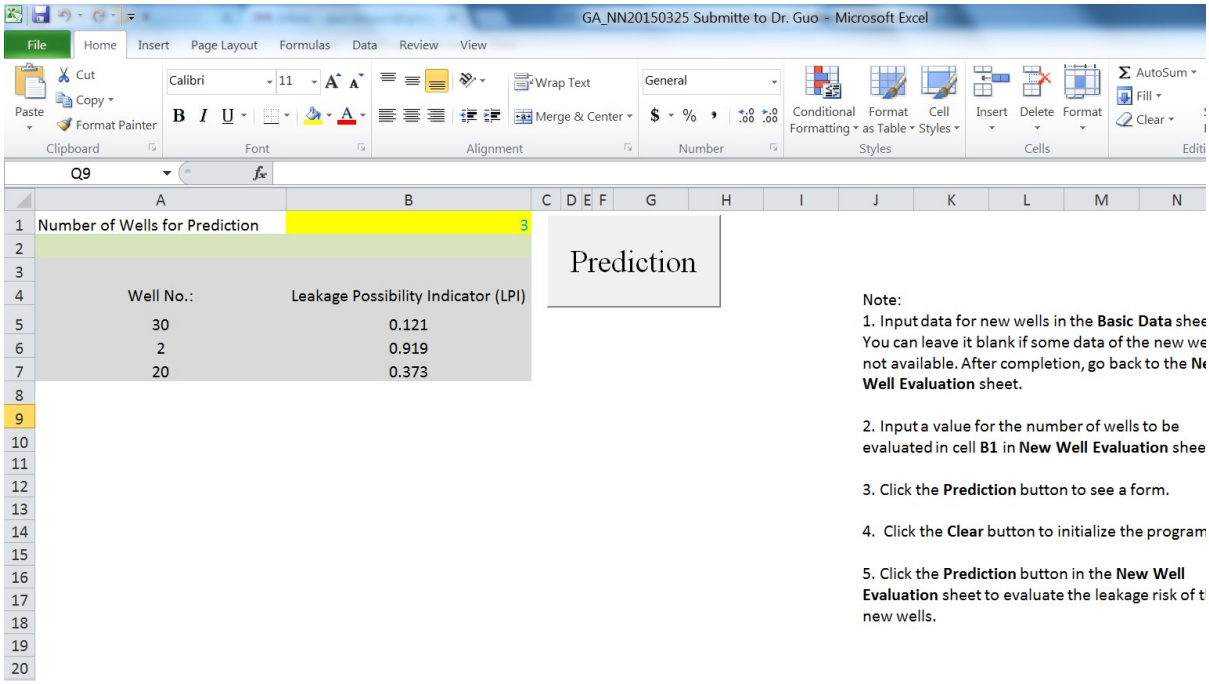


Figure 26: New Well Evaluation sheet of the Statistical INGA model.

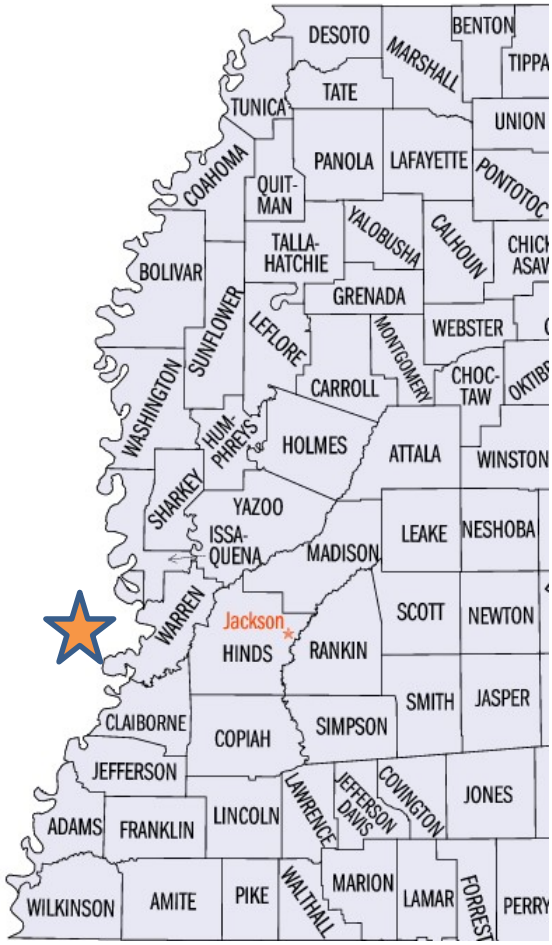


Figure 27: Location of test site in the Cranfield Field, Adams County, Mississippi.

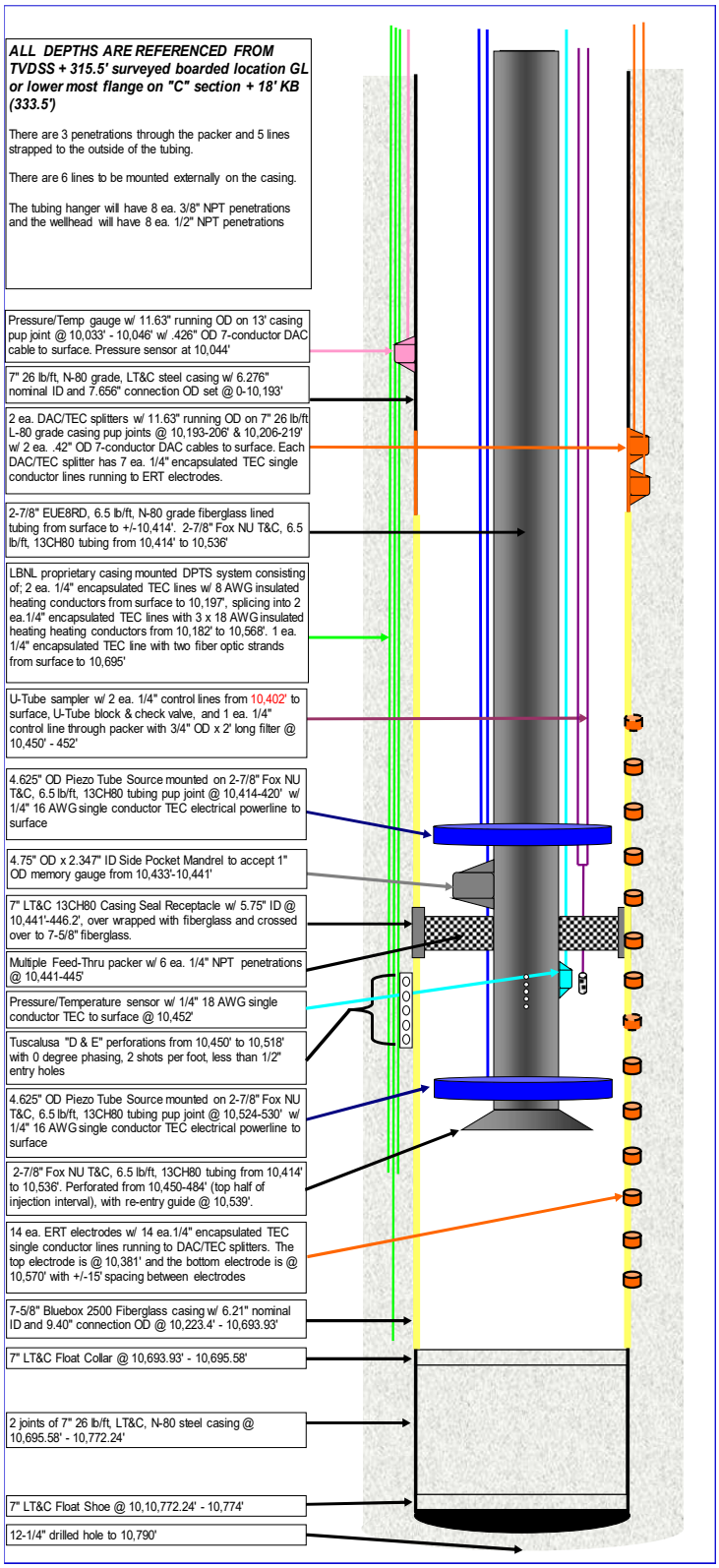


Figure 28: Schematic of completion of wells CFU31F2 and CFU31F3 in the Cranfield Field.

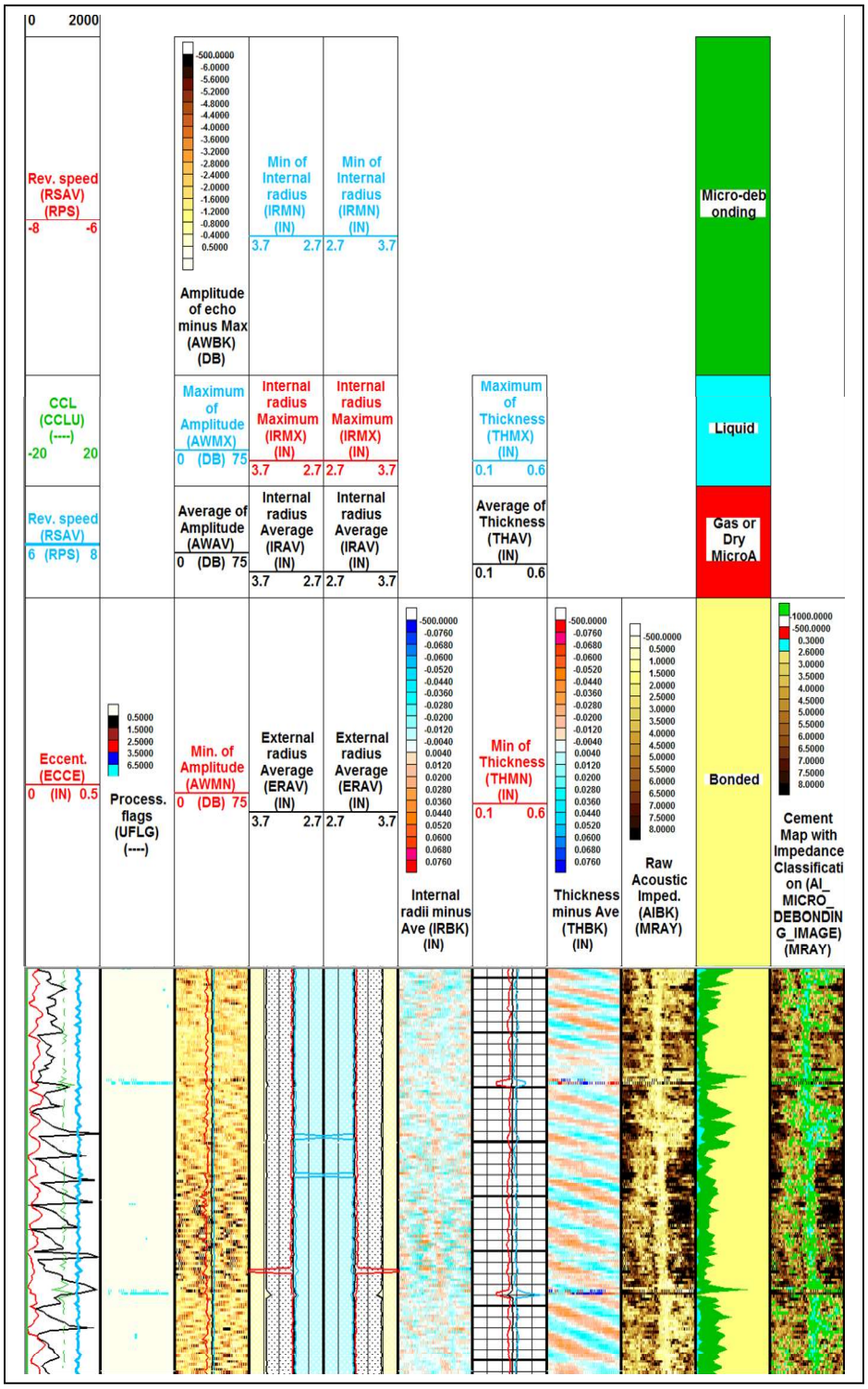


Figure 29: Maps of well members identified by an Ultrasonic Imager Tool in well CFU31F2.

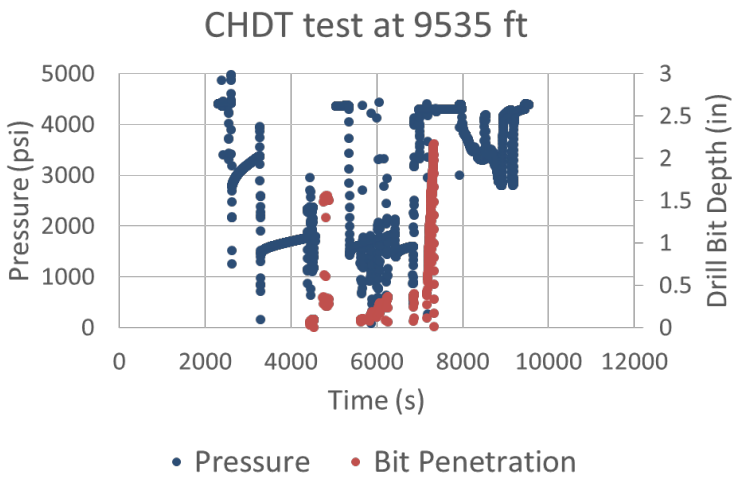


Figure 30: Pressure test data recorded in well CFU31F3 in the Cranfield Field.

**Location of Sidewall Cores from Well CFU31F2**
**Cranfield Field, Adams County, Mississippi**

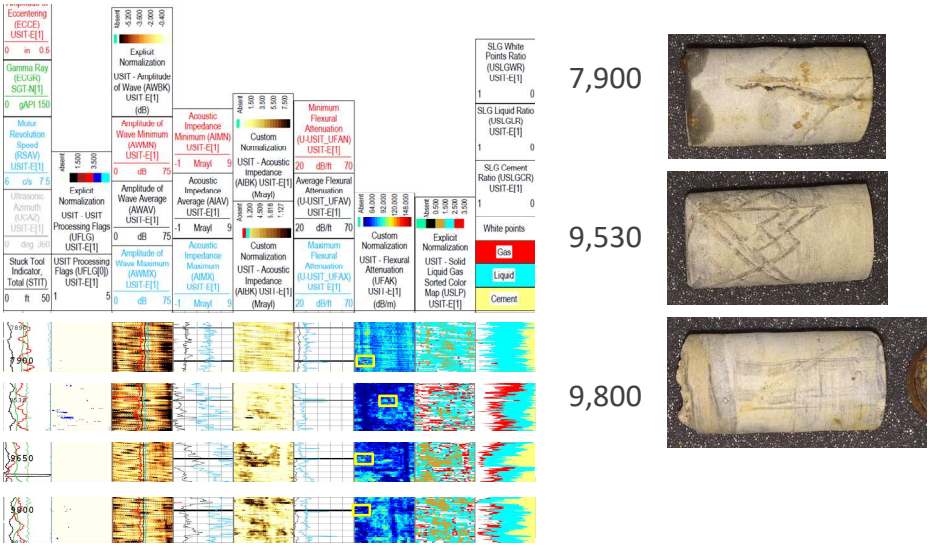


Figure 31: Sidewall coring intervals in well CFU31F2 in the Cranfield Field.

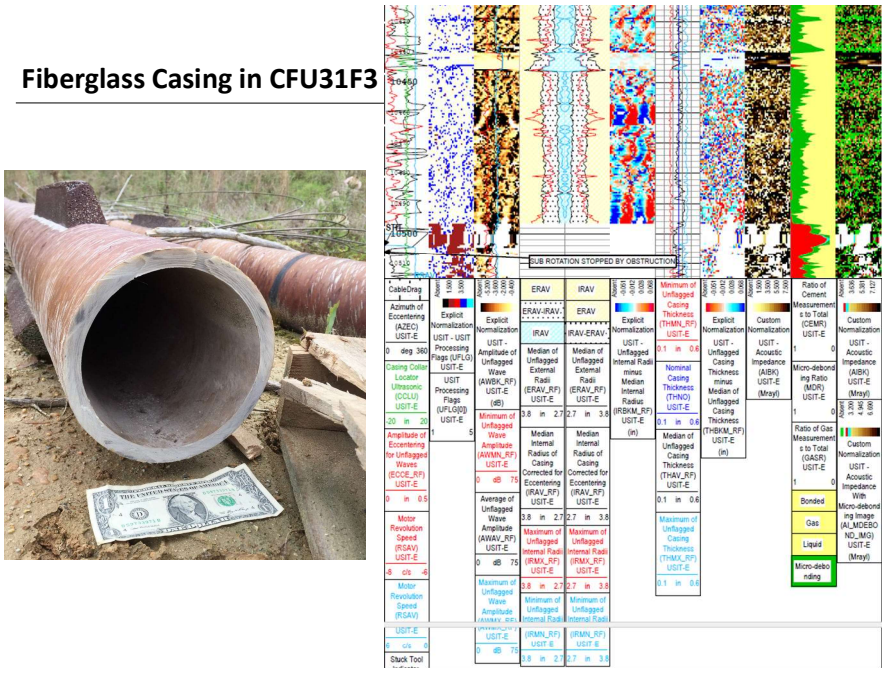


Figure 32: Fiberglass casing set in well CFU31F3 in the Cranfield Field.


Figure 33: Core samples taken from the sidewall in well CFU31F3 in the Cranfield Field.

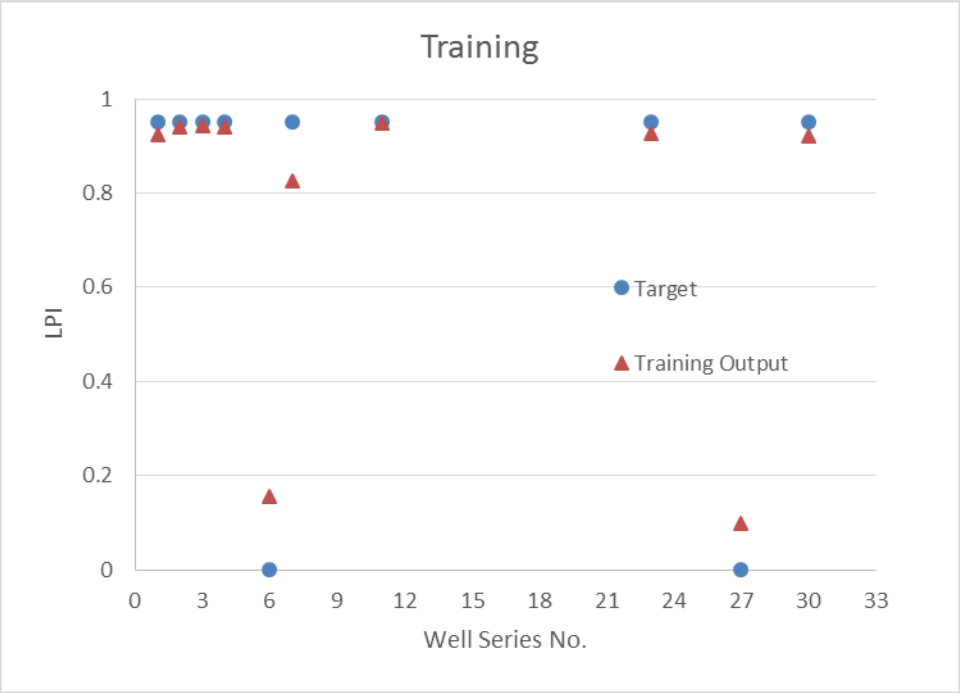


Figure 34: Performance of Statistical INGA model training (Target = known true value).


Figure 35: Comparison of Statistical INGA model-predicted and the true values of LPI.

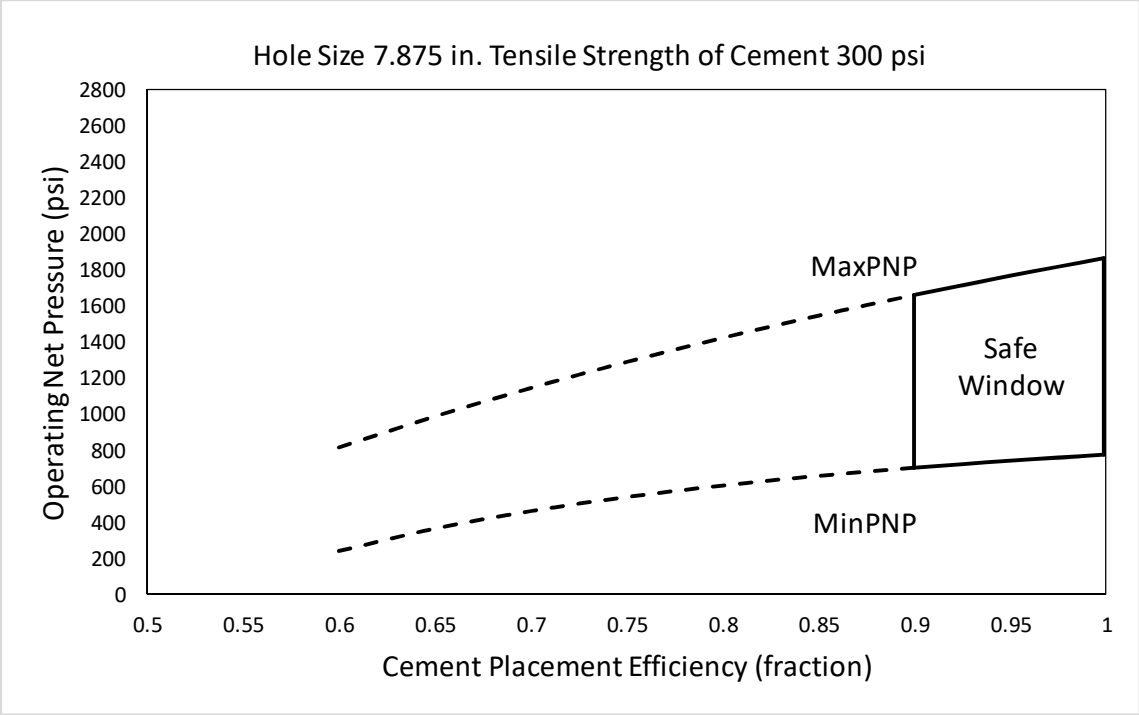


Figure 36: Operating Net Pressure window for wells completed with 7.875" casing with tensile strength of cement 300 psi.

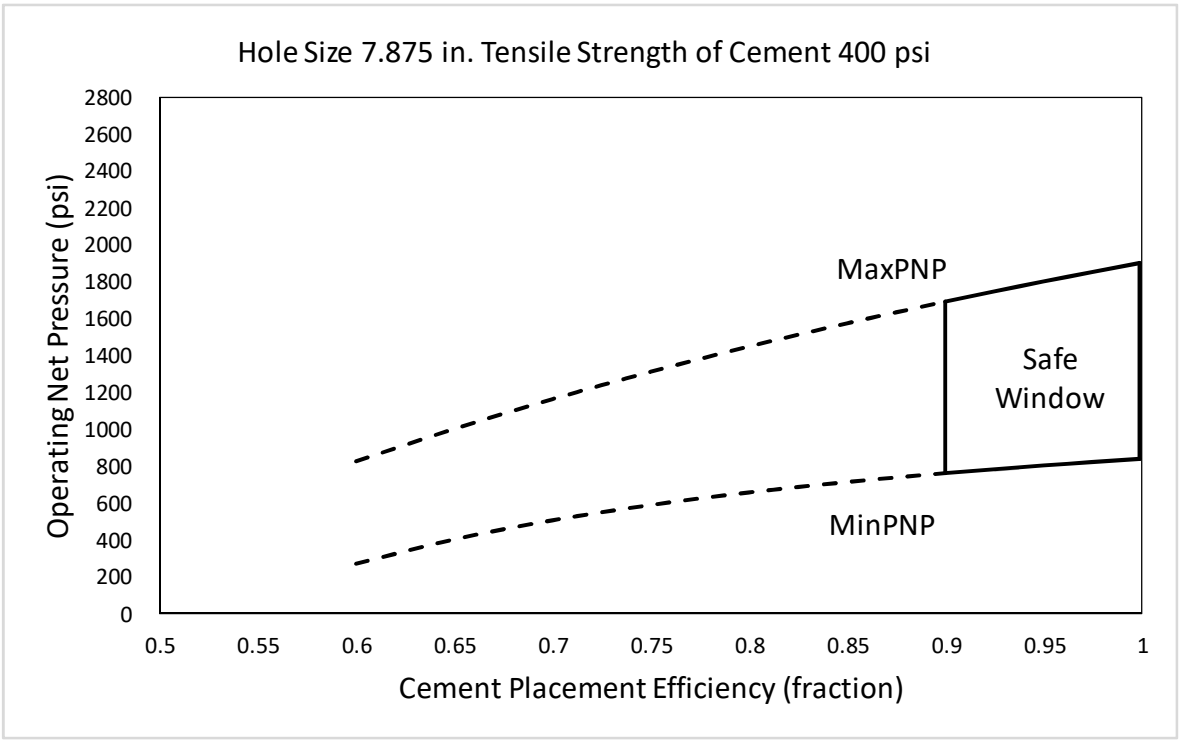


Figure 37: Operating Net Pressure window for wells completed with 7.875" casing with tensile strength of cement 400 psi.

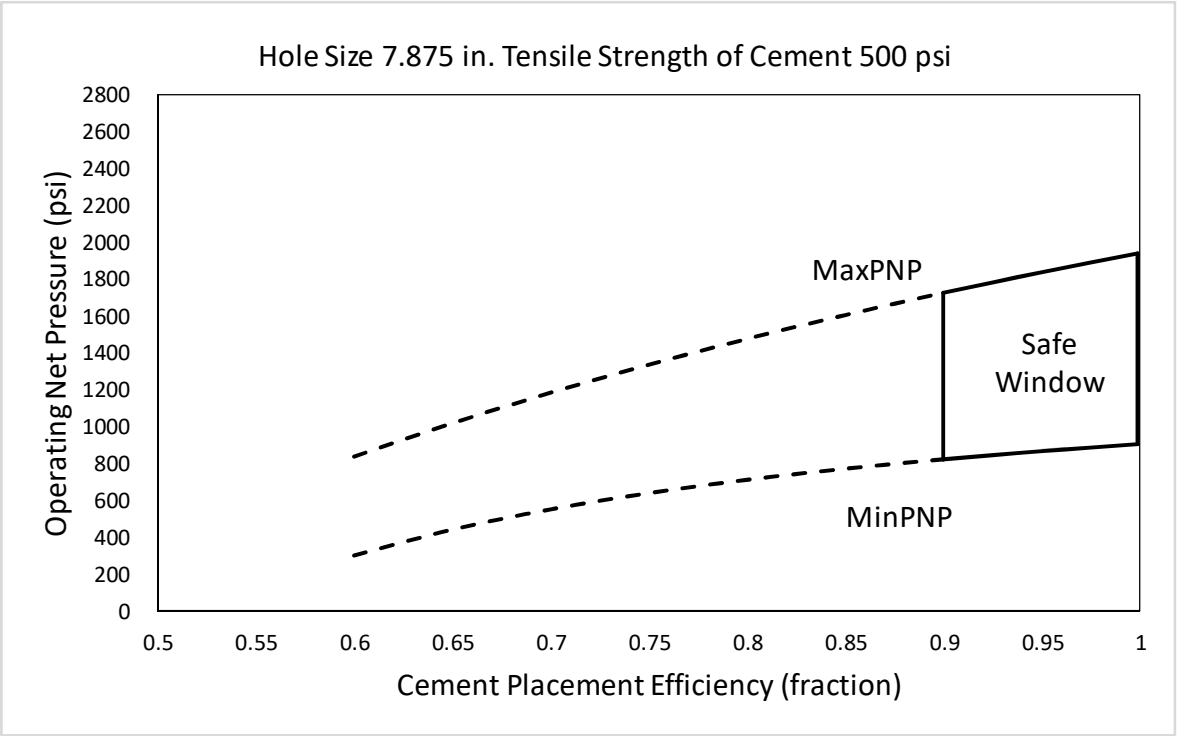


Figure 38: Operating Net Pressure window for wells completed with 7.875" casing with tensile strength of cement 500 psi.

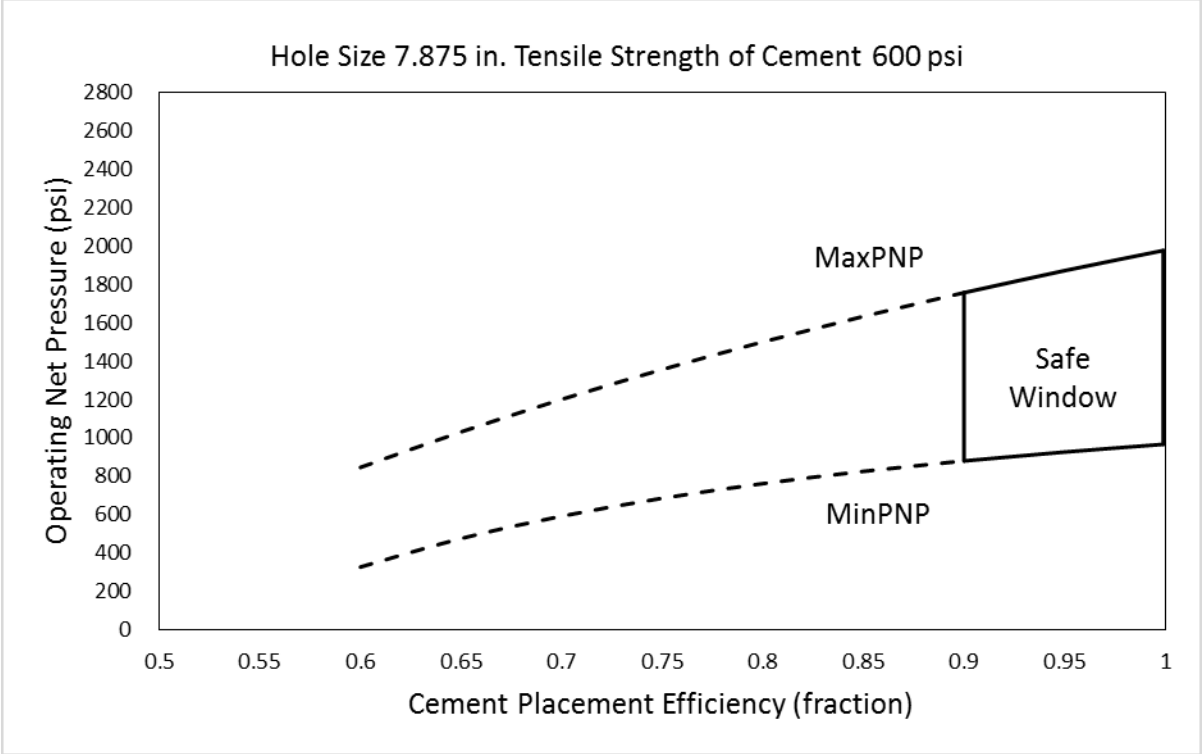


Figure 39: Operating Net Pressure window for wells completed with 7.875" casing with tensile strength of cement 600 psi.

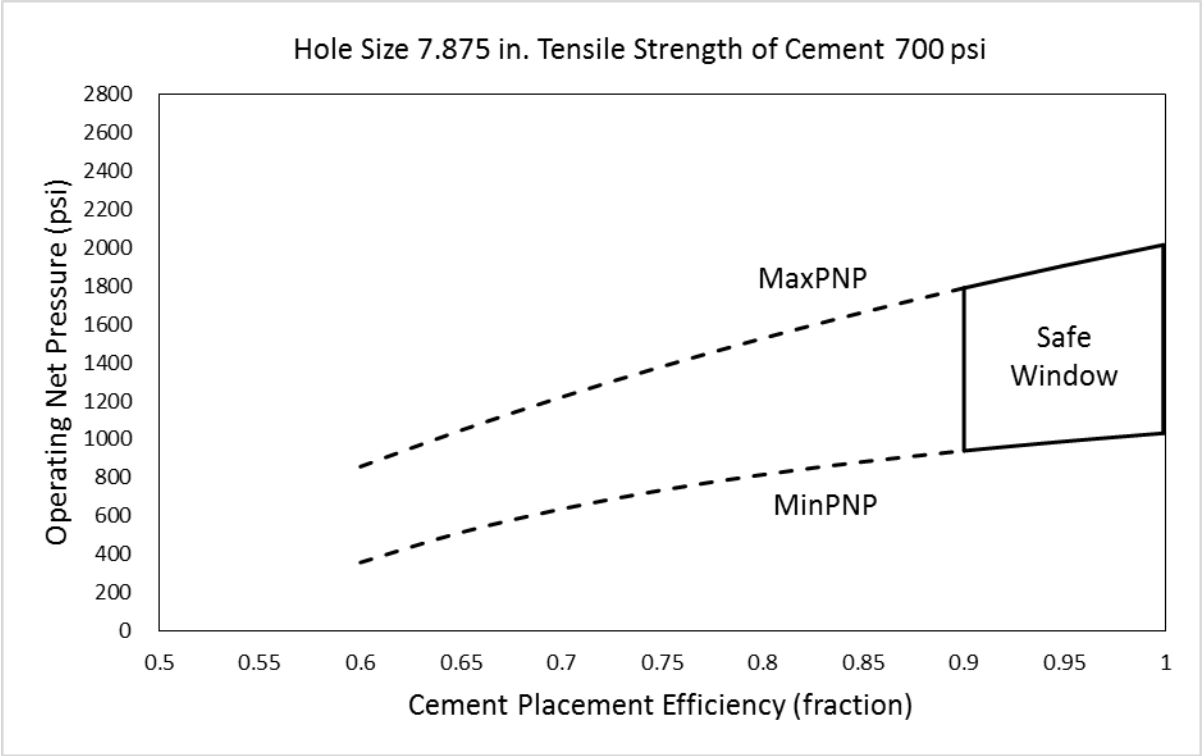


Figure 40: Operating Net Pressure window for wells completed with 7.875" casing with tensile strength of cement 700 psi.

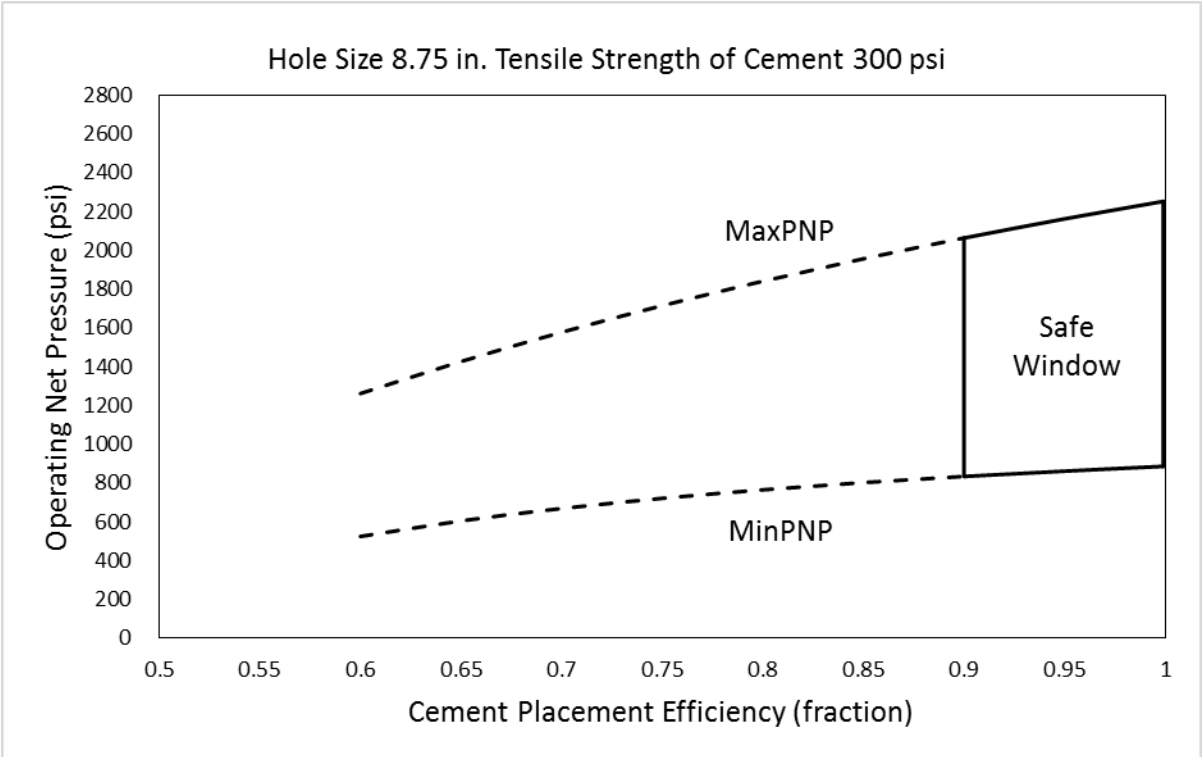


Figure 41: Operating Net Pressure window for wells completed with 8.75" casing with tensile strength of cement 300 psi.

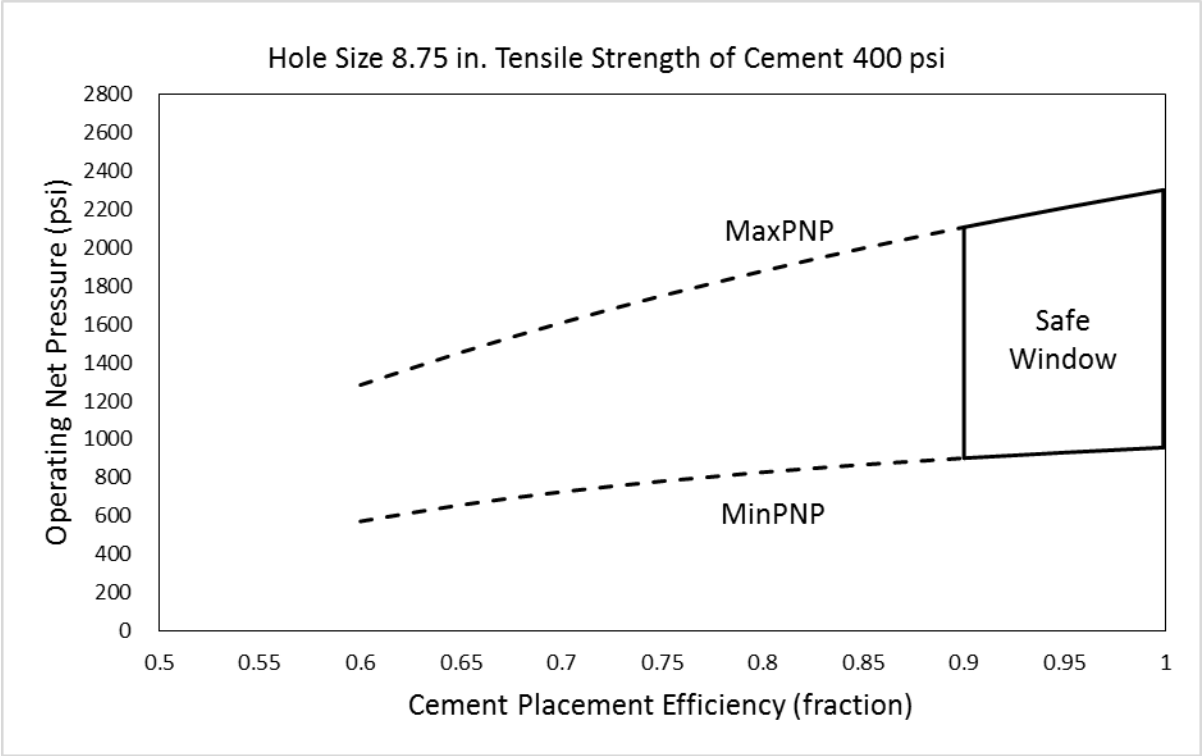


Figure 42: Operating Net Pressure window for wells completed with 8.75" casing with tensile strength of cement 400 psi.

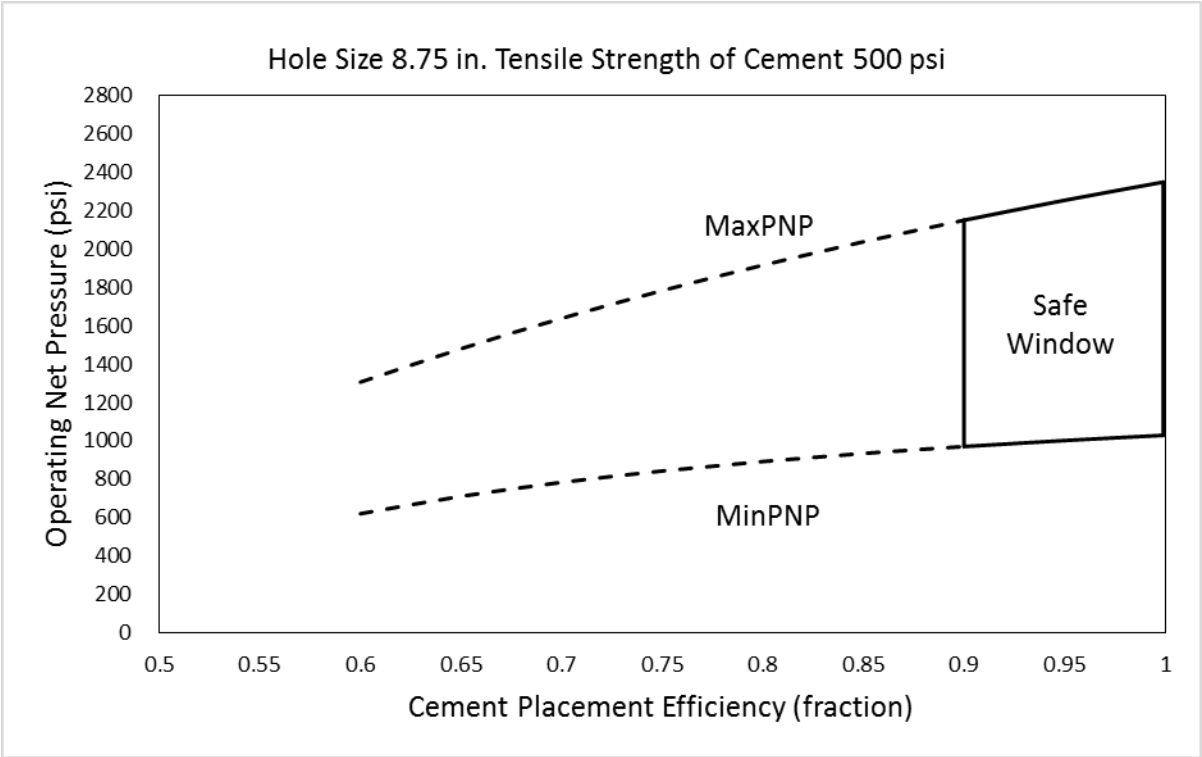


Figure 43: Operating Net Pressure window for wells completed with 8.75" casing with tensile strength of cement 500 psi.

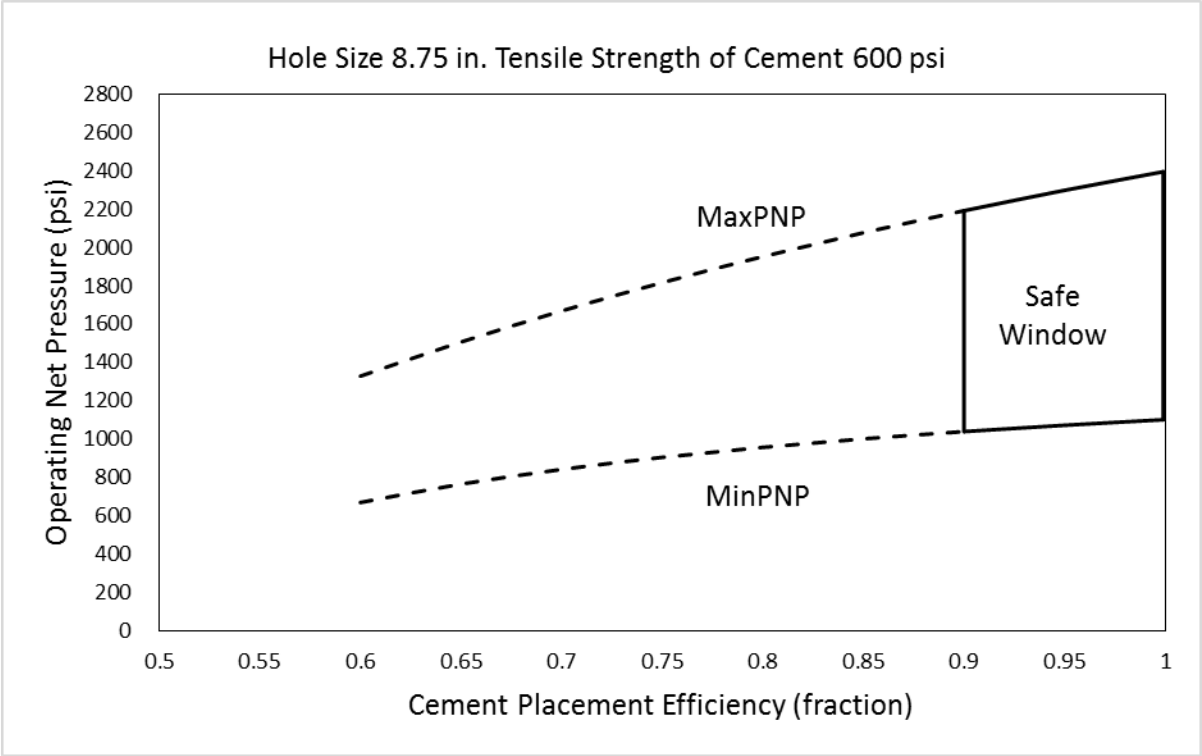


Figure 44: Operating Net Pressure window for wells completed with 8.75" casing with tensile strength of cement 600 psi.

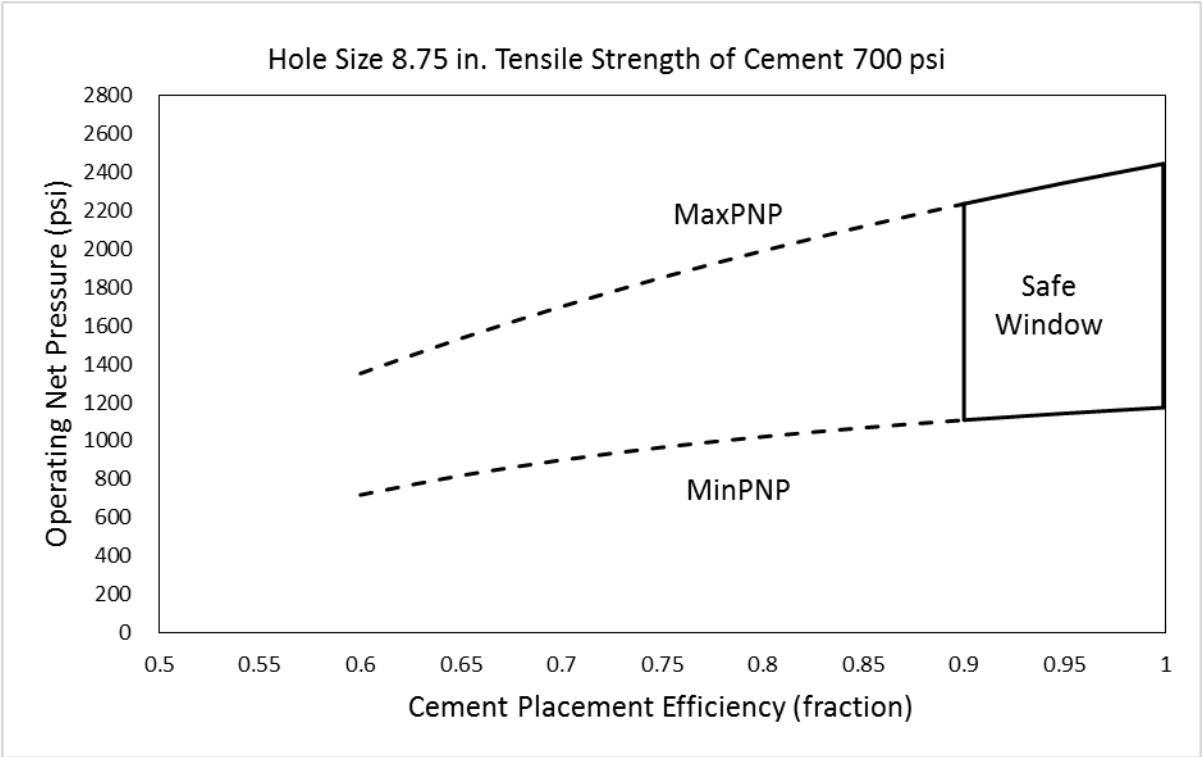


Figure 45: Operating Net Pressure window for wells completed with 8.75" casing with tensile strength of cement 700 psi.

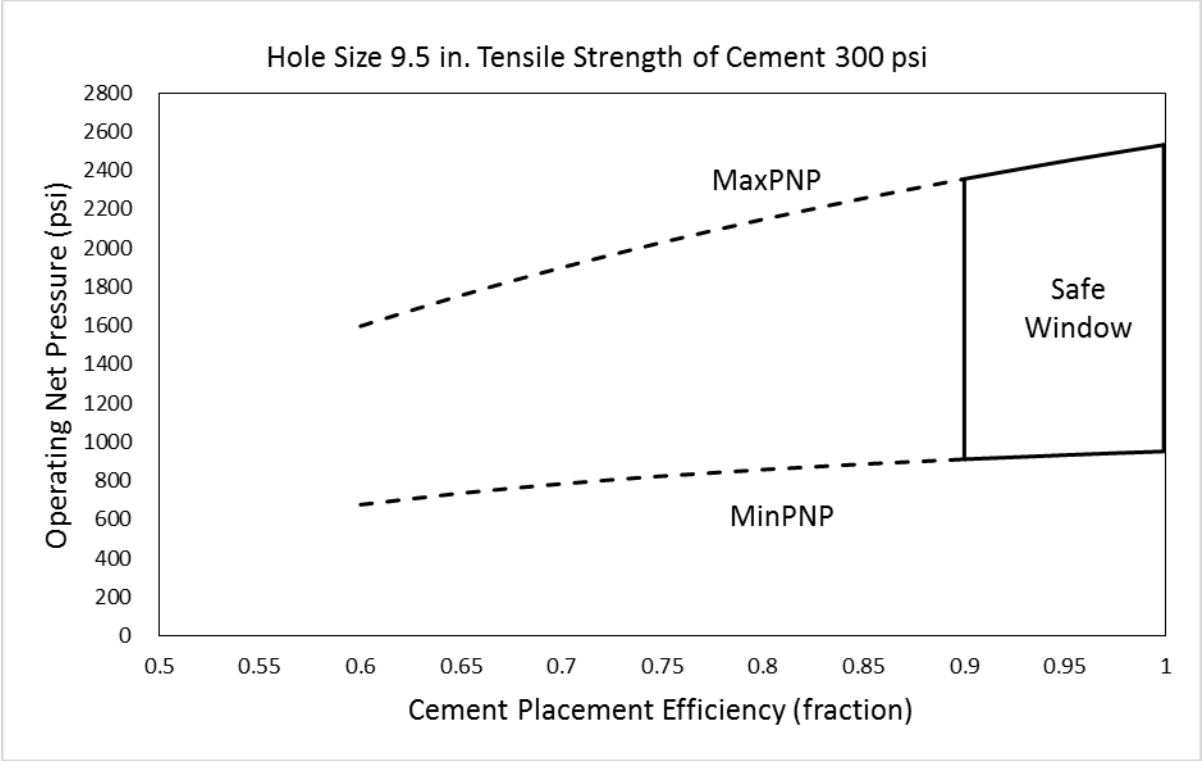


Figure 46: Operating Net Pressure window for wells completed with 9.5" casing with tensile strength of cement 300 psi.

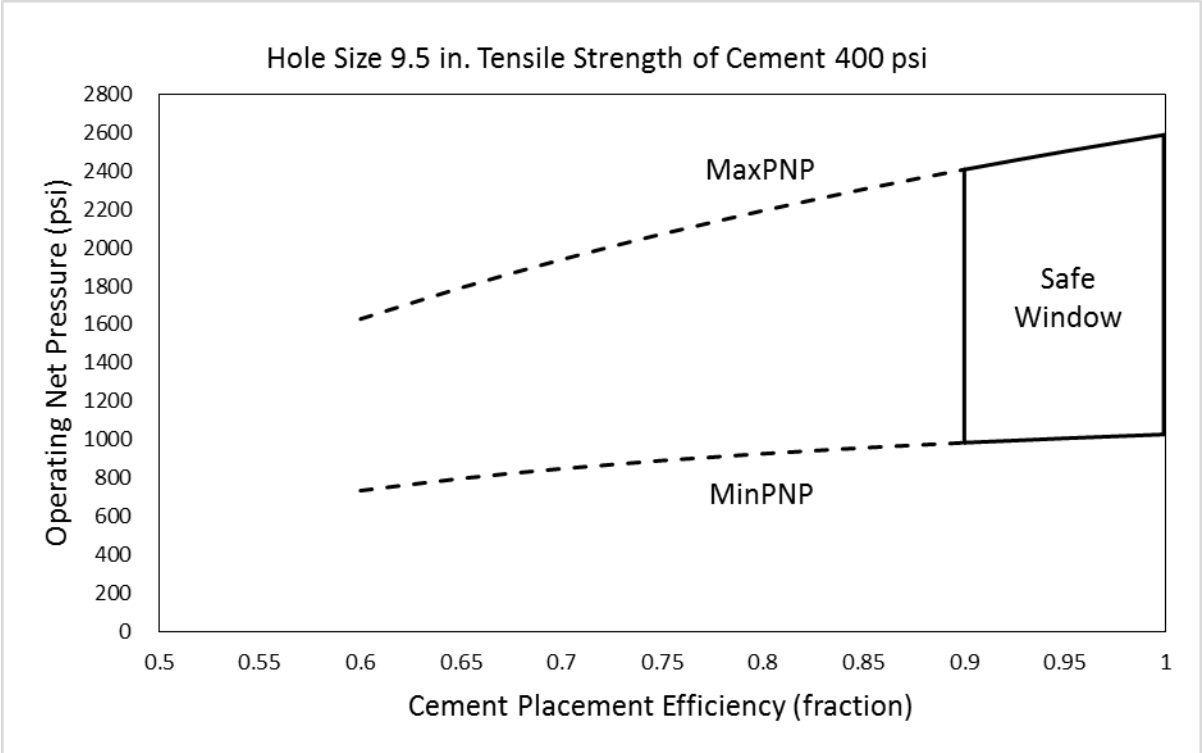


Figure 47: Operating Net Pressure window for wells completed with 9.5" casing with tensile strength of cement 400 psi.

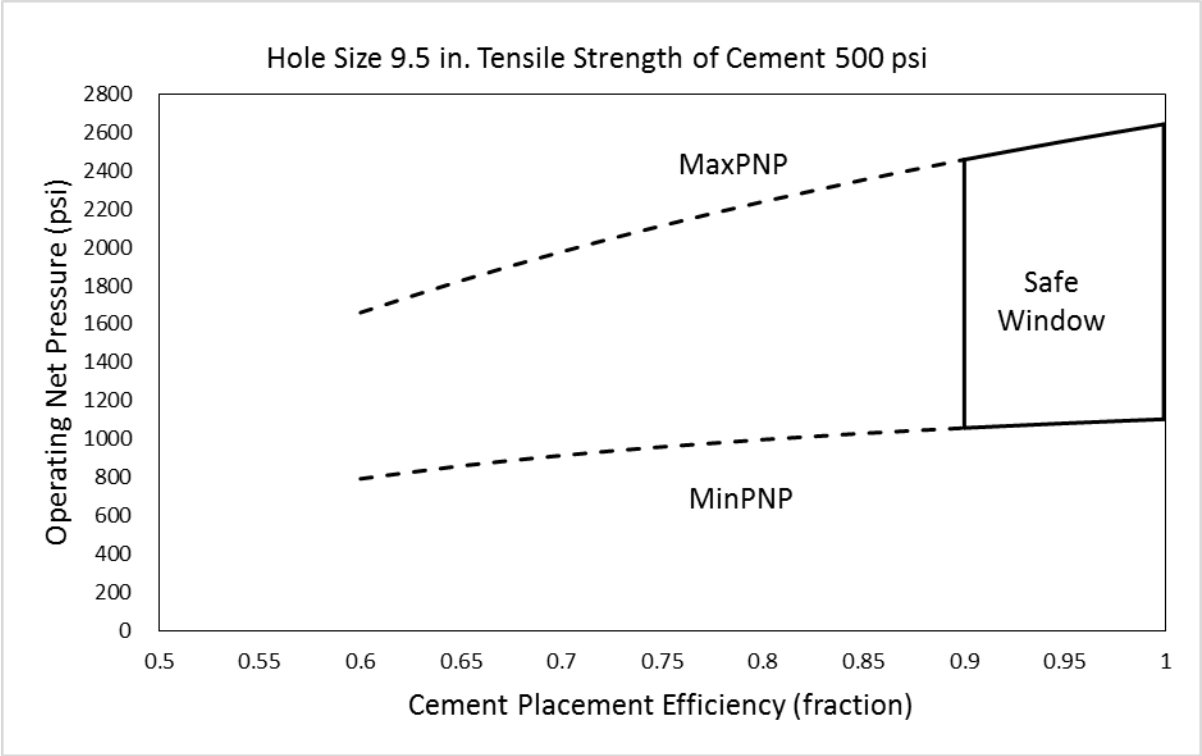


Figure 48: Operating Net Pressure window for wells completed with 9.5" casing with tensile strength of cement 500 psi.

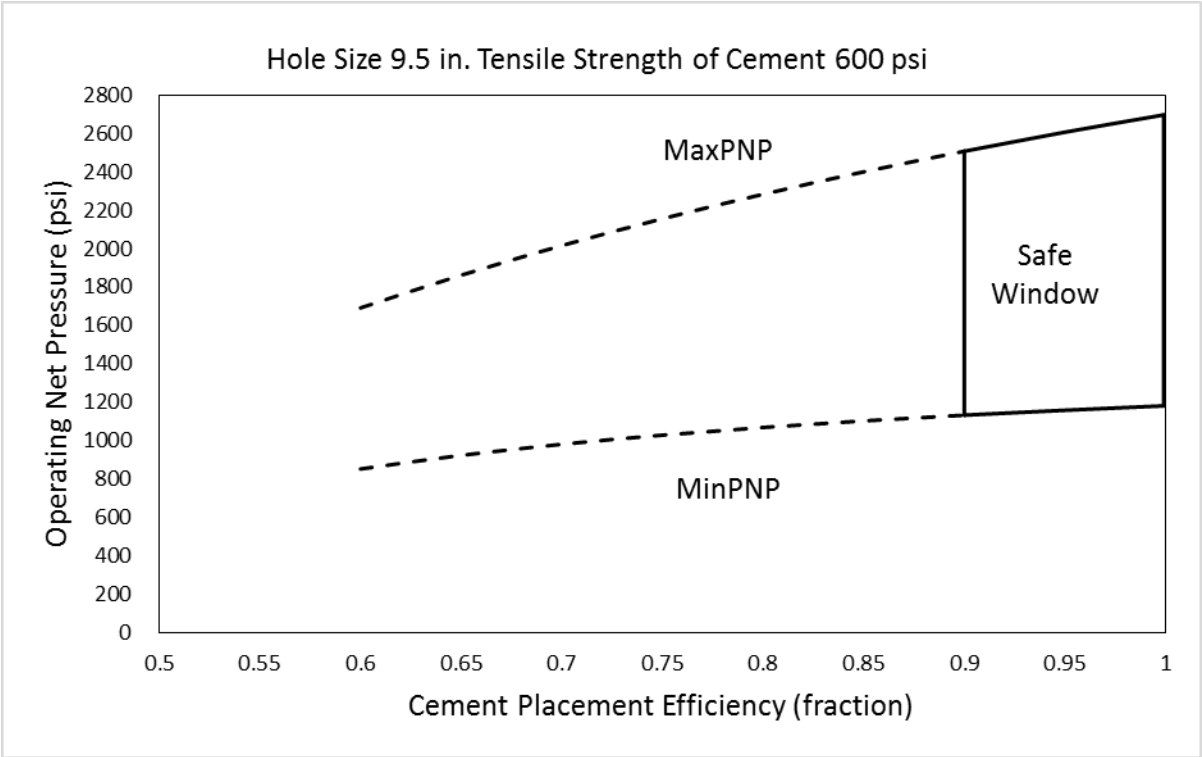


Figure 49: Operating Net Pressure window for wells completed with 9.5" casing with tensile strength of cement 600 psi.

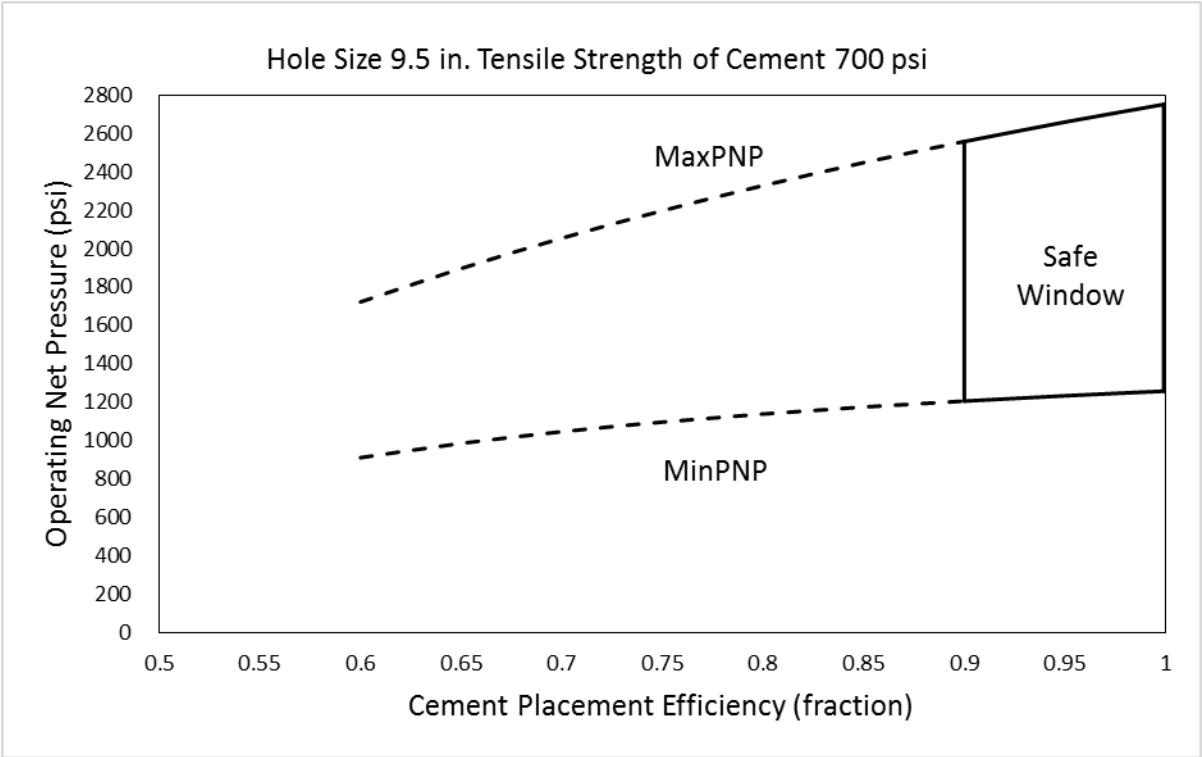


Figure 50: Operating Net Pressure window for wells completed with 9.5" casing with tensile strength of cement 700 psi.

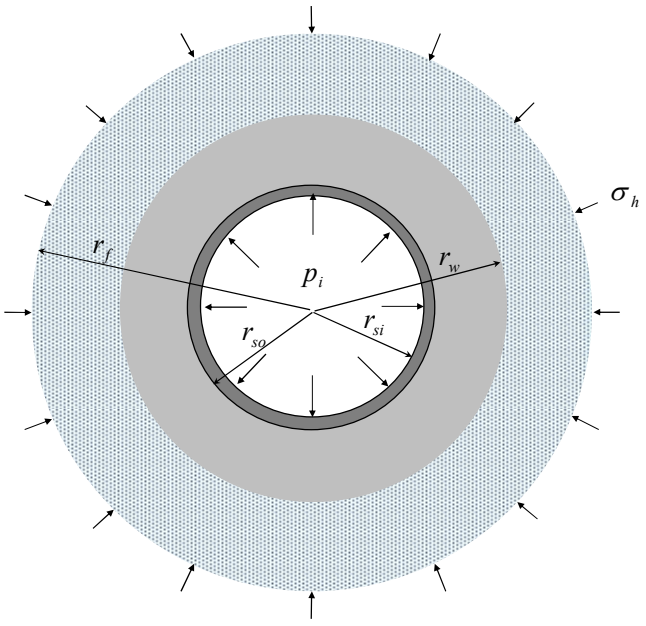


Figure A- 1:  A cross section of perfect cement collar around well casing.

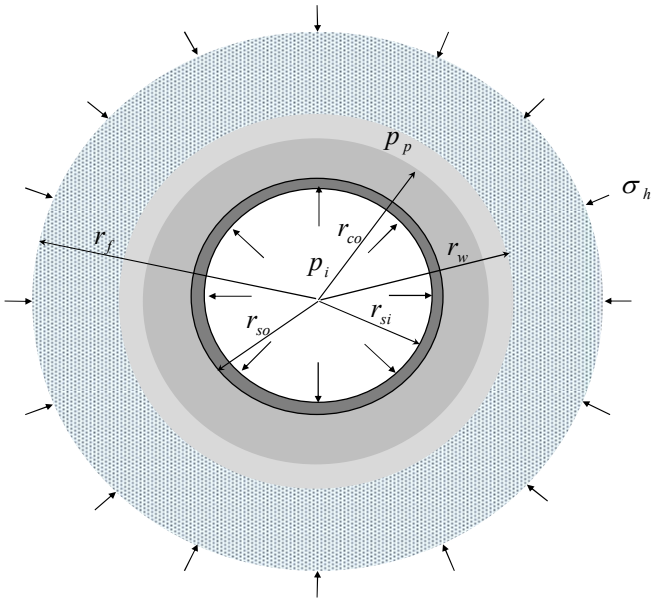


Figure A- 2: A cross section of imperfect cement collar around well casing.

## Appendix A: Derivation of the Maximum Permissible Pressure

Under the radial loads (pressure or stress) the stresses in thick-pipe can be calculated using Lame's solutions:[17]

$$\sigma_r = \frac{p_i r_i^2 - p_o r_o^2}{\left(r_o^2 - r_i^2\right)} - \frac{r_i^2 r_o^2 \left(p_i - p_o\right)}{r^2 \left(r_o^2 - r_i^2\right)} \tag{A.1}$$

and

$$\sigma_\theta = \frac{p_i r_i^2 - p_o r_o^2}{\left(r_o^2 - r_i^2\right)} + \frac{r_i^2 r_o^2 \left(p_i - p_o\right)}{r^2 \left(r_o^2 - r_i^2\right)} \tag{A.2}$$

where $\sigma_r$ = radial stress

$\sigma_\theta$ = tangential (loop) stress

$p_i$ = internal pressure

$p_o$ = external pressure

$r$ = radius

$r_i$ = inner radius

$r_o$ = outer radius

It can be shown that the tangential stress reaches its peak value at the inner wall of pipe ($r = r_i$). The stresses at the inner wall are thus expresses as:

$$\sigma_{ri} = -p_i \tag{A.3}$$

and

$$\sigma_{\theta i} = \frac{p_i\left(r_i^2 + r_o^2\right) - 2p_o r_o^2}{\left(r_o^2 - r_i^2\right)} \ . \tag{A.4}$$

Figure A-1 illustrates a cross-section of a well casing cemented in a formation with a rock stress $\sigma_h$. Since the tensile strength of cement concrete is much lower than its compressive strength, tensile failure is expected when the injection pressure inside the casing reaches a certain level.

When Lame's solutions are applied to the cement collar, the tangential stress at the inner wall of the collar is given by:

$$\sigma_{\theta ci} = \frac{p_{ci}\left(r_{so}^2 + r_w^2\right) - 2p_{co} r_w^2}{\left(r_w^2 - r_{so}^2\right)} \ . \tag{A.5}$$

The worst situation is that the annular space between for casing and the formation rock is not completely filled with cement and the external pressure for the cement collar is the formation pore pressure. This is illustrated in Figure A-2.

Then Eq. (A.5) becomes:

$$\sigma_{\theta ci} = \frac{p_{ci}\left(r_{so}^2 + r_{co}^2\right) - 2p_p r_{co}^2}{\left(r_{co}^2 - r_{so}^2\right)} \tag{A.6}$$

where $p_p$ is formation pore pressure. The cement collar will failure when the tangential stress reaches the tensile strength of cement concrete. At the failure condition, Eq. (A.6) takes the form of:

$$\sigma_T = \frac{p_{ci}\left(r_{so}^2 + r_{co}^2\right) - 2p_p r_{co}^2}{\left(r_{co}^2 - r_{so}^2\right)} \tag{A.7}$$

where $\sigma_T$ is the tensile strength of cement concrete. The internal pressure for the cement collar to cause failure can be solved from Eq. (A.7):

$$p_{ci} = \frac{\sigma_T\left(r_{co}^2 - r_{so}^2\right) + 2p_p r_{co}^2}{\left(r_{so}^2 + r_{co}^2\right)}. \tag{A.8}$$

where $r_{co}$ is the outer diameter of the cement collar.

Under the radial loads (pressure or stress) the radial displacement in a thick-wall casing can be calculated by:[17]

$$u_r = \frac{(1-\nu)}{E}\frac{\left(p_i r_i^2 - p_o r_o^2\right)r}{\left(r_o^2 - r_i^2\right)} + \frac{(1+\nu)}{E}\frac{\left(p_i - p_o\right)r_i^2 r_o^2}{\left(r_o^2 - r_i^2\right)r} \tag{A.9}$$

where $E$ is Young's modulus and $\nu$ is Poison's ratio of material. An expression for the radial displacement at the outer wall of the pipe can be obtain from Eq. (A.9) by setting $r = r_o$

$$u_r = \frac{r_o}{E\left(r_o^2 - r_i^2\right)}\left\{2p_i r_i^2 + p_o\left[\nu\left(r_o^2 - r_i^2\right) - \left(r_o^2 + r_i^2\right)\right]\right\}. \tag{A.10}$$

Because the tensile strength of cement concrete is very low (300 psi ~700 psi), it is conservative to assume that negligible deformation of cement collar should occur before its tensile failure. This is equivalent to an assumption of zero displacement at the interface between the casing and the cement collar. Applying Eq. (A.10) to the casing under the cement-failure condition gives:

$$0 = \frac{r_{so}}{E\left(r_{so}^2 - r_{si}^2\right)}\left\{2p_{si}r_{si}^2 + p_{ci}\left[\nu\left(r_{so}^2 - r_{si}^2\right) - \left(r_{so}^2 + r_{si}^2\right)\right]\right\}. \tag{A.11}$$

which is solved for the internal pressure of casing required to cause failure of cement collar:

$$p_{si} = \frac{p_{ci}\left[\left(r_{so}^2 + r_{si}^2\right) - \nu\left(r_{so}^2 - r_{si}^2\right)\right]}{2r_{si}^2}. \tag{A.12}$$

Substituting Eq. (A.8) into Eq. (A.12) results in an expression for the casing internal pressure to cause cement collar failure:

$$p_{si} = \frac{\left[\left(r_{so}^2 + r_{si}^2\right) - \nu\left(r_{so}^2 - r_{si}^2\right)\right]\left[\sigma_T\left(r_{co}^2 - r_{so}^2\right) + 2p_p r_{co}^2\right]}{2r_{si}^2\left(r_{so}^2 + r_{co}^2\right)}, \tag{A.13}$$

which is called the Maximum Permissible Pressure (MaxPP) in this study.

## Appendix B: Derivation of the Minimum Permissible Pressure

Figure A-1 illustrates a cross-section of a well casing cemented in a formation with a rock stress $\sigma_h$. The worst situation is that the annular space between casing and the formation rock is not completely filled with cement and the external pressure for the cement collar is the formation pore pressure. This is illustrated in Figure A-2.

According to Lame's solutions for thick-wall pipe, the pipe material will yield first at the inner wall. The tangential stress at the inner wall of the cement sheath is given by:[17]

$$\sigma_{\theta ci} = \frac{p_{ci}\left(r_{ci}^2 + r_{co}^2\right) - 2p_{co}r_{co}^2}{\left(r_{co}^2 - r_{ci}^2\right)} \tag{B.1}$$

where

$\sigma_{\theta ci}$ = tangential stress at the inner wall of the cement sheath

$p_{ci}$ = pressure or radial stress at the inner wall of the cement sheath

$p_{co}$ = pressure or radial stress at the outer wall of the cement sheath

$r_{ci}$ = inner radius of cement sheath

$r_{co}$ = outer radius of cement sheath

If the cement completely fills the annulus, as shown in Figure A-1, the radial stress at the outer wall of cement sheath can be much higher than the formation stress $\sigma_h$. In conservative analysis, the value of $p_{co}$ should be taken as the formation stress $\sigma_h$ and $r_{co}$ is taken as the wellbore radius $r_w$. However, if the cement does not completely fill

the annulus, as shown in Figure 5, the value of $p_{co}$ should be taken as the formation pore pressure $p_p$ and $r_{co}$ should be estimated based on cement bonding logs.

Under the radial loads (pressure or stress) the radial displacement in a thick-wall casing can be calculated by:[17]

$$u_r = \frac{(1-\nu)}{E}\frac{\left(p_i r_i^2 - p_o r_o^2\right)r}{\left(r_o^2 - r_i^2\right)} + \frac{(1+\nu)}{E}\frac{\left(p_i - p_o\right)r_i^2 r_o^2}{\left(r_o^2 - r_i^2\right)r} \tag{B.2}$$

where

$\nu$ = Poison's ratio of casing material

$E$ = Young's modulus of casing material

$p_i$ = casing inner pressure

$p_o$ = casing outer pressure or radial stress

$r_i$ = inner radius of casing

$r_o$ = outer radius of casing

$r$ = radial distance from the axis of casing

$u_r$ = radial displacement at radial distance $r$

An expression for the radial displacement at the outer wall of the casing can be obtained from Eq. (B.2) by setting $r = r_o$:

$$u_r = \frac{r_o}{E\left(r_o^2 - r_i^2\right)}\left\{2p_i r_i^2 + p_o\left[\nu\left(r_o^2 - r_i^2\right) - \left(r_o^2 + r_i^2\right)\right]\right\}. \tag{B.3}$$

Because the tensile strength of cement concrete is very low (300 psi ~700 psi), it is conservative to assume that negligible deformation of cement sheath should occur before its failure. This is equivalent to an assumption of zero displacement at the interface between the casing and the cement sheath. Applying Eq. (B.3) to the casing under the cement-failure condition gives:

$$0 = \frac{r_o}{E\left(r_o^2 - r_i^2\right)}\left\{2p_i r_i^2 + p_o\left[\nu\left(r_o^2 - r_i^2\right) - \left(r_o^2 + r_i^2\right)\right]\right\}. \tag{B.4}$$

The casing outer pressure or radial stress at the outer wall of casing is equal to the radial stress at the inner wall of cement sheath, i.e., $p_o = p_{ci} = -\sigma_{r\,ci}$ at $r_o = r_{ci}$. It is solved from Eq. (B.4) to get:

$$\sigma_{rci} = -p_{ci} = \frac{-2p_i r_i^2}{\left(r_o^2 + r_i^2\right) - \nu\left(r_o^2 - r_i^2\right)}. \tag{B.5}$$

The tangential and radial stresses given by Eqs. (B.1) and (B.5), respectively, can be used for failure analysis to determine the Minimum Permissible Pressure $p_i$.